INSTITUTE FOR SPACE STUDIES

STELLAR ENERGY SOURCES
(revised July, 1963)

Hubert Reeves

FACILITY FORM 602

N 66-80594
(ACCESSION NUMBER)

(THRU)

186
(PAGES)

None
(CODE)

(NASA CR OR TMX OR AD NUMBER)

(CATEGORY)

GODDARD SPACE FLIGHT CENTER
NATIONAL AERONAUTICS AND SPACE ADMINISTRATION

STELLAR ENERGY SOURCES
(revised July, 1963)

by Hubert Reeves
University of Montreal
and
Goddard Institute for Space Studies

To be published in the Vol VIII, "Stellar Interiors," of the series "Stars and Stellar Systems," edited by Aller and Middlehurst. University of Chicago Press.

This work was prepared while the author was a Research Associate at the Institute for Space Studies, under an appointment by the National Academy of Sciences - National Research Council.

1. History of a Star

Throughout its life a star transforms nuclear and gravitational energy into photons and neutrinos. The star lives on its nuclear resources during the so-called nuclear burning stages. During such stages the rate of energy released from some particular nuclear reaction is just sufficient to compensate for the radiation loss. The star stops its gravitational contraction for the time being, to resume it only after the exhaustion of the particular fuel involved.

By now, two neatly defined burning stages can be identified with fair confidence: the hydrogen and helium burning stages. During the hydrogen burning stage, four hydrogren nuclei are transformed into one helium nucleus with an energy release of 26.730 Mev (6.682 Mev per nucleon).

Four main mechanisms are responsible for this conversion. These mechanisms are described in Tables 1 and 2. According to the mass of the star, the hydrogen burning stage will take place at temperatures ranging from ten to thirty million degrees. Some of these reactions are accompanied by neutrino emission. About five per cent of the energy will escape under the form of neutrinos.

Stars in the hydrogen burning stage are identified with stars in the main sequence of the Herzsprung-Russell diagram. The upper half of the main sequence represents stars living mostly on the CN cycles (PPIV), while the lower half represents stars living on some combination of the three first cycles.

After the exhaustion of the hydrogen in the core, a star resumes its contraction again but still obtains some of its energy from hydrogen burning in a thin shell surrounding the helium core. The red giant branch in the H-R diagram can be considered with good confidence as representing stars in this stage of evolution.

The helium burning stage starts when the core becomes hot enough to initiate the thermonuclear reactions between the helium nuclei themselves (Table 3). This occurs at temperatures varying from 10^8 ^oK to 3×10^8 ^oK, ($T_8 = 1$ to 3). The isotopic outcome of the burning consists mainly of C^{12} and O^{16}. Only in the very massive stars does it appear possible to obtain Ne^{20} or Mg^{24} from the helium burning stage.

The energy released during this stage depends on the final isotopic abundance. It is 7.275 Mev for each C^{12} made (0.6062 Mev per nucleon); 14.436 Mev for each O^{16} (0.9022 Mev

per nucleon); 19.167 Mev for Ne^{20} (0.9583 Mev per nucleon) and 28.481 Mev for Mg^{24} (1.187 Mev per nucleon). These reactions do not create neutrinos.

Stars in the helium burning stage are usually identified with stars in the tip of the red giant branch. The presence of any further burning stages is still highly hypothetical. The next candidate as fuel nuclei is C^{12} (through its fusion with another C^{12}). Rough estimates show that it would become active at temperatures varying from 0.6 to 1.0 billion degrees. After that, the photodisintegration of the Ne^{20} could trigger another burning stage, and still later the fusion of two O^{16} nuclei (both in the range from T_9 = 1.3 to 2.0).

We have good reason to believe that at this stage the core becomes the seat of intense neutrino-producing reactions. As the temperature rises, these neutrinos carry away an increasingly large fraction of the stellar energy. At temperatures neighboring the billion degree mark, these neutrinos appear to have become the main source of energy dissipation.

The following nuclear reactions (further photo-disintegration and re-combination) would be spread over a range of temperature (from two to about four billion degrees).

Figure 1

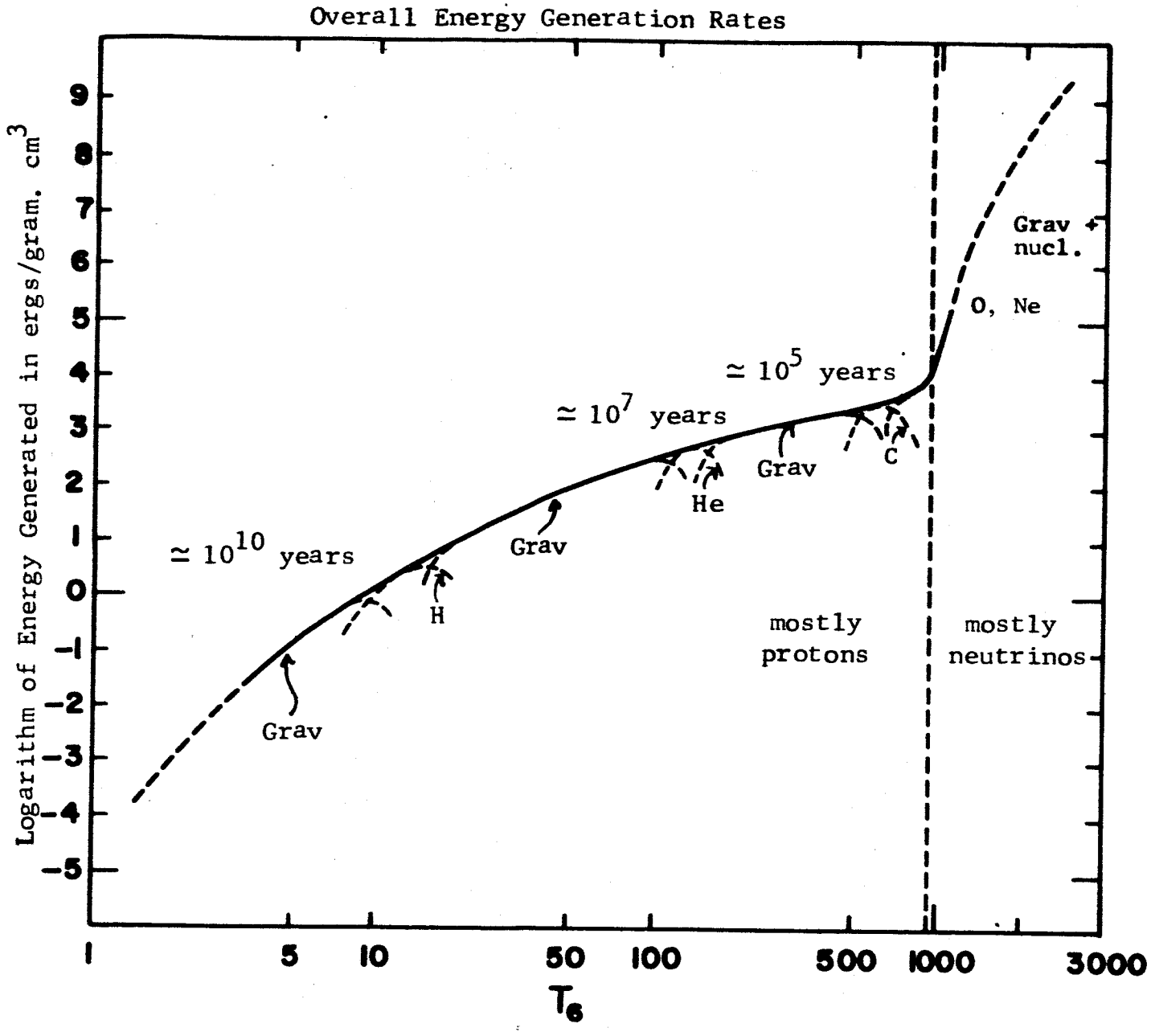

Figure 1.

A very rough sketch of the energy generated by a star of about one solar mass which (we assume) would reach up to a few billion degrees. The origin of the energy is identified by "Grav" for gravitational contraction, and by the name of the nuclear fuel for nuclear burning stages. The dashed lines represent the individual contributions of these two modes. The solid (envelope) line is the sum of both; the total luminosity of the star in erg/gr. sec. We identify roughly the region where the luminosity switches from photons to neutrinos.

Figure 2

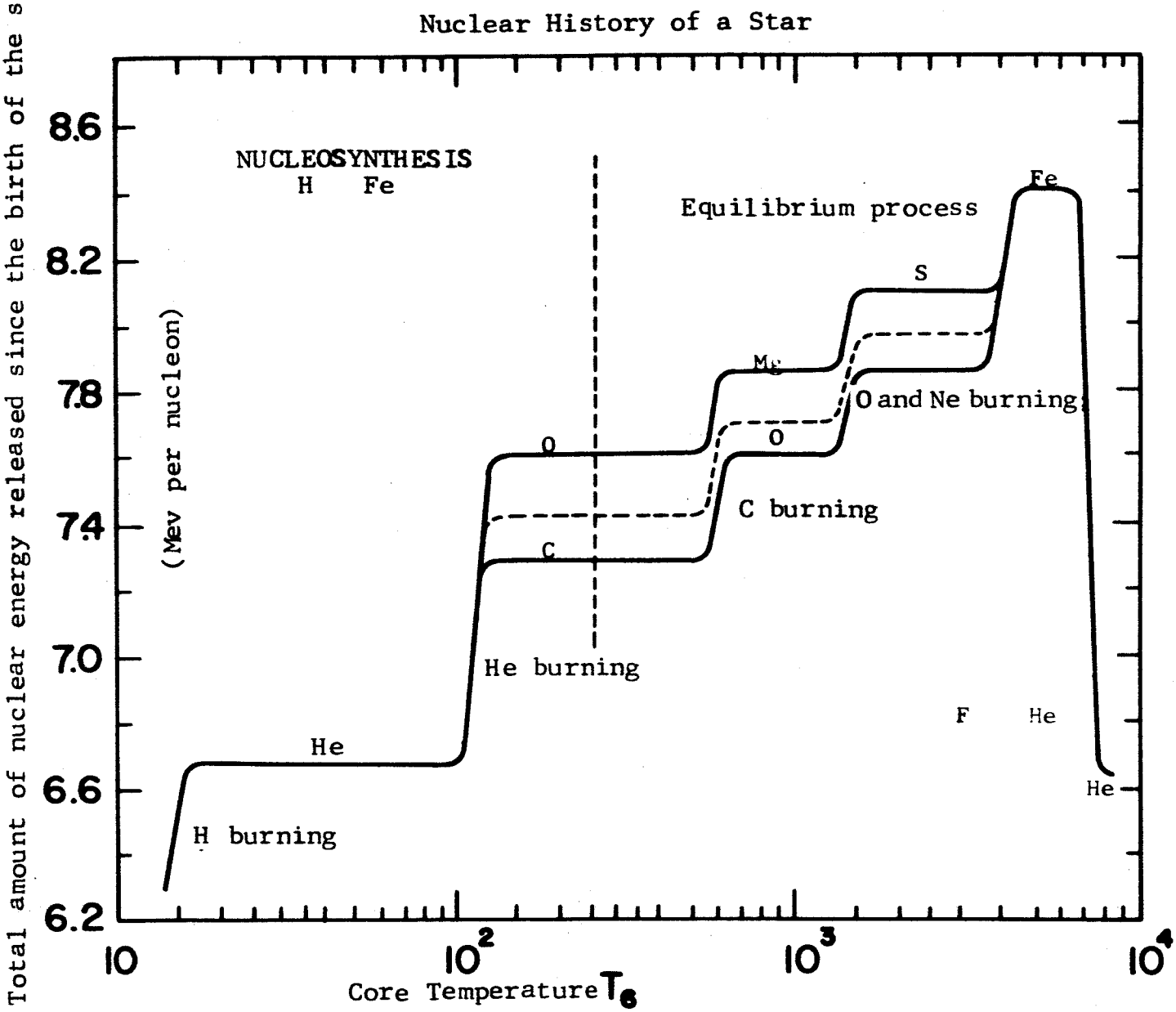

Figure 2.

The curve represents the total amount of nuclear energy (per nucleon) released since the birth of the star, as a function of the core temperature. During the nuclear burning stages the curve rises sharply (almost isothermal processes). During the periods of gravitational contraction the isotopic composition does not change (flat regions). After the He burning stage the core contains C^{12} and O^{16} in fractional abundances depending upon the initial mass. The C and O curves are then lower and upper limits respectively. The dashed line is a typical case. The same kind of statement applies to the rest of the graph.

Figure 3

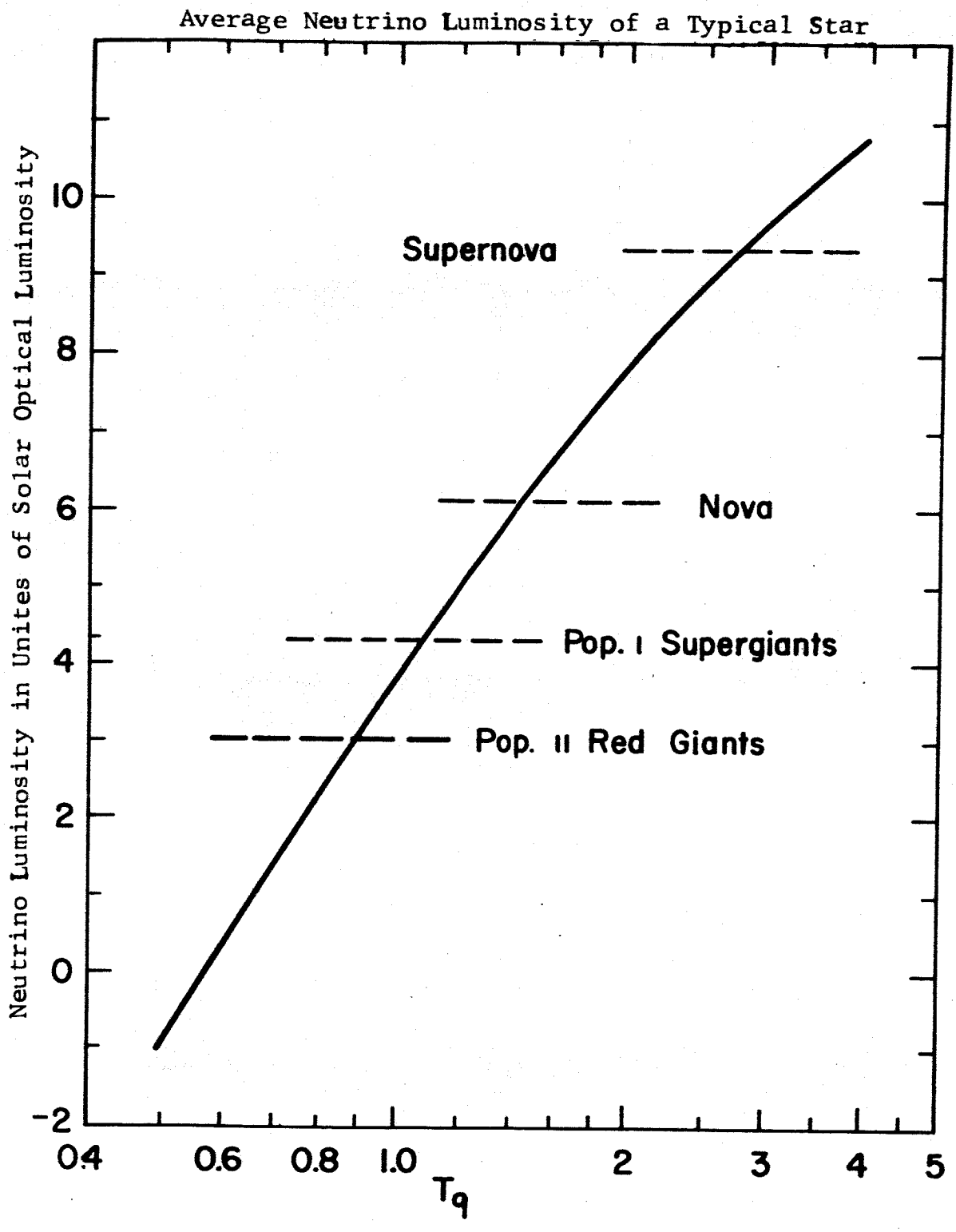

Average neutrino luminosity of a typical star. This graph was obtained by dividing the central neutrino luminosity per gr/cm. sec by about one hundred, in order to obtain an average value over the whole star. For comparison average optical luminosities are given for various steady states of stars (giants) and also transient states (novae and supernovae).

2. Formalism

The aim of the present paper is to review somewhat critically the whole problem of nuclear energy generation rate during stellar evolution. The computation of these rates depends, amongst other things, upon the cross sections for the various nuclear events responsible for the energy production. Except for one case (the $H^1 + H^1$ reaction) these cross sections cannot be calculated; they must be measured by laboratory experiments. Furthermore, in most cases the measurements were made at energies somewhat higher than the energies of stellar interest, (a few times kT). In these cases some methods of extrapolation are used to find the cross section in the proper range of energies.

We intend to consider each reaction of interest in detail. The diagrams exhibiting the energy levels of the nuclei involved will be given for most reactions. In these diagrams we shall include the break-up energies for some constituents of interest, together with the stellar energy ranges at various temperatures. This way one can judge whether the reaction should be resonant or not, and if so,

which resonance levels are expected to play a dominant role. Further, if any new levels are discovered in the future or if the existence of some of the levels already shown become dubious, the diagram will allow a quick estimate of the importance of the resulting modifications in the computed rate.

Most of the parameters relevant to the various reactions are given in the Tables. We shall give for each reaction the range of energy which has been explored experimentally. We shall then describe the method of extrapolation and give the accuracy of the results. In a number of cases the experimenters have been contacted to obtain a re-evaluation of the uncertainty in their results. Using these new estimates, values will be recommended here that may differ somewhat from the values used by previous authors. The margin of errors quoted will tend to be pessimistic, although not unduly so.

From the computed reaction rates, energy generation rates will be calculated. These last rates depend on the slowest reaction of a given set of reactions, but also in some cases, on the rate of some other reactions. These effects will be discussed. Calculations will be made which,

Table 4

MASS TABLE $A \leq 56$

SYMBOL	NAME	Z	MASS (a.m.u.: O^{16} = 16.00) (Error in milli-a.m.u.)	MASS EXCESS (kev: O^{16} = 0.00)
H^{1}	Hydrogen	1	1.00814563 ± 0.00007	7584.76 ± 0.06
D^{2}	Deuterium	1	2.01474251 ± 0.00009	13727.42 ± 0.08
He^{3}	Helium	2	3.0169888 ± 0.0002	15819.0 ± 0.2
He^{4}	Helium	2	4.0038761 ± 0.0004	3609.2 ± 0.3
Li^{6}	Lithium	3	6.017039 ± 0.001	15865. ± 1.
Li^{7}	Lithium	3	7.018236 ± 0.001	16980. ± 1.
Be^{9}	Beryllium	4	9.0150509 ± 0.0009	14014.6 ± 0.8
B^{10}	Boron	5	10.0161222 ± 0.0007	15012.1 ± 0.7
B^{11}	Boron	5	11.0128051 ± 0.0005	11923.4 ± 0.4
C^{12}	Carbon	6	12.0038150 ± 0.0002	3552.3 ± 0.2
C^{13}	Carbon	6	13.0074883 ± 0.0008	6972.7 ± 0.7
N^{14}	Nitrogen	7	14.0075262 ± 0.0002	7008.0 ± 0.2
N^{15}	Nitrogen	7	15.0048769 ± 0.0009	4541.1 ± 0.8
O^{16}	Oxygen	8	16.000000	0
O^{17}	Oxygen	8	17.0045377 ± 0.0009	4225.3 ± 0.8
O^{18}	Oxygen	8	18.0048821 ± 0.0003	4545.9 ± 0.2
F^{19}	Fluorine	9	19.0044445 ± 0.0007	4138.5 ± 0.6

Table 4

SYMBOL	NAME	Z	MASS (a.m.u.: O^{16} = 16.00)	MASS EXCESS (kev: O^{16} = 0.00)
			(Error in milli-a.m.u.)	
Ne^{20}	Neon	10	19.9987964 ± 0.0004	-1120.8 ± 0.4
Ne^{21}	Neon	10	21.000524 ± 0.002	488. ± 2.
Ne^{22}	Neon	10	21.9983759 ± 0.0004	-1512.3 ± 0.4
Na^{23}	Sodium	11	22.997081 ± 0.002	-2718. ± 2.
Mg^{24}	Magnesium	12	23.992670 ± 0.002	-6825. ± 2.
Mg^{25}	Magnesium	12	24.993738 ± 0.002	-5788.8 ± 2.
Mg^{26}	Magnesium	12	25.990851 ± 0.002	-8519. ± 2.
Al^{27}	Aluminium	13	26.990113 ± 0.002	-9206. ± 2.
Si^{28}	Silicon	14	27.985822 ± 0.003	-13202. ± 3.
Si^{29}	Silicon	14	28.985703 ± 0.004	-13313. ± 3.
Si^{30}	Silicon	14	29.983290 ± 0.004	-15560. ± 4.
P^{31}	Phosphorous	15	30.983611 ± 0.002	-15261. ± 1.
S^{32}	Sulfur	16	31.982238 ± 0.001	-16538.8 ± 0.9
S^{33}	Sulfur	16	32.981943 ± 0.003	-16814. ± 3.
S^{34}	Sulfur	16	33.978663 ± 0.003	-19867. ± 3.
Cl^{35}	Chlorine	17	34.979972 ± 0.003	-18649. ± 3.
S^{36}	Sulfur	16	35.978524 ± 0.004	-19996. ± 3.
A^{36}	Argon	18	35.978983 ± 0.003	-19570. ± 3.
Cl^{37}	Chlorine	17	36.977648 ± 0.002	-20813. ± 2.

Table 4

SYMBOL	NAME	Z	MASS (a.m.u.: O^{16} = 16.00)	MASS EXCESS (kev: O^{16} = 0.00)
			(Error in milli-a.m.u.)	
A^{38}	Argon	18	37.974794 ± 0.003	-23471. ± 2.
K^{39}	Potassium	19	38.976101 ± 0.003	-22253. ± 3.
A^{40}	Argon	18	39.9750886 ± 0.006	-23196.2 ± 0.6
K^{40}	Potassium	19	39.976713 ± 0.004	-21683. ± 3.
Ca^{40}	Calcium	20	39.975294 ± 0.004	-23005. ± 4.
K^{41}	Potassium	19	40.974858 ± 0.005	-23411. ± 4.
Ca^{42}	Calcium	20	41.971967 ± 0.004	-26103. ± 4.
Ca^{43}	Calcium	20	42.972437 ± 0.005	-25665. ± 5.
Ca^{44}	Calcium	20	43.969464 ± 0.005	-28434. ± 5.
Sc^{45}	Scandium	21	44.970211 ± 0.004	-27738. ± 4.
Ca^{46}	Calcium	20	45.968298 ± 0.004	-29519. ± 4.
Ti^{46}	Titanium	22	45.967242 ± 0.004	-30502. ± 3.
Ti^{47}	Titanium	22	46.966685 ± 0.008	-31021. ± 8.
Ca^{48}	Calcium	20	47.96776 ± 0.02	-30017. ± 14.
Ti^{48}	Titanium	22	47.963191 ± 0.005	-34274. ± 4.
Ti^{49}	Titanium	22	48.963428 ± 0.005	-34054. ± 4.
Ti^{50}	Titanium	22	49.960667 ± 0.006	-36624. ± 5.
V^{50}	Vanadium	23	49.963044 ± 0.005	-34412. ± 5.
Cr^{50}	Chromium	24	49.961929 ± 0.005	-35449. ± 5.

Table 4

SYMBOL	NAME	Z	MASS (a.m.u.: O^{16} = 16.00)	MASS EXCESS (kev: O^{16} = 0.00)
			(Error in milli-a.m.u.)	
V^{51}	Vanadium	23	50.960174 ± 0.005	-37084. ± 5.
Cr^{52}	Chromium	24	51.957027 ± 0.005	-40015. ± 4.
Cr^{53}	Chromium	24	52.957482 ± 0.005	-39591. ± 4.
Cr^{54}	Chromium	24	53.57508 ± 0.007	-40945 ± 5.
Fe^{54}	Iron	26	53.956769 ± 0.007	-40254. ± 6.
Mn^{55}	Manganese	25	54.955519 ± 0.005	-41418. ± 5.
Fe^{56}	Iron	26	55.952714 ± 0.007	-44030. ± 6.
Fe^{57}	Iron	26	56.953494 ± 0.007	-43304. ± 6.
Fe^{58}	Iron	26	57.951690 ± 0.008	-44984. ± 7.

however, will not prejudice the chemical composition of the gas considered.

For uniformity, the masses and Q values (with the O^{16} scale) were all taken from the latest (1960) nuclear data tables of the U.S.A.E.C. (Everling, Koenig, Mattauch, and Wapstra 1960). In Table 4 these masses are given in a.m.u. (scale of O^{16}) together with the mass excesses in kev. The energy diagrams were taken from the Landolt-Börnstein handbook (1961) but again with the Q values from the U.S.A.E.C.. Corrections to the diagram were made whenever newer data was available.

Unless otherwise noted, the kinetic energies quoted are always energies in the center of momentum system. We shall use three units of temperature; T_6 (units of 10^6 ^oK) for the hydrogen burning, T_8 (units of 10^8 ^oK) for helium burning and T_9 (units of 10^9 ^oK) for the rest of the stages. In analytical formulae the temperature units will always be identified.

The stable chemical elements will be identified by their atomic numbers, (although we shall sometimes write α for the He^4 particle). N_i will represent the number densities and X_i the <u>fractional mass</u> (in a given gas).

In the diagrams the energy levels are in Mev, the notation "2^-; 0" under a level indicates that the spin is 2, the parity is (-), and the isotopic spin is 0. Bracketed numbers are doubtful. Whenever we have taken away a part of the diagram, the number of levels in that range are given, as for instance, "11 levels" in Figure 4. Finally, a vertical bar outside the diagram with the label $T_8 = 20$ means that at this temperature the most likely candidate for a given nuclear reaction is to be found in the corresponding energy range (the Gamow peak). The center of the range is also indicated.

In the Tables of the reaction rates, we have often identified the level which gives the dominant contribution at a given temperature. For instance, the notation (6.87 - N.R. - 10) attached to a certain portion of a column means that in the corresponding range of temperatures, the 6.87 Mev level in the compound nucleus is dominant, that the contribution is non-resonant (N.R.), and that the rate may be inaccurate by a factor of 10.

2.1 Thermonuclear Reaction Rates

We consider a gas composed of two types of particles, 1 and 2, reacting together to give two new particles, 3 and 4. The number of reactions per second per unit volume can be written as:

$$I_{1,2} = \int_{v_t}^{\infty} N(v)\,[v\sigma(v)]\,dv \tag{1}$$

Here v is the relative velocity between two reacting particles; $\sigma(v)$ is the nuclear cross section for the reaction under consideration, at the velocity v; N(v) is the number of pairs of particles with velocity v; v_t is the threshold velocity for the reaction (usually $v_t = 0$).

In most cases of astrophysical interest, the atomic gas is not degenerate and may adequately be represented by a Maxwellian distribution. The distribution of the <u>relative</u> velocities between pairs of particles (the only one that matters for us) is easily seen to be also Maxwellian, and given by

$$N(v) = \frac{2N_1N_2}{\sqrt{2\pi}}\,\frac{M^{3/2}v^2}{(kT)^{3/2}}\exp(-Mv^2/2kT) \tag{2}$$

M is the reduced mass, $M = A_1A_2/A_1 + A_2$ in a.m.u.; N_1, N_2 are the numbers of atoms 1 and 2 per unit volume.

We shall frequently use the following quantity,

$$\langle \sigma v \rangle_{2,1} = \int N(v)[\sigma(v)v]dv \Big/ \int N(v)\,dv = I_{1,2}/N_1 N_2 \tag{3}$$

In words, $\langle \sigma v \rangle$ is the reaction probability per unit pair of particles 1 and 2 in a unit volume per unit time.

In terms of $\langle \sigma v \rangle$ one can obtain a collection of useful quantities:

$$P_{2,1} = N_1 \langle \sigma v \rangle_{2,1} \tag{4}$$

is the probability of a reaction between an atom of species 2 with N_1 atoms of species 1 per unit volume. We recall that $N_1 = \mathcal{N}\rho\chi_{A_1}/A_1$ where $\mathcal{N}$ is Avogadro's number (6.02×10^{23} in c.g.s.), ρ is the total density of the gas, A_1 is the mass number of species 1 and χ_A is the fractional density of that species. $1/P_{2,1}$ is the mean life of the atom of species 2 in these conditions.

$$r_{2,1} = \frac{N_2 N_1 \langle \sigma v \rangle_{2,1}}{\rho} = N_2 \frac{P_{2,1}}{\rho} \tag{5}$$

is the number of reactions per gram per second, if the species 1 and 2 are different. If we are considering reactions of a certain species with itself (e.g. $H^1 + H^1$) then:

$$r_{1,1} = \frac{N_1^2}{2} \frac{\langle \sigma v \rangle_{1,1}}{\rho} = \frac{N_1 P_{1,1}}{2\rho} \tag{6}$$

Given that $Q_{2,1}$ is the energy released in any one reaction; then $\mathcal{E}$, the rate of energy generation per gram per second is:

$$\mathcal{E}_{2,1} = r_{2,1} Q_{2,1} = \frac{N_1 N_2 \langle \sigma v \rangle_{2,1} Q_{2,1}}{\rho} = \frac{N_2 P_{2,1} Q_{2,1}}{\rho} \text{ erg/gm-sec.} \tag{7}$$

for different reacting species, or

$$\mathcal{E}_{1,1} = \frac{N_1^2}{2} \frac{\langle \sigma v \rangle_{1,1}}{\rho} Q_{1,1} = \frac{N_1 P_{1,1} Q_{1,1}}{2\rho} \qquad \text{(same species)} \tag{8}$$

The heart of the problem is the estimation of $\sigma(E)$. In some cases σ (E) has been measured experimentally in the region of astrophysical interest. In other cases, σ (E) must be either extrapolated from higher energy measurements or must be estimated from various nuclear models.

When the rest-mass energy of the two particles 1 and 2 corresponds to a region of the energy diagram of the

compound system (compound nucleus) where the resonances are well separated (which happens mostly for light nuclei), the contribution from any one of these resonances at energy E_r to the process involved (1 + 2 → 3 + 4) is well represented by a Breit-Wigner one level formula:

$$\sigma_{B.W.}(E_r) = \pi \lambda\!\!\!^{-2} \omega \, \Gamma_{2,1} \, \Gamma_{3,4} / [(\Gamma^2/4) + (E - E_r)^2] \qquad (9)$$

here $\lambda\!\!\!^{-}$ is the De Broglie wave length ($\lambda\!\!\!^{-} = \hbar/p$); (numerically, $\pi \lambda\!\!\!^{-2} = \frac{0.647}{E}\frac{1}{M}$ barns; 1 barn = 10^{-24} cm^2, if E is in Mev and M in a.m.u.); $\Gamma_{2,1}$ is the partial width for the reaction (2 + 1); $\Gamma_{3,4}$ is the partial width for the 3 + 4 breakup. Finally, the term ω is a statistical factor:

$$\omega = (2j_{CN} + 1)/(2j_1 + 1)(2j_2 + 1) \qquad (10)$$

j_1 is the spin of particle 1, j_2 the spin of particle 2 and j_{CN} is the spin of the resonant level.

The partial widths can be further factored into the product of a transmission factor and a so-called reduced width γ^*. γ^* is usually split into:

$$\gamma^* = \Theta_{1,2}^2 \gamma_w^*$$

where γ_w^* is the Wigner-Teichmann upper limit to the reduced width ($\gamma_w^2 = 1.5\hbar^2/MR^2$ in c.g.s. system) and $\theta_{1,2}^2$ is a constant, smaller than unity which depends upon the internal structure of the resonance level. R is the nuclear radius of interaction.

If we consider a collision of particles with relative angular momentum ℓ, and relative energy $E = \frac{\hbar^2 k^2}{2M}$ the transmission factor is often written as $T_\ell(E)(kR/2)$. This factor expresses the probability that the two constituents will overcome their various barriers (Coulomb, centrifugal and also the sudden change in the potential as the nuclear surface is crossed), and will penetrate each other.

When written down explicitly, T_ℓ (E) (for charged particles) presents itself as a complicated mixture of the regular (F_ℓ) and irregular (G_ℓ) solution to the wave equation outside of the nuclear boundary. (Feshbach, Shapiro and Weisskopf 1953.) However, at low energy (low compared to the height of the barriers) the factor T_ℓ (E) can be approximated by simpler expressions.

The highest barrier is usually the Coulomb barrier

$$\left[B_c = \frac{Z_1 Z_2 e^2}{R} \simeq \frac{1.44\, Z_1 Z_2}{R} \right.$$ in Mev, if R is in

fermis ($1f = 10^{-13}$cm.)]. In cases where E << B we are justified in writing:

$$\Gamma_{1,2} = \gamma^{*} \xi_{\ell}^{2} e^{-2\pi\eta} \tag{11}$$

where $\xi_{\ell}^{2} = (G_0^2/G_\ell^2)(2y^{1/2} e^{4y^{1/2}})$

with $4y^{1/2} = 4\left[\frac{2Z_1 Z_2 e^2 MR}{\hbar^2}\right]^{1/2} = 1.054\,[Z_1 Z_2 M(\text{a.m.u.})\,R(f)]^{1/2}$

and is almost independent of the energy. The factor $(e^{-2\pi\eta}) = e^{-2\pi Z_1 Z_2 e^2/\hbar v}$ (the so-called Gamow factor) represents the strong energy dependence brought in by the Coulomb repulsion. Numerically, if E is in Kev:

$$\exp(-2\pi\eta) = \exp(-31.285\, Z_1 Z_2\, M^{1/2}/E^{1/2}) \tag{12}$$

Away from the resonances the Breit-Wigner formula is no more accurate. However, if again E << B, the experimental cross sections do still exhibit the Gamow factor energy dependence. It is customary to then use the so-called astrophysical S factor defined as:

$$\sigma = \frac{S}{E} e^{-2\pi\eta} \tag{13}$$

The S factor is then almost energy independent. If we introduce Equation 13 into Equation 3 we see that the integrand has a peak (the Gamow peak) which represents the best candidates for nuclear reactions. The center, E_o, and the width ΔE_o of the peak are both increasing functions of the temperature. Numerical values for different frequently used temperature units are given in Table 5.

The expression $<\sigma v>$ can be approximately integrated by a technique described in Salpeter (1952). The result, usually called the non-resonant (n.r.) approximation, is:

$$\log_{10} \langle \sigma v \rangle_{n.r.} = -15.4 - \log(M Z_1 Z_2) + \log S + 2 \log \tau - 0.434 \tau \quad (14)$$

where M is in a.m.u., and τ, a dimensionless parameter is given by: $\tau = 3E_o/kT$. (See Table 5.) In many cases the factor S was experimentally found to be slightly energy dependent. In such cases, we use the two first terms of a series expansion:

$$S(E) = S(0) + E\,(dS/dE) \quad (15)$$

Various workers have analyzed their data to obtain by

extrapolation the value of S(0) at zero energy, and an average value <dS/dE> at low energies.

In these cases we use in Equation 14 the value of S at the Gamow peak (S_{eff}):

$$S_{eff}(T) = S(0)g(T) = S(0)\left[1 + \frac{5}{12\tau} + \frac{\langle dS/dE \rangle}{S(0)}\left(E_0(T) + \frac{35}{36}kT\right)\right] \quad (16)$$

(the term ($5/12\tau$) is actually a correction term to the integral itself.)

For convenience in tabulation we also define:

$$g(T) = [1 + UT^{1/3} + VT^{2/3} + WT] \quad (17)$$

In most instances we shall characterize a non-resonant reaction by giving its ($p_{2,1}/\rho X_1$) (See Equation 4.) We shall write it as:

$$\frac{p_{2,1}}{\rho X_1} = A f_{2,1}\, g_{2,1}\, e^{-B/T^{1/3}}/T^{2/3} \quad (18)$$

A is a numerical constant (to be gotten from Equation 14), $f_{2,1}$ is the electron screening factor (to be discussed later); $g_{2,1}$ is defined in Equation 16 and $B = \tau T^{1/3}$. From Equation 7 or 8, we can obtain ($\mathcal{E}$), the energy generation rate for a given reaction. We shall also introduce n, the logarithmic derivative of $\mathcal{E}$ with respect to T:

$$n \equiv \frac{T}{\mathcal{E}} \frac{d\mathcal{E}}{dT} \tag{19}$$

In certain cases the "non-resonant" contribution from a given resonance can be approximated by evaluating its Breit-Wigner cross section at the Gamow peak (E_o). Comparing Equations 9, 11 and 13, we get an effective S factor given by:

$$S_{BW} = (\pi \lambda^2 \times E)(\omega \xi_\ell^2 \gamma^2 \Gamma_{3,4}) \Big/ \left[\frac{\Gamma^2(E_o)}{4} + (E_o - E_r)^2 \right] \tag{20}$$

Experimental determination of $\Gamma_{1,2}$ at the resonances yields immediately the value of $[\gamma^2 \xi_\ell^2]$. If no experimental results are available one must guess the value of R, the nuclear radius of interaction, to be used in computation of ξ_ℓ^2 and of $\theta_{1,2}^2$. The uncertainty in $\theta_{1,2}^2$ usually brings the biggest uncertainty in the rate.

For the later stages of stellar evolution one has to deal with particles having energies approaching the Coulomb barrier energies. In such cases one has to include an extra term in the expansion of the Coulomb wave function.

To take into account this modification we shall redefine and prime some of the expressions used previously. First we want to extract from some of the "constants" the energy

Table 5

Useful Parameters for Computation of Thermonuclear Reaction Rates

	Kev	Mev
$2\pi\eta E^{1/2}/(Z_1^2 Z_2^2 M)^{1/2}$	3.1285×10^{1}	9.8935×10^{-1}
$\frac{4^{3/2}}{6\eta^2}\left(\frac{MR^3}{Z_1 Z_2}\right)^{-1/2} E^{-1}$	1.2150×10^{-4}	1.2150×10^{-1}

	T_6	T_8	T_9
$E_0/T^{2/3}(Z_1^2 Z_2^2 M)^{1/3}$ (kev)	1.22	26.3	122
$\Delta E_0/T^{5/6}(Z_1^2 Z_2^2 M)^{1/6}$ (Kev)	.75	35	237
$\tau\,(Z_1^2 Z_2^2 M)^{-1/3} T^{1/3}$	4.2483×10^{1}	9.1528	4.2483
$\frac{\epsilon}{\left(\frac{MR^3}{Z_1 Z_2}\right)^{1/2} T}$	1.05×10^{-5}	1.05×10^{-3}	1.05×10^{-2}
kT (kev)	$8.6164 \times 10^{-2} T_6$	$8.6164 T_8$	$8.6164 \times 10^{1} T_9$

dependence inflicted on them by the increased bombarding energies. We define:

$$\xi_\ell'^2 = \xi_\ell^2 e^{y^{3/2}/6\eta^2} = \left(\frac{G_0}{G_\ell}\right)^2 2y^{1/2} e^{4y^{1/2}} \tag{21}$$

$$S' = Se^{(y^{3/2}/6\eta^2)} = \sigma E \exp\left(2\pi\eta + y^{3/2}/6\eta^2\right) \tag{22}$$

For numerical values of $y^{3/2}/6\eta^2$, see Table 5.

Then $\xi_\ell'^2$ and S' are almost energy independent and we have:

$$\Gamma_{1,2} = \gamma^* \exp\left(-2\pi\eta - y^{3/2}/6\eta^2\right)\xi_\ell'^2 \tag{23}$$

The effect of this term will be to "reduce" the value of the Gamow energy to $E_0' = E_0\left(1 + \frac{2\epsilon}{3}\right)$; $\epsilon \simeq (y^{3/2}/6\eta^2)kT$ the Gamow width to $\Delta E_0' = \Delta E_0\left(1 - \frac{5\epsilon}{6}\right)$. Finally we replace τ , such as in Equation 14 by $\tau' = (1+\epsilon/3)\tau$ to obtain the correct rate. Numerical values of ϵ are given in Table 5.

Lastly, when some resonance falls in (or close to) the Gamow peak, the term $<\sigma v>$ comes dominantly from this resonance, and we have (the so-called resonant contribution):

$$\frac{P_{1,2}}{\rho Y_1} = \frac{\omega N}{A_1} e^{-E_r/kT} \left(\frac{2\pi\hbar^2}{MKT}\right)^2 \frac{\Gamma_{1,2}\,\Gamma_{3,4}}{\Gamma\hbar} \quad \text{(in c.g.s. units)} \tag{24}$$

This yields (in units of T_8):

$$\log_{10} \langle \sigma v \rangle_r = -11.09 + \log \omega \left(\frac{\Gamma_{1,2} \Gamma_{3,4}}{\Gamma} \right) - \frac{3}{2} \log M - \frac{3}{2} \log T_8 - 50.4\, E_r / T_8 \qquad (24a)$$

with Γ's and E_r in Mev.

2.3 Electron Screening Factors

Electron screening factors have been first calculated by Schatzman (1948). The limiting cases have been considered by Salpeter (1954). He has shown that the effective increase in the nuclear reaction rate due to electron screening can be described in terms of a potential energy term U_o. He gives recipes to evaluate this term and shows that the correct rate is obtained by multiplying the unscreened rate by $\exp(-U_o/kT)$. (U_o is always a negative quantity.)

To evaluate U_o one must first find if the screening is weak or strong, i.e. if the electrostatic interaction energy between neighboring nuclei is small or large compared to the thermal energy. Intermediate cases require special attention. If the weak screening condition applies one obtains:

$$-U_o/KT = 0.188\, Z_1 Z_2 \mathcal{S} \rho^{1/2} / T_6^{3/2} \tag{25}$$

where Z_1, Z_2 are the charges of the two particles involved ($Z_1 \geq Z_2$), ρ is the density in grams and $\mathcal{S}$ is defined by:

$$\mathcal{J} = \left\{ \sum_i \frac{X_i (\eta_i + \eta_i^2)}{A_i} \right\}^{1/2} \tag{26}$$

where η_i are the charges of the various nuclei in the stellar core with the sum over i referring to a sum over all the constituents of the gas.

The criterion for the validity of the weak screening approximation can be written as $(-U_o/kT)\ (\eta/Z_2) < 1$, where η is the average charge of the gas. If the electron gas is partly degenerate one has to redefine $\mathcal{J}$:

$$\mathcal{J}_{deg.} = \left\{ \sum X_i \frac{\eta_i^2}{A_i} + (f'/f) \sum X_i \frac{\eta_i}{A_i} \right\}^{1/2} \tag{27}$$

In Figure 5 the function $f'(\eta)/f(\eta)$ is plotted as a function of D, the degeneracy parameter (the ratio of the Fermi energy to the mean thermal energy). The value of D is given by:

$D = 0.3\ (\frac{\rho}{\mu})^{2/3}\ \frac{1}{T_6}$ for non-relativistic cases: $(\frac{\rho}{\mu}) << 10^6$

and $D = \frac{60}{T_6}\ (\frac{\rho}{\mu})^{1/3}$ for relativistic cases; $(\frac{\rho}{\mu}) >> 10^6$

μ is the number of nucleons per electron in the gas,

$$\mu = (\Sigma X_i \frac{Z_i}{A_i})^{-1}$$

If the condition for weak screening is violated, one computes the strong screening potential by the formula:

$$\frac{-U_o}{kT} = 0.20\left[(Z_1+Z_2)^{5/3} - Z_1^{5/3} - Z_2^{5/3}\right]\left(\frac{\rho}{\mu}\right)^{1/3}\frac{1}{T_6} \tag{28}$$

This formula is valid if 1) $Z_1 << \rho^{1/3}$

and 2) $\frac{0.23Z_1^{2/3}}{T_6}\gamma\left(\frac{\rho}{\mu}\right)^{1/3} >> 1$

If these two conditions do not apply (intermediate screening) one has to consider more involved techniques. However, a graphic interpolation from weak screening to the strong screening may yield a first estimate of the correct value.

The results of Salpeter are based on the assumption that all atoms in the gas are completely ionized. To test this assumption, we define an ionization parameter (I_z) for a given atom of charge Z as the ratio of the ionization potential of a K-shell electron in a hydrogen-like atom to the mean thermal energy. The assumption is valid if:

$$I_z = \frac{Ze^2}{2a_{oz}}\frac{1}{(kT)} = \frac{0.16Z^2}{T_6} << 1 \tag{29}$$

where a_{oz} is the Bohr radius for an atom of charge Z. This parameter is usually much smaller than one. One notable exception is the CNO cycle at low temperatures. There one would have to use a more accurate formalism

Figure 5

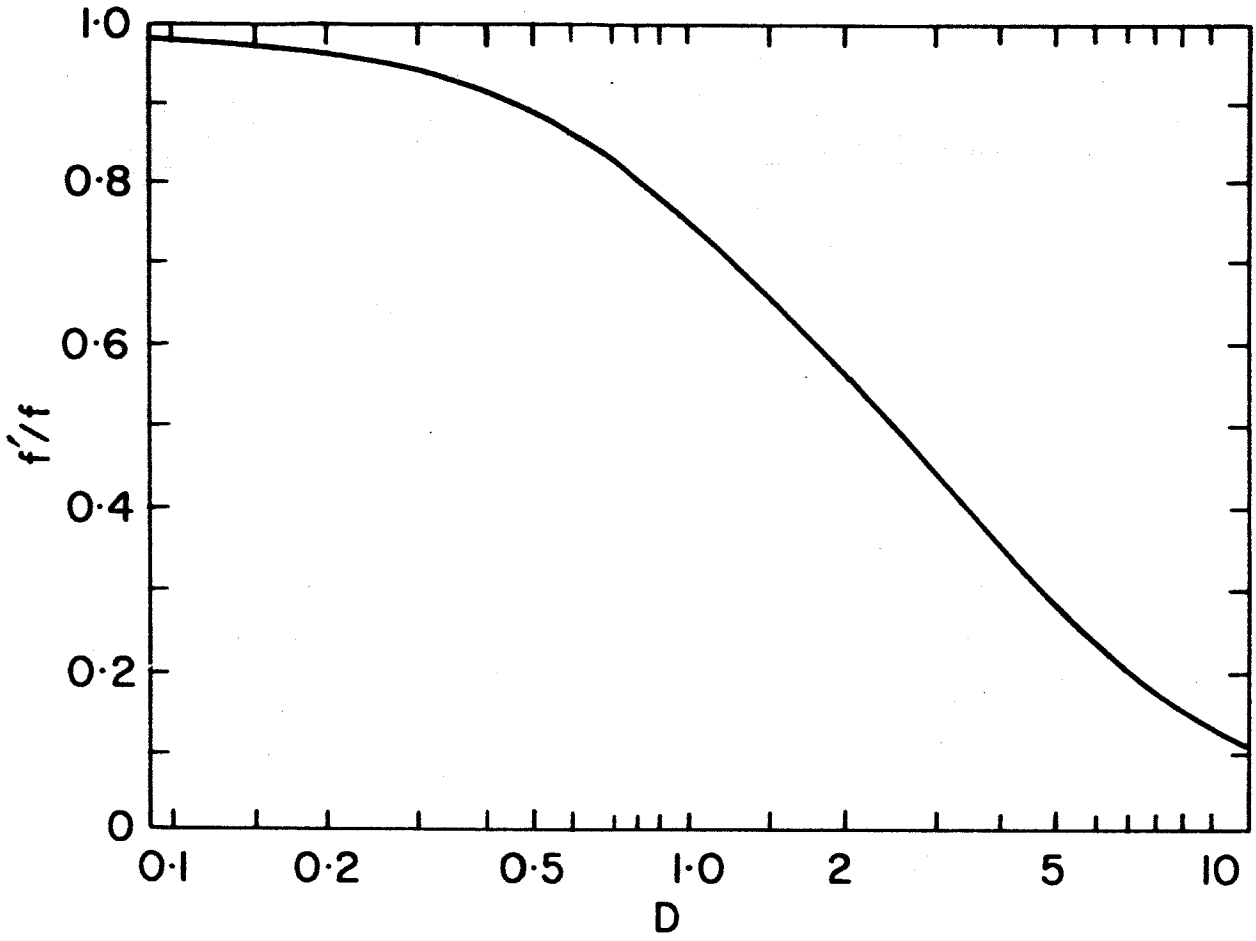

Plot of the Electron Screening Parameter as a Function of D, the Degeneracy Parameter.

such as given in Schatzman (1948) or Keller (1953). However, it usually turns out that in such cases the CNO cycle is not the dominant mode of energy production. The formalism of Salpeter, while somewhat inaccurate still remains then perfectly adequate.

3. Hydrogen Burning Stage

In the stars the fusion of four protons into one helium nucleus is accomplished through two important mechanisms: the proton-proton chain and the carbon-nitrogen cycle. In the proton-proton chain one starts by adding three protons together to form a helium-3 nucleus. This nucleus then reacts with another helium-3 or with an already present helium-4 nucleus to eventually become a helium-4 nucleus. The detailed possible mechanisms are given in Table 1.

The rate of energy generation is governed mostly by the rate of the proton-proton reaction. It is also governed by the number of subsequent reactions which can become in equilibrium with this reaction. One should notice here that the PPI requires for its completion two helium-3 nuclei while PPII and PPIII require only one (the helium-4 used in these models acts only as a catalyst). Hence the <u>rate</u> of energy generation is twice as large for these modes. In that sense the energy generation rate depends also on the abundance of helium-4.

In the carbon-nitrogen cycle (also referred to as PPIV) four protons are successively added to a nucleus of C^{12}. With the addition of the last proton the nucleus breaks into C^{12} and He^4. Sometimes the break-up does not occur and O^{16} is formed. This nucleus then accepts two more protons and breaks into N^{14} and He^4. This is called the CNO bi-cycle.

We shall discuss in detail the set of nuclear reactions involved in the hydrogen burning. Recent improvements in the experimental techniques as well as in the theoretical understanding allows one to compute the rates with fair confidence and even permits the addition of some refinements.

The set of reactions considered are listed in Tables 6 and 7 together with some of the relevant nuclear parameters. It appears fairly certain that with the exception of the O^{17} (H^1, He^4) N^{14}, the reactions involved in the proton-proton branches or the CNO cycle are all non-resonant, although the presence of resonances in the stellar energy range cannot yet be completely ruled out. To discuss these reaction rates it is convenient to use T_6 as a unit of temperature. The results will all be given in terms of this unit. The results concerning the CNO bi-cycle came mostly from the work of

Caughlan and Fowler (1962).

In the diagram we have indicated the position and width of the Gamow peak at $T_6 = 100$, which is certainly an upper limit of the temperature of the hydrogen burning stage.

TABLE 1

THE PROTON-PROTON CHAIN

$$H^1 + H^1 \rightarrow H^2 + e^+ + \nu$$

PP I $$H^2 + H^1 \rightarrow He^3 + \gamma$$

$$He^3 + He^3 \rightarrow He^4 + 2H^1$$

or

$$He^3 + He^4 \rightarrow Be^7 + \gamma$$

PP II

$$Be^7 + e^- \rightarrow Li^7 + \nu$$

$$Li^7 + H^1 \rightarrow Be^8 + \gamma$$

$$Be^8 \rightarrow 2He^4$$

or

$$Be^7 + H^1 \rightarrow B^8 + \gamma$$

PP III

$$B^8 \rightarrow Be^{8*} + e^+ + \nu$$

$$Be^{8*} \rightarrow 2He^4$$

Table 6

PARAMETERS FOR PROTON-PROTON REACTION

REACTION	REDUCED MASS $M = \frac{A_1 A_2}{A_1 + A_2}$ a.m.u.	$Z_1 Z_2 \sqrt{M}$	$\frac{E_o}{T_6^{2/3}} = 1.220 (Z_1^2 Z_2^2 M)^{1/3}$ (kev)	$\frac{\Delta E_o}{T_6^{5/6}} = 0.75 (Z_1^2 Z_2^2 M)^{1/6}$ (kev)
$H^1 + H^1 \rightarrow H^2 + e^+ + \nu$	0.5041 ± 0.0001	0.70998 ± 0.00009	0.971	0.67
$H^1 + H^2 \rightarrow He^3 + \gamma$	0.6719 ± 0.0001	0.81971 ± 0.00006	1.07	0.70
$He^3 + He^3 \rightarrow He^4 + 2H^1$	1.5085 ± 0.0001	4.9128 ± 0.0002	3.53	1.3
$He^3 + He^4 \rightarrow Be^7 + \gamma$	1.7205 ± 0.0001	5.2468 ± 0.0002	3.68	1.3
$Be^7 + e^- \rightarrow Li^7 + \nu$				
$Li^7 + H^1 \rightarrow He^4 + He^4$	0.8815 ± 0.0001	2.8167 ± 0.0002	2.43	1.1
$Be^7 + H^1 \rightarrow B^8 + \gamma$	0.8815 ± 0.0001	3.7556 ± 0.0003	2.95	1.2
$B^8 \rightarrow Be^8 + e^+ + \nu$				

REACTION	$B_6 = 42.483(Z_1^2 Z_2^2 M)^{1/3}$	$2\pi\eta E^{1/2}$(kev) = $31.285(Z_1^2 Z_2^2 M)^{1/2}$	Q value (kev) ($4H^1 \rightarrow He^4 \Rightarrow$ 26.730 Mev)	Neutrino E_{max} (kev) = ($\Delta m - 2m_e c^2$)
$H^1 + H^1 \rightarrow H^2 + e^+ + \nu$	33.810 ± 0.003	22.212 ± 0.003	1442.10 ± 0.20	420.16 ± 0.20
$H^1 + H^2 \rightarrow He^3 + \gamma$	37.210 ± 0.002	25.645 ± 0.003	5493.15 ± 0.16	
$He^3 + He^3 \rightarrow He^4 + 2H^1$	122.774 ± 0.004	153.70 ± 0.02	12859.31 ± 0.48	
$He^3 + He^4 \rightarrow Be^7 + \gamma$	128.277 ± 0.004	164.15 ± 0.02	1587.4 ± 1.2	
$Be^7 + e^- \rightarrow Li^7 + \nu$			860.7 ± 2.2	
$Li^7 + H^1 \rightarrow He^4 + He^4$	84.731 ± 0.004	88.121 ± 0.010	17346.5 ± 1.2	
$Be^7 + H^1 \rightarrow B^8 + \gamma$	102.645 ± 0.005	117.50 ± 0.01	133.1 ± 1.8	
$B^8 \rightarrow Be^8 + e^+ + \nu$			17980.0 ± 2.3	16958.1 ± 2.3

Table 6

REACTION	Average Neutrino Energy Loss (Mev)	S(0) (kev - barns)	<dS/dE> barns	A $\left(\frac{P}{\rho X_1} = Afg \exp(-B/T_6^{1/3}) T_6^{-2/3}\right)$
$H^1 + H^1 \rightarrow H^2 + e^+ + \nu$	0.263	$(3.36 \pm 0.4) \times 10^{-22}$	2.7×10^{-24}	$(3.3 \pm 0.4) \times 10^{-13}$
$H^1 + H^2 \rightarrow He^3 + \gamma$		$(2.5 \pm 0.4) \times 10^{-4}$	7.9×10^{-6}	$(2.2 \pm 0.4) \times 10^{5}$
$He^3 + He^3 \rightarrow He^4 + 2H^1$		1.2×10^{3}		$(P_{3,3}/\rho X_3)$ $(4.3) \times 10^{11}$
$He^3 + He^4 \rightarrow Be^7 + \gamma$		(0.47 ± 0.07)	-2.8×10^{-4}	$(P_{3,4}/\rho X_4)$ $(1.2 \pm 0.2) \times 10^{8}$
$Be^7 + e^- \rightarrow Li^7 + \nu$	0.80			
$Li^7 + H^1 \rightarrow He^4 + He^4$		(100 ± 25)		$(1.2 \pm 0.3) \times 10^{11}$
$Be^7 + H^1 \rightarrow B^8 + \gamma$		$(2 \pm 1) \times 10^{-2}$		$(2.6 \pm 1.3) \times 10^{7}$
$B^8 \rightarrow Be^8 + e^+ + \nu$	7.2			

Table 6

Table 6

$$g = (1 + UT_6^{1/3} + VT_6^{2/3} + WT_6)$$

REACTION	U $U = 5/12B$	V $V = \frac{E_o}{T_6^{2/3}} \frac{\langle dS/dE \rangle}{S(0)}$	W $W = \frac{35}{36} \frac{\langle dS/dE \rangle}{S(0)} k$	f Electron Screening Factor (Weak)
$H^1 + H^1 \rightarrow H^2 + e^+ + \nu$	1.23×10^{-2}	7.80×10^{-3}	6.73×10^{-4}	$(1 + 0.25\rho^{1/2}/T_6^{3/2})$
$H^1 + H^2 \rightarrow He^3 + \gamma$	1.12×10^{-2}	3.12×10^{-2}	2.45×10^{-3}	$(1 + 0.25\rho^{1/2}/T_6^{3/2})$
$He^3 + He^3 \rightarrow He^4 + 2H^1$	3.39×10^{-3}			$(1 + 1.0\rho^{1/2}/T_6^{3/2})$
$He^3 + He^4 \rightarrow Be^7 + \gamma$	3.25×10^{-3}	-2.15×10^{-3}	-4.90×10^{-5}	$(1 + 1.0\rho^{1/2}/T_6^{3/2})$
$Be^7 + e^- \rightarrow Li^7 + \nu$				
$Li^7 + H^1 \rightarrow He^4 + He^4$	4.92×10^{-3}			$(1 + 0.75\rho^{1/2}/T_6^{3/2})$
$Be^7 + H^1 \rightarrow B^8 + \gamma$	4.06×10^{-3}			$(1 + 1.0\rho^{1/2}/T_6^{3/2})$
$B^8 \rightarrow Be^8 + e^+ + \nu$				

3.1 Electron Screening for Hydrogen Burning Cases

For stars on the main sequence, the factor $\rho^{1/2}/T_6^{3/2}$ varies from 0.02 for $M = 10\ M_\odot$ to 2.4 for $M = 0.1\ M_\odot$ (Kumar 1962). For $M > 0.6\ M_\odot$, D is less than 0.6, then from Figure 5, $f'/f \simeq 1$. In this case $\mathcal{J}$ is $\simeq 1.4(1 - 0.13\,\mathcal{X}_4)$. (Again $\mathcal{X}_4$ is the concentration by weight of the helium in the gas.) $(-U_o/kT)$ becomes $0.27(Z_1Z_2)(1 - 0.13\,\mathcal{X}_4)\,\rho^{1/2}/T_6^{3/2}$. The product Z_1Z_2 is never larger than 8, hence all main sequence stars with $M > 0.6\ M_\odot$ are eligible for the weak screening formula.

The maximum value of $0.27Z_1Z_2\,\rho^{1/2}/T_6^{3/2}$ is about 0.40 when the proton-proton branch is dominant, and even less when the CNO cycle is dominant. Hence, in view of the approximation already used in deriving these formulae one may well put $\mathcal{X}_4 = 0.5$ everywhere and expand the exponential:

$$\exp(-U_o/kT) = \left[1 + 0.25Z_1Z_2\ \frac{\rho^{1/2}}{T_6^{3/2}}\right] \equiv f\ .$$

In Tables 6 and 7 we shall list the value of f, assuming that the weak screening approximation applies. As

discussed before it should apply inside all the main sequence stars with $M > 0.6\ M_{\odot}$. In hydrogen burning shells the electron screening is usually negligible. For main sequence stars with $M < 0.6\ M_{\odot}$, the strong screening approximation or some accurate estimates should be used.

The case of CN burning stars of low temperature has been discussed previously.

3.2 Hydrogen Thermonuclear Reactions (Proton-Proton)

$$H^1 + H^1 \rightarrow H^2 + e^+ + \nu$$

Since there is no bound system to be formed with two protons, this reaction can occur only if the protons are brought together by a nuclear collision. During the short time of the encounter, one of the protons has a chance to beta-decay thereby becoming a neutron, a positive electron and a neutrino. The neutron can then be captured by another proton to form a deuteron. This reaction has never been observed in the lab. Its extremely small calculated cross section (10^{-23} barns) explains this fact and suggests that it might never be detected directly. However, the present state of nuclear physics and of weak interaction theories makes its existence practically compelling.

The computation of the cross section for this reaction requires knowledge of the Gamow-Teller beta-decay coupling constant.

The decay rate is given by

$$\beta = 4\left(\frac{G^2}{2\pi^3}\right)\left(\frac{m_e c^2}{\hbar}\right) f(w)\left|\phi_i \phi_f \, d\tau\right|^2$$

where G is the interaction coupling constant which will

be explained below, w is the maximum energy of the electron (or positron) in units of $m_e c^2$, and f(w) is computed in Fermi's theory. ϕ_i is the initial wave function, and ϕ_f is the final wave function. The uncertainties in β come from two sources; the uncertainty due to a lack of knowledge of the initial and the final state, wave functions, and a lack of knowledge of the coupling constant G.

In most literature, instead of G, g_β is quoted. g_β is defined as

$$g_\beta = 4\left(\frac{G^2}{2\pi^3}\right)\left(\frac{m_e c^2}{\hbar}\right) \tag{29a}$$

and $$G = g m_p^2 \left(\frac{m_e}{m_p}\right)^2 \left(\frac{g_{GT}}{g_F}\right)$$

Experimentally $g(m_p)^2 = (1.01 \pm 0.01) \times 10^{-5}$. g_{GT} and g_F are the Gamow-Teller part and the Fermi part of the weak coupling constants.

We write $a = \frac{g_{GT}}{g_F}$. Numerically,

$$g_\beta = 4.49 \times 10^{-4} a^2$$

To determine a, one may use the experimentally determined half-life of the neutron and the decay of O^{14} nuclei.

Wu (private communication) has determined

$$a^2 = 1.42 \pm 0.08$$

Hence

$$g_\beta = 6.36 \pm 0.36$$

Fowler has substantially revised the above data. The uncertainties in our knowledge of g_β is thus around 5%.

With this value of g_β, the S factor becomes $S(0) = 3.36 \pm 0.4 \times 10^{-22}$ Kev barns while $\langle \frac{dS}{dE} \rangle = 2.7 \times 10^{-24}$ barns (Chiu, private communication). $H^1 + H^2 \rightarrow He^3 + \gamma$

This reaction has recently been analyzed by Griffiths, Lal and Scarfe (Griffiths, 1961) down to energies of 16 Kev (24 Kev lab). The cross section can be accounted for in terms of a direct capture process. Both the S and P wave contribute significantly to the capture rate, even at the lowest energies. The reaction can be characterized by the following parameters:

$$S(0) = 2.7 \times 10^{-4} \text{ Kev barns}$$

$$\langle dS/dE \rangle = 0.067 \times 10^{-4} \text{ barns}$$

Note: In a later report by the same authors (to be published) the values $S(0) = (2.5 \pm 0.4) \times 10^{-4}$ Kev barns and $\langle dS/dE \rangle = 0.079 \times 10^{-4}$ barns are given.

It is not easy to determine the margin of uncertainty on these results. According to one author (Dr. Griffiths, private communication), it may be as large as 50%, but probably somewhat smaller. It is worthwhile noting that this value of S is some three or four times larger than the values used previously. The ratio of H^2/H^1 in stars should consequently be decreased by the same amount.

$H_e^3 + He^3 \rightarrow He^4 + 2H^1$

The reaction has been studied in the laboratory (Good, Kunz and Moak, 1954) at energies from 50 to 400 Kev (c.m.). The cross section follows a simple Gamow-type curve up to $E \simeq 175$ Kev. The experimenters find that at E = 100 Kev, the cross section is at least 2.5 μ b. From this one gets that the S(0) factor is larger than 1.2×10^3 Kev barn. Dr. Good (private communication) believes that this number should be at the same time a good estimate and a lower limit. He sets the upper limit as 2.4×10^3 Kev barns, although such a high value of S appears very unlikely. The experiments do not allow a determination of $\langle dS/dE \rangle$.

Figure 6

Energy Diagram of Be^7

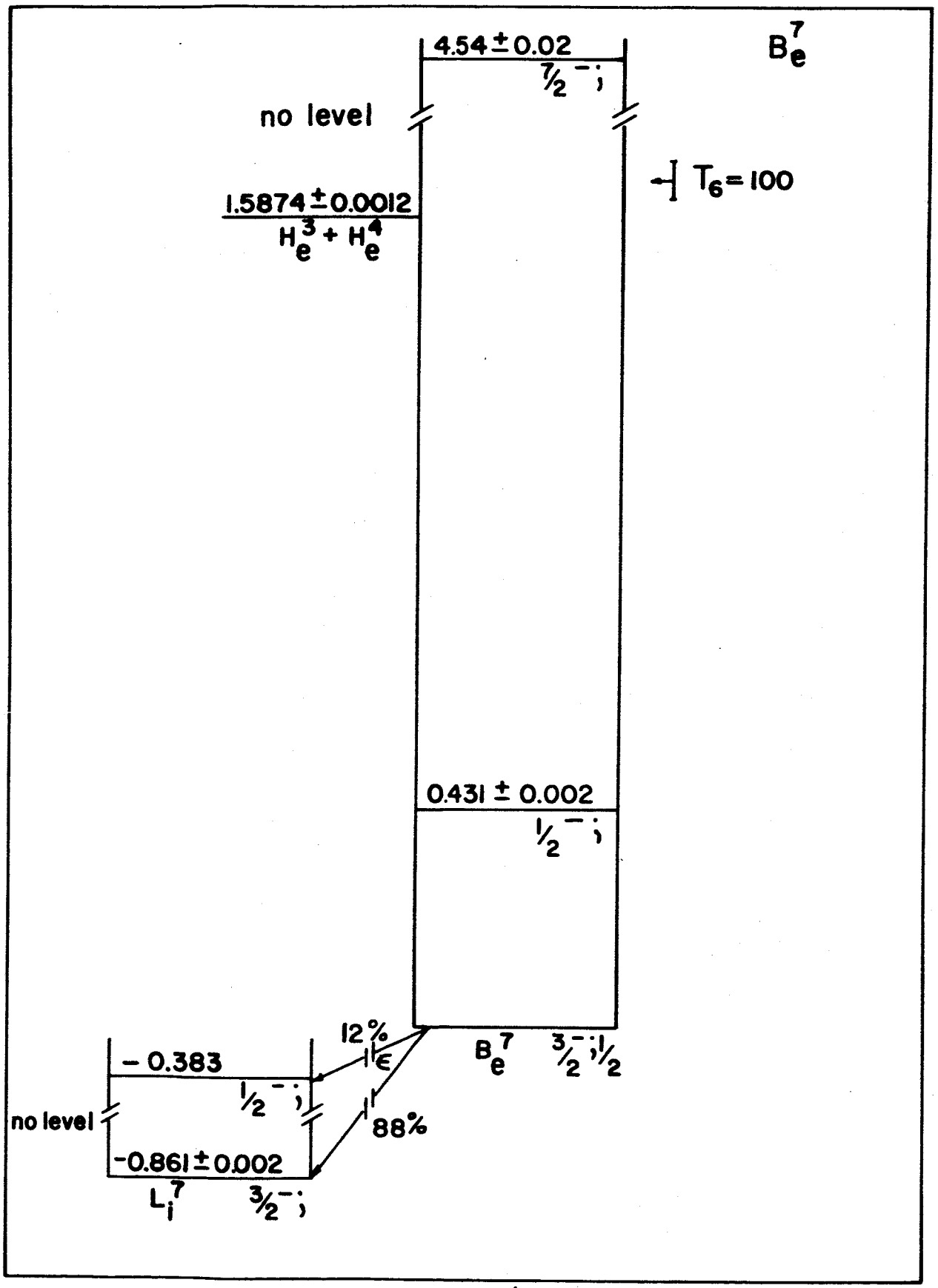

$He^3 + He^4 \rightarrow Be^7 + \gamma$

The importance of this reaction for stellar energy sources has been first pointed out by Fowler (1951) and Schatzman (1951). Measurements have been made by Holmgren and Johnston (Holmgren 1959) at $E_{c.m.}$ = 206, 309 and 404 Kev. From the energy diagram (Figure 6) the process is clearly non-resonant. In fact, it shows the characteristics of a direct capture process (Christy and Duck 1961). Consequently the experimental curve was simply fitted by a Gamow-type curve. According to Dr. Holmgren (private communication) the best experimental value of $S(0)_{c.m.}$ is 1.0 ± 0.4 Kev barn. The slope of S is negative and has a value $\langle dS/dE \rangle = -7 \times 10^{-4}$ barn.

Note: Parker and Kavanagh (to be published) have obtained: $S(0) = 0.47 \pm 0.07$ Kev barns and $\langle dS/dE \rangle = -2.8 \times 10^{-4}$ barns. These new values have been used in the present work.

Figure 7

Energy Diagram of Be^8

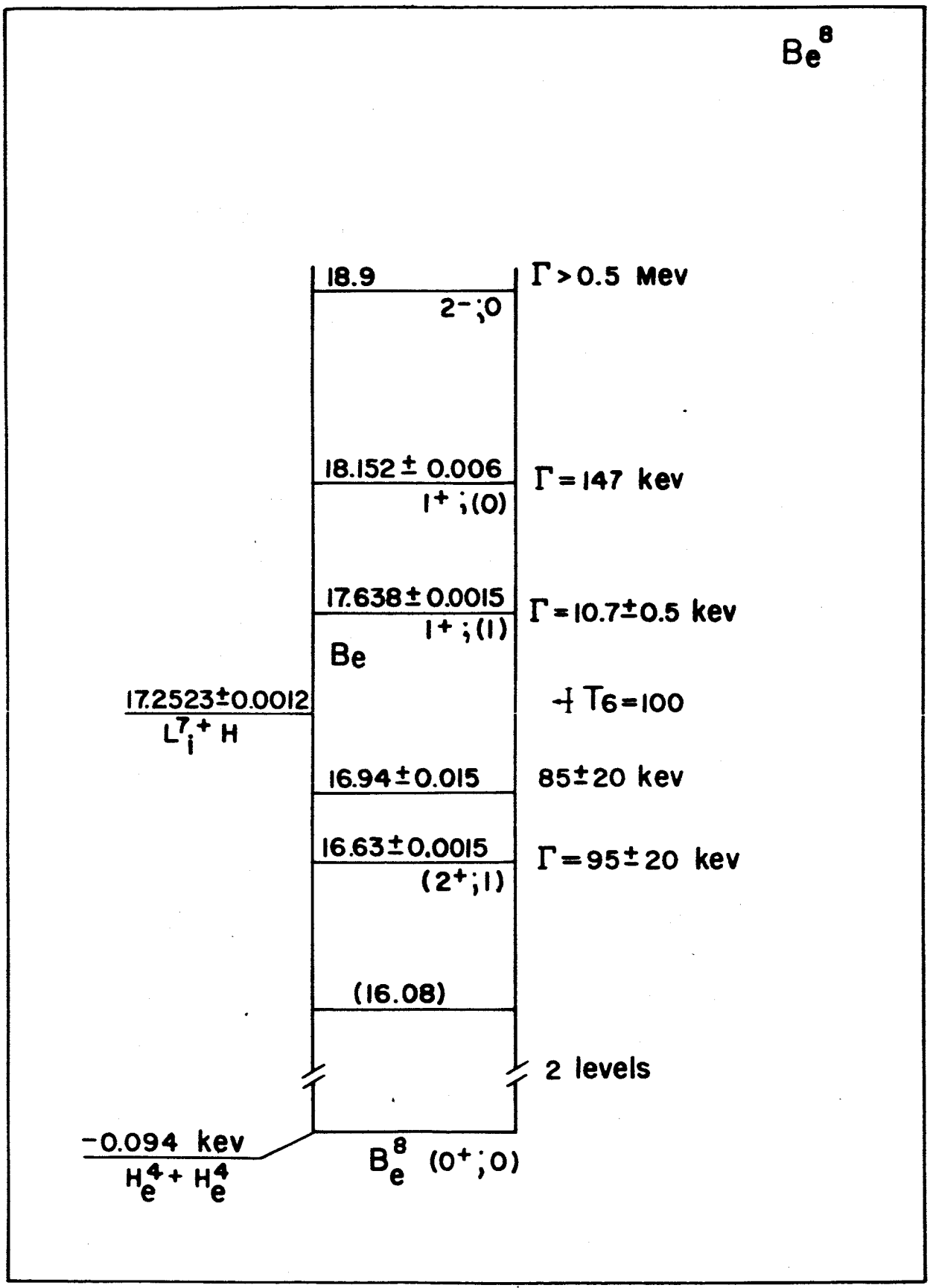

$$Li^7 + H^1 \rightarrow He^4 + He^4$$
$$\rightarrow Be^8 + \gamma$$

These two reactions have been studied in the range from 30 to 250 Kev (c.m.) (Sawyer and Phillips 1953). The first one is more than one hundred times faster than the second one everywhere in the range. Previous measurements had shown an isotropic yield at 100 Kev. Assuming isotropy all through the range; the cross sections were calculated from the 90° yield.

The product of the yield times the energy was plotted as a function of $E^{-1/2}$ in order to detect any energy dependence of the factor S (Figure 7). Within the experimental uncertainty no such dependence could be found.

The value of S_0 is 100 Kev barns with a probable error of 25%.

$$Be^7 + H^1 \rightarrow \gamma + B^8$$

The existence of an excited level at E_r = 600 Kev has been questioned. We have not included this level in

Figure 8

Energy Diagram of B^8

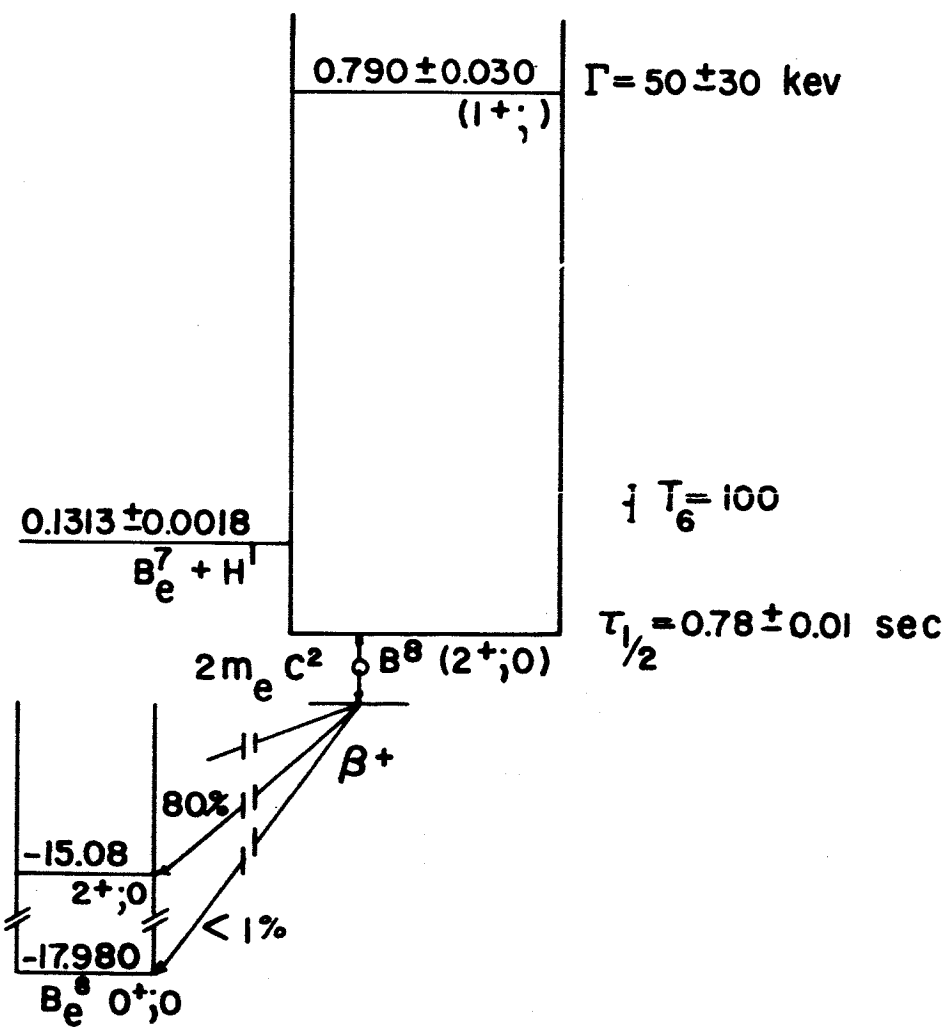

the diagram (Figure 8). This reaction has been described by Christy and Duck (Christy 1961) as a direct capture process. Its cross section has been measured by Kavanagh (1960) at $E_{c.m.}$ = 700 Kev, and 1225 Kev. He finds $\sigma(700)$ = (0.48 $\pm$ 0.18 μb) and $\sigma(1225)$ = (0.50 $\pm$ 0.20 μ b). Although the first measurement could be expected to feel the influence of the resonance at 790 Kev, Kavanagh estimates that the resonant contribution is probably negligible. He evaluates S_0 = 0.020 $\pm$ 0.010 Kev-b.

$Be^7 + e^- \rightarrow Li^7 + \nu$

The free electron gas in a stellar core is expected to initiate this reaction. An accurate calculation has been made by Bahcall (Bahcall 1962) taking into account the nucleus electron Coulomb interaction, relativistic and nuclear size corrections, the imperfect overlap between initial and final atomic states, and electron screening in bound decay. The probability of electron capture is given as:

$$P_{Be^7+e^-\rightarrow Li^7+\nu} = \frac{2.12 \times 10^{-9} \rho (1+X_1)}{T_6^{1/2}} \text{ sec}^{-1} \qquad (30)$$

within a few per cent. (X_1 is the fractional weight of hydrogen.)

TABLE 2

THE CNO BI-CYCLE

PP IV

$$C^{12} + H^{1} \rightarrow N^{13} + \gamma$$

$$N^{13} \rightarrow C^{13} + e^{+} + \nu$$

$$C^{13} + H^{1} \rightarrow N^{14} + \gamma$$

$$N^{14} + H^{1} \rightarrow O^{15} + \gamma$$

$$O^{15} \rightarrow N^{15} + e^{+} + \nu$$

$$N^{15} + H^{1} \rightarrow C^{12} + He^{4}$$

$$N^{15} + H^{1} \rightarrow O^{16} + \gamma$$

$$O^{16} + H^{1} \rightarrow F^{17} + \gamma$$

$$F^{17} \rightarrow O^{17} + e^{+} + \nu$$

$$O^{17} + H^{1} \rightarrow N^{14} + He^{4}$$

Figure 9

Energy Diagram of N^{13}

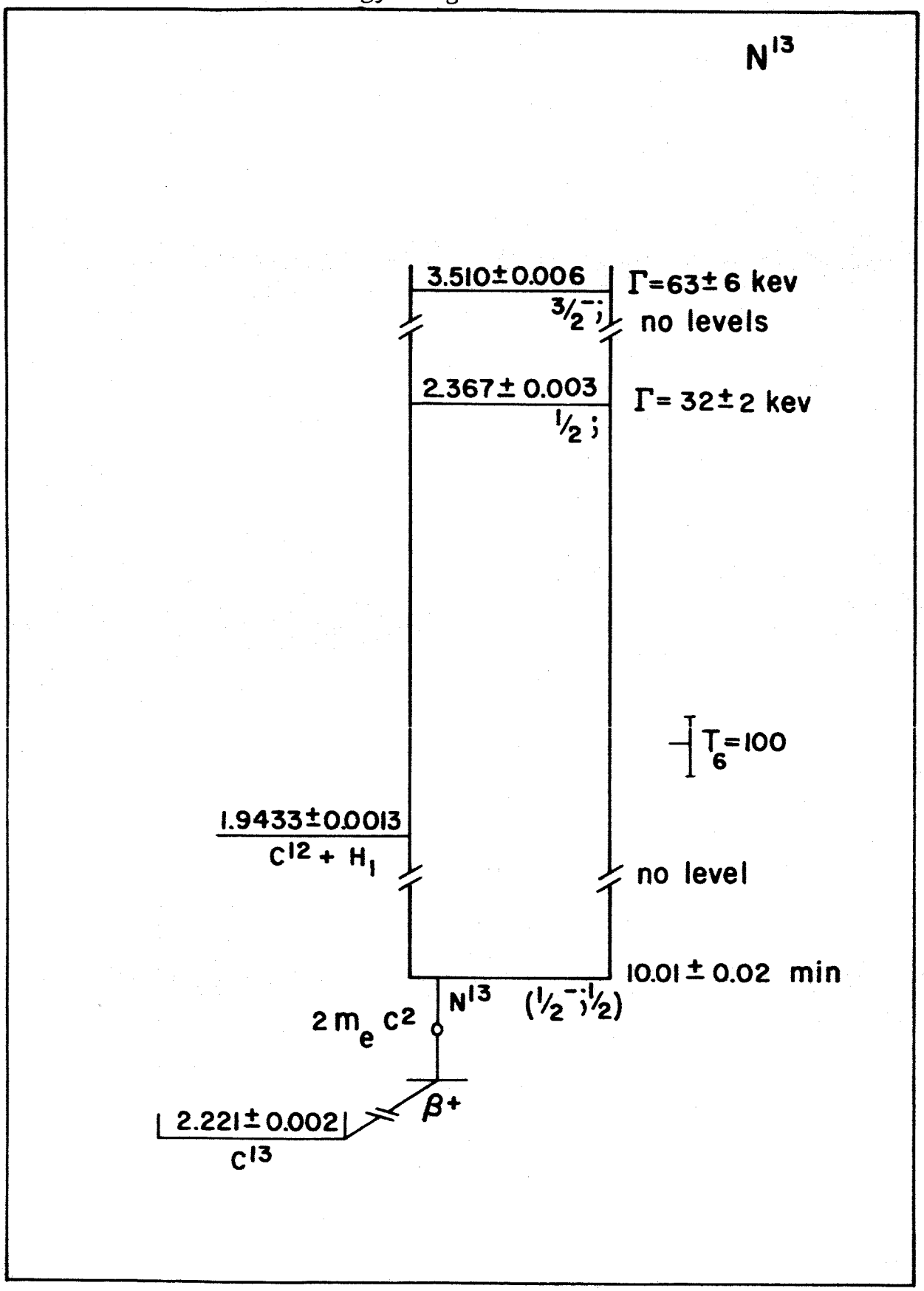

3.3 Hydrogen Thermonuclear Reactions (CNO)

$C^{12} + H^{1} \rightarrow N^{13} + \gamma$

Measurements have been made down to E_p = 80 Kev ($E_{c.m.}$ = 74 Kev) by Lamb and Hester, (Lamb 1957a) and others. A resonance at E_{lab} = 462 Kev (E^{+} = 2.367: γ_p^2 = 1695 Kev; $\omega\Gamma_\gamma$ = 1.52 ev) is the most important factor in the cross section. In the low energy part of the range one has to consider the interference of the resonance tail with the non-resonant rate (Figure 9).

The extrapolation to low energy has been made by Hebbard and Vogl (Hebbard, 1960) in the following way; first they have calculated the contribution of the resonance tail of the 462 Kev level from a single level Breit-Wigner formula, including all energy dependence. Then, they have divided the experimental cross section by this computed cross section. This way the non-resonant factor could be obtained and extrapolated to low energies. They find $S = 1.33 \pm 0.15$ Kev barn at $E_{c.m.}$ = 25 Kev.

The lifetime of N^{13} against photodisintegration is given by: $\log t = [119/T_8 - 15.3]$ sec. For $T_8 > 7.5$ it becomes shorter than the lifetime against beta disintegration.

Figure 4

Energy Diagram of N^{14}

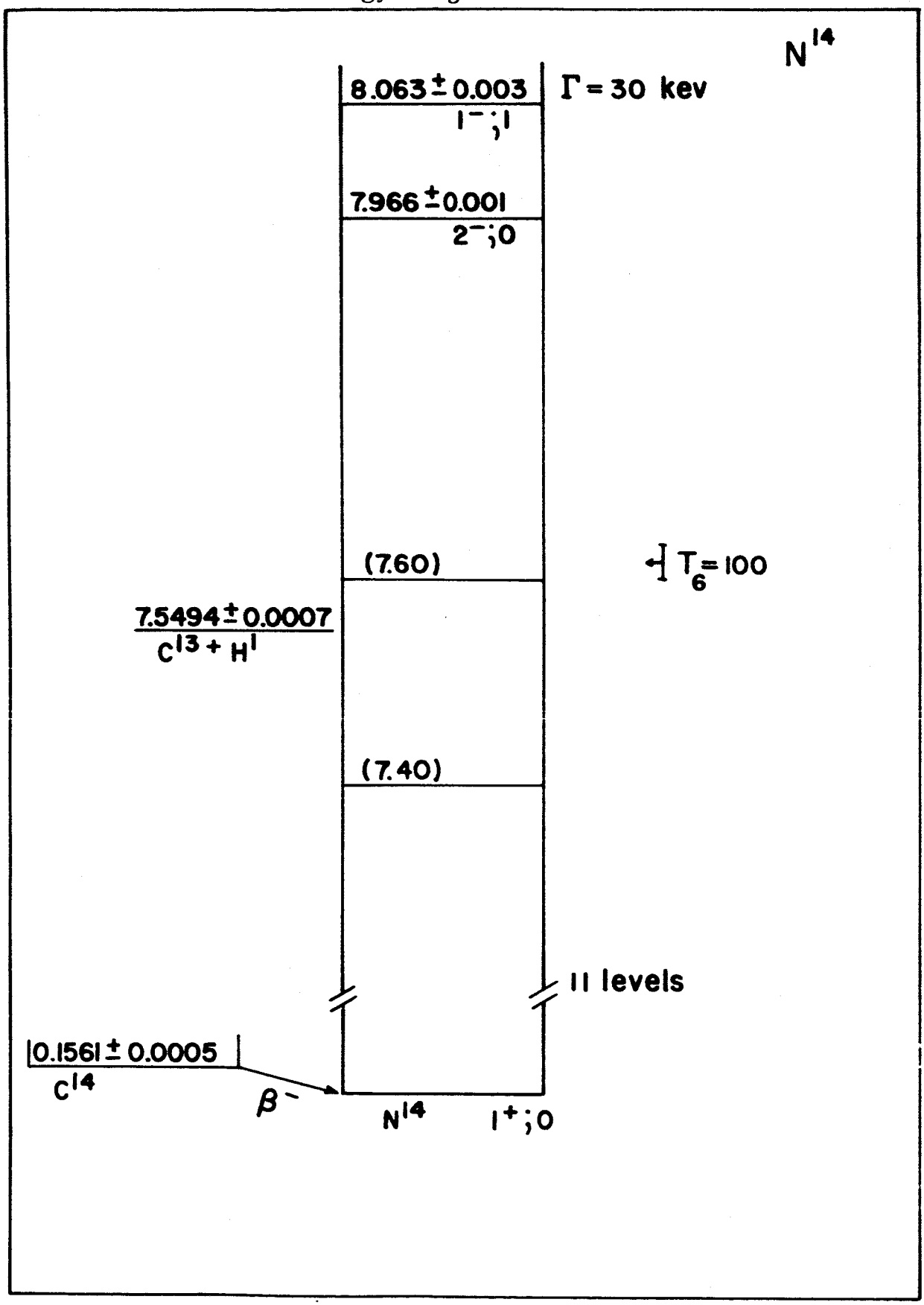

$C^{13} + H^{1} \rightarrow N^{14} + \gamma$

As seen from the diagram (Figure 4) the Q value for the $(C^{13} + H^{1})$ breakup is situated in a rather well populated area of the energy spectrum of N^{14}. For this reason, the extrapolation of the capture cross section to low energies has always been a difficult problem. The resonances are, in this area, separated by a few hundred Kev. One of these resonances may well be located in the region just above the breakup point. Because of the Coulomb effect it would be very difficult to analyze the contribution of this reaction to the thermonuclear reaction rate. An experiment on $N^{14}(H^{1}, H^{1})N^{14*}$ (Burge and Prowse (1956) had suggested in particular the presence of a level at 7.60 Mev). However, a recent examination of the energy level scheme of N^{14} through the $N^{15}(He^{3}, He^{4})N^{14*}$ (Clayton 1962) has failed to confirm the presence of such a level. Further, a rerun of the $N^{14}(H^{1}, H^{1})N^{14*}$ by Brown (private communication from Clayton), although not completely finished at the present time, does not exhibit the 7.60 Mev inelastic peak observed by Burge and Prowse. Hence it appears resonable to assume that the $N^{14}(H^{1}\gamma)O^{15}$ is a

Figure 10

Energy Diagram of O^{15}

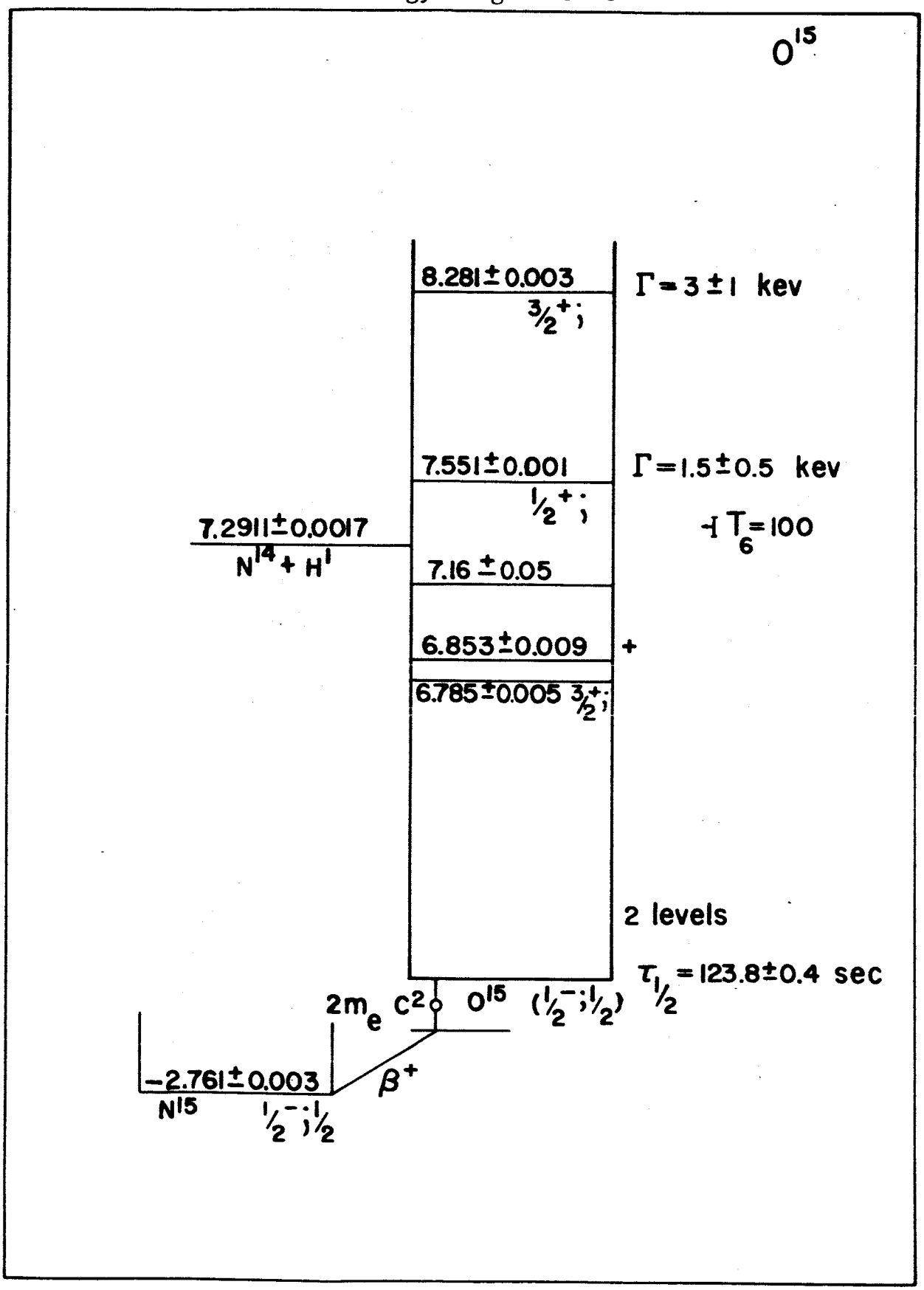

non-resonant reaction.

The physicists at the Kellogg Lab (Hebbard 1960) have recently measured the cross section for the radiative capture ($C^{13}(P,\gamma)N^{14}$) down to energies of 140 Kev.

The extrapolation to low energies has been done with a technique very similar to the technique used in the $C^{12}(H^1\gamma)N^{13}$. The non-resonant cross section is governed mostly by a resonance at E_p = 550 Kev ($E_{c.m.}$ = 510 Kev) with a reduced proton width γ_p^2 = 455 Kev. They find S = 6.0 $\pm$ 0.8 Kev barn at $E_{c.m.}$ = 25 Kev.

$N^{14} + H^1 \rightarrow O^{15} + \gamma$

The radiative capture cross section has been measured by Lamb and Hester (Lamb 1957b) in the range E_{lab} = 100 to 135 Kev. In this range they match the measured cross section with a value S = 2.7 $\pm$ 0.2 Kev barn. Another set of measurements by Pixley (yet unpublished) in the range E_{lab} = 450 to 650 Kev yields S = 1.76 Kev barn. Extrapolating from these two sets: S(0) = 3.12; $\langle dS/dE \rangle$ = -2.7×10^{-3} barns (Figure 10).

Figure 11

Energy Diagram of O^{16}

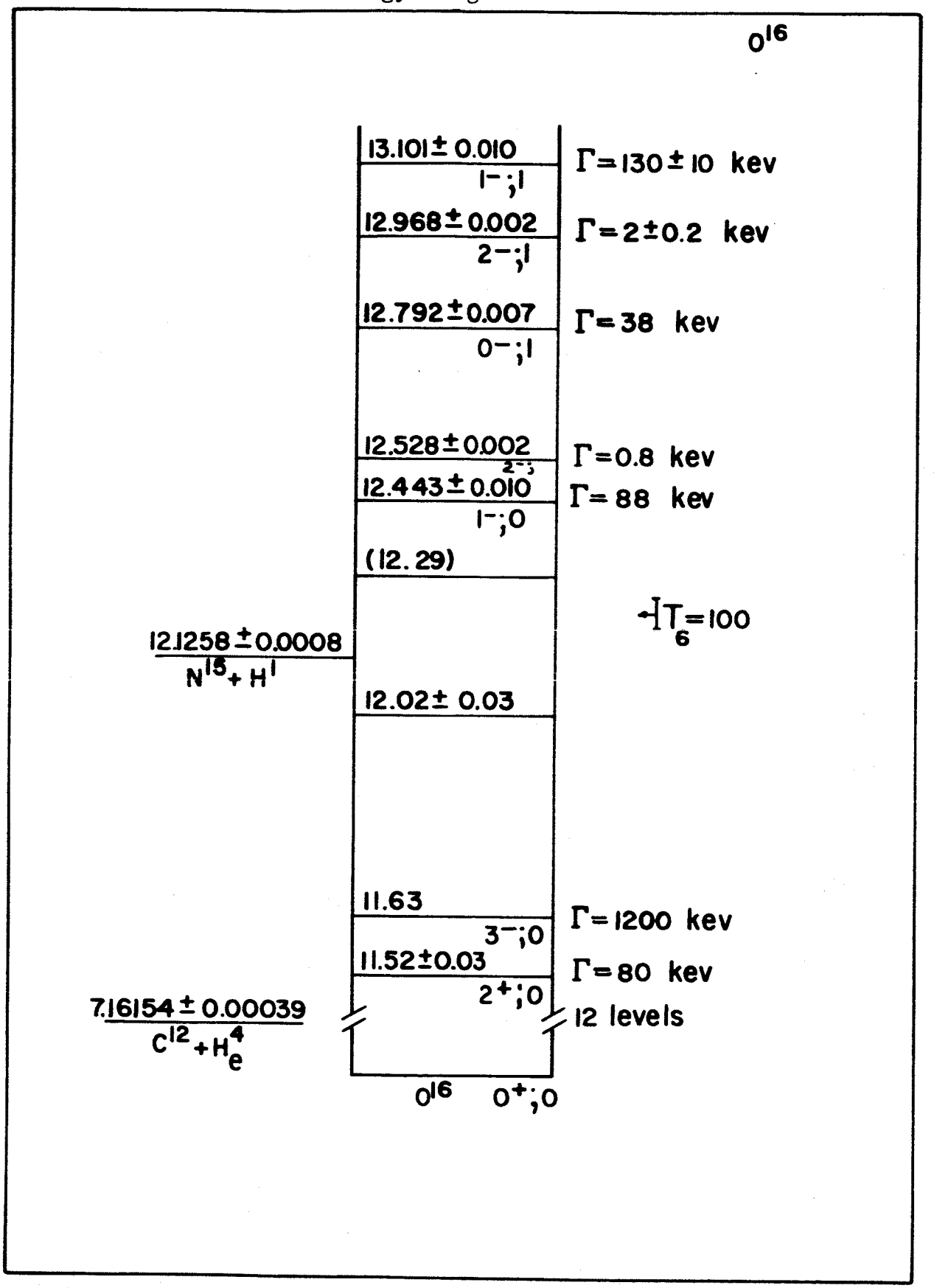

$$N^{15} + H^{1} \rightarrow C^{12} + He^{4}$$
$$\rightarrow O^{16} + \gamma$$

The cross section for the $N^{15} + H^{1} \rightarrow C^{12} + He^{4}$ has been measured down to E_{lab} = 100 Kev by Schardt, Fowler and Lauritsen, (Schardt 1952) and other workers. Two groups of alpha particles are observed, one group (α_0) accompanying C^{12} nuclei in the ground state; another group (α_1) with C^{12} in the first excited state (4.43 Mev). The yield for the first group is by far the largest at low energies, as can be expected from arguments concerning the Coulomb barrier. It is the only one that we shall consider.

As C^{12} and He^{4} are both spinless particles, they can only come from the state of so-called "natural" parity in O^{16} (0^+, 1^-, 2^+, 3^-, etc.). Indeed the cross section exhibits maxima at the 12.44, 13.10, and 13.25 Mev levels, which are respectively 1^-, 1^-, and 3^-. The $N^{15} + H^{1} \rightarrow O^{16} + \gamma$ has been measured by Hebbard (1960) to $E_{lab} \simeq 200$ Kev. The cross section is resonant at $E^* = 12.44$ and 13.10 (Figure 11).

Hebbard has analyzed the integrated cross sections with the multi-channel two level Breit Wigner expression. He included in his analysis the four channels of O^{16} breaking up

Figure 12

Energy Diagram of F^{17}

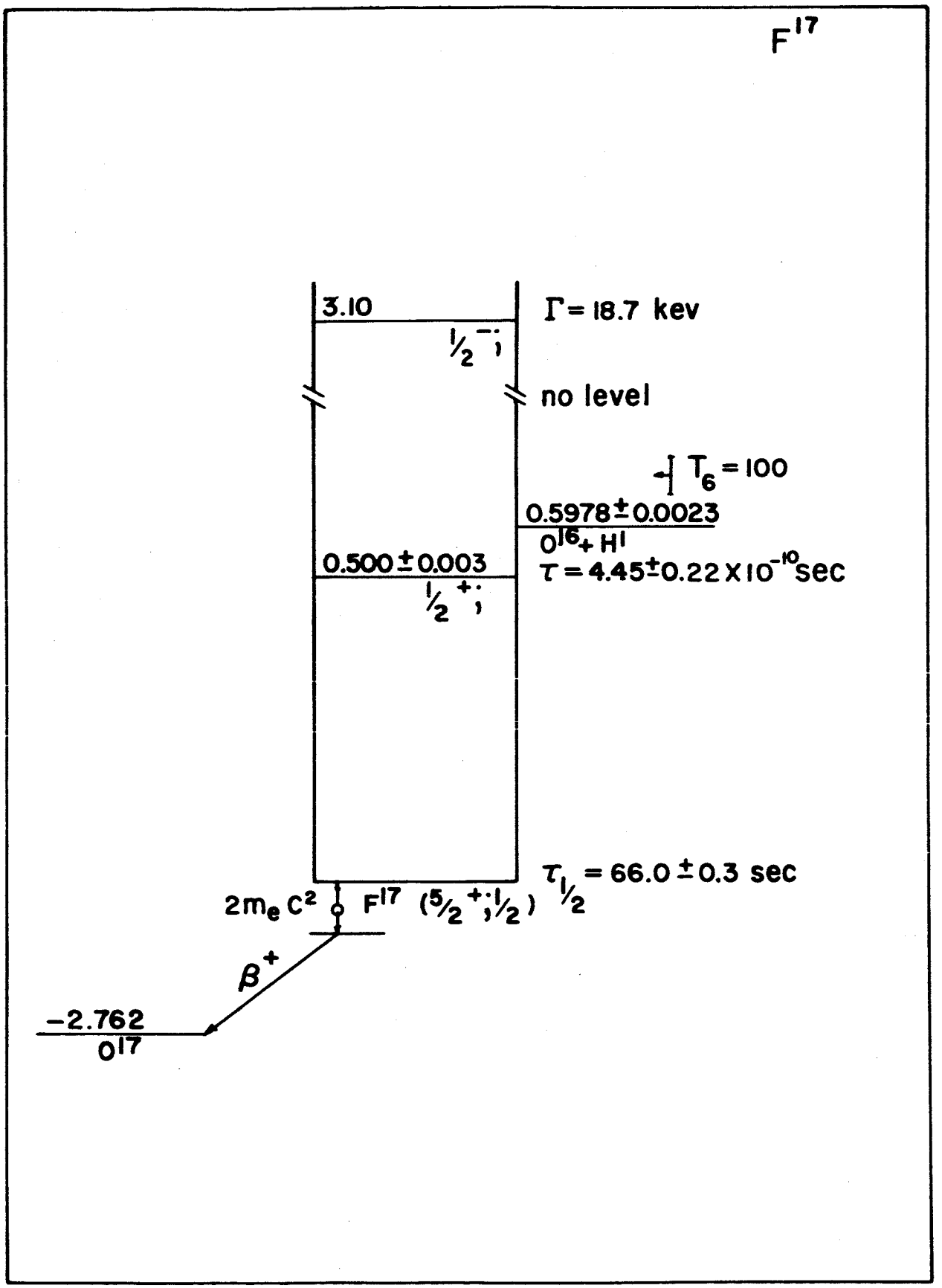

into $N^{15} + H^1$, $C^{12} + \alpha_0$, $C^{12} + \alpha_1$ and $O^{16} + \gamma$. The experimental points are resonably well fitted by his theoretical curve.

Extrapolation of the theoretical curve allows a determination of the S factor. He obtains: S = 32 Kev barns and 7.2×10^4 Kev barns respectively for $N^{15} + H^1 \rightarrow O^{16} + \gamma$ and $N^{15} + H^1 \rightarrow C^{12} + He^4$, at E = 25 Kev.

$O^{16} + H^1 \rightarrow F^{17} + \gamma$

Measurements of the radiative proton capture by oxygen have been made by Tanner (1959) at 616 Kev (lab) and by Hester, Pixley and Lamb (1958) in the range from 140 to 170 Kev (lab). Tanner finds S = 6. $\pm$ 1.4 Kev barns. Using the formalism of Christy and Duck, Fowler and Caughlan have extrapolated these results to low energies. They get S(0) = 10.6 Kev barns and $\langle dS/dE \rangle = -2.8 \times 10^{-2}$. (Figure 12)

Note: A theoretical analysis of the same data plus newer points has been made by Lal (1961). He finds S(0) = 12 Kev barns.

Figure 13

Energy Diagram of F^{18}

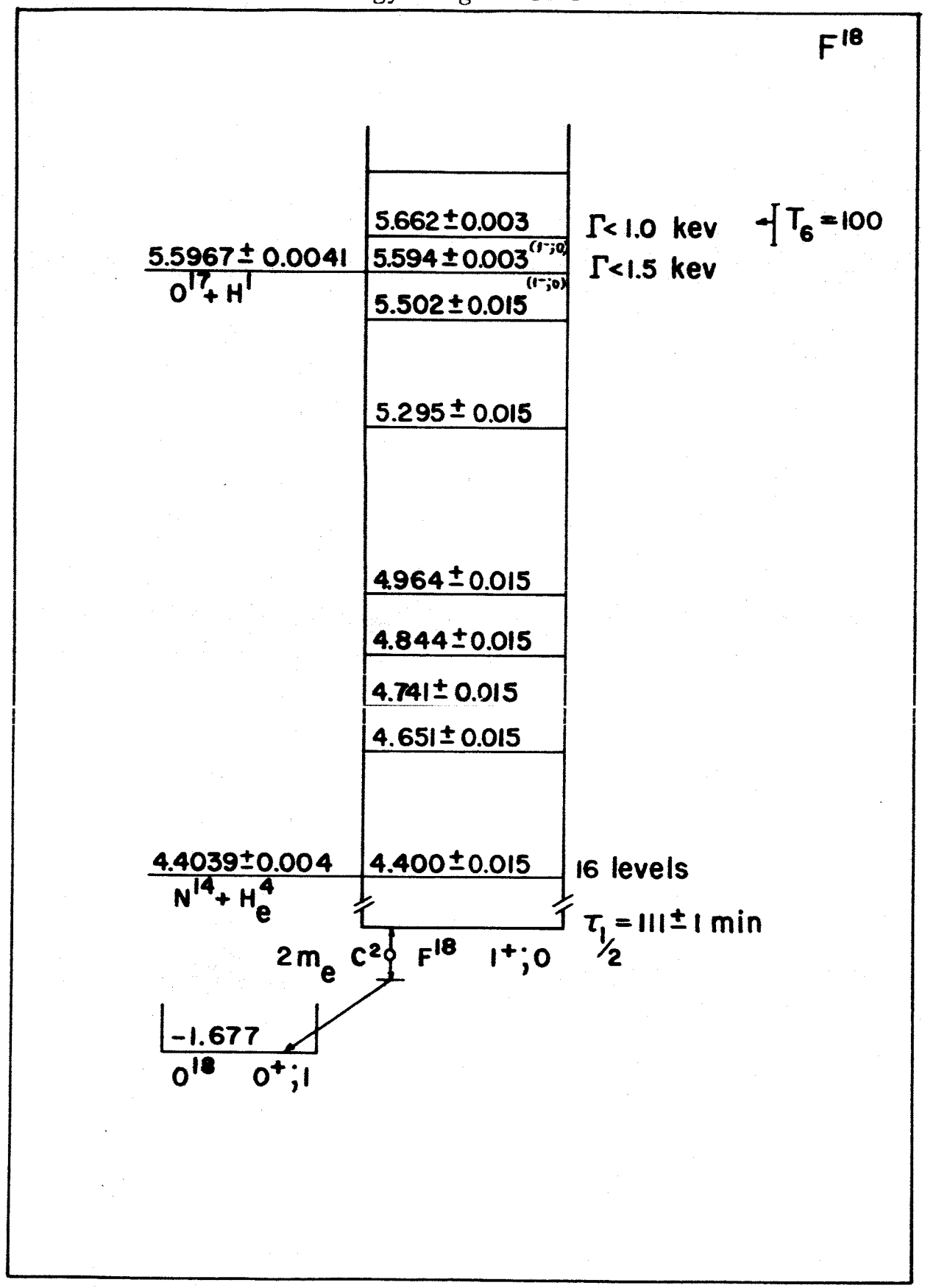

$$O^{17} + H^{1} \rightarrow N^{14} + He^{4}$$
$$\rightarrow F^{18} + \gamma$$

Because of the abundance of levels in the corresponding region of the compound nucleus the rate is most likely resonant. Close to the break-up point one finds two (1^-) resonances at $E_r = -3 \pm 7$ Kev and at $E_r = 65 \pm 7$ Kev. Silverstein, Hardie, Oppliger, and Salisbury (Silverstein 1960) have made some measurements of the properties of these levels. In both cases, the total width is $\simeq$ 200 ev, and is most likely due to the alpha particle width. Hence, one can obtain a good estimate of θ_α^2, (the alpha reduced width of these levels); one gets $\theta_\alpha^2 \simeq 0.14$. (The ($H^1$ γ) reaction is neglected as its radiation width is undoubtedly much smaller than 200 ev. (Figure 13)).

Brown (1962) has used these two levels to compute the reaction rate. One important quantity for computation of the resonant nuclear reaction is θ_p^2, the proton reduced width. Unfortunately nothing is known about the θ_p^2 of these two levels. To obtain an estimate Brown assumed that the θ_p^2 of these levels is similar to the θ_p^2 of some neighboring levels at higher excitation energy. He sets

$\theta_p^2 \simeq 7 \times 10^{-3}$. This estimate is probably within a factor 10 of the correct value but may possibly be wrong by a factor of one hundred.

Since the two levels are both (1^-) and since they are so close to each other one should worry about interference effects. In particular, one does not know whether the interference will be destructive or constructive. Brown has carried out calculations for the two cases and has shown that the thermonuclear rates would be the same for $T_6 > 22$ but could differ by factors of 10 to 100 at lower temperatures.

He then shows that the observed terrestrial O^{17}/O^{16} ratio is better explained in terms of the destructive interference. On this account Fowler and Caughlan accept the choice of destructive interference.

In the absence of better argumentation we shall make the same choice but remember that it rests on rather unsafe grounds.

Above $T_6 = 30$, the rate can be written with the help of a resonant formula of the form:

$$\frac{P}{\rho Y_1 f_{n,1}} = 10^{2.4} e^{-755/T_6} / T_6^{3/2} \qquad (T_6 > 30)$$

At lower temperatures the values of $p/\rho \chi_1 f_{17,1}$ were computed numerically by Brown. The results are given in Table 8.

This rate is the poorest known of all the rates discussed so far. The influence of the uncertainties attached to this particular reaction rate on our knowledge of the energy generation rate will be discussed in later paragraphs.

PARAMETERS FOR CNO CYCLE

REACTION	REDUCED MASS $M = \frac{A_1 A_2}{A_1 + A_2}$ a.m.u.	$Z_1 Z_2 \sqrt{M}$	$E_0/T_6^{2/3} = 1.220(Z_1^2 Z_2^2 M)^{1/3}$ (kev)	$\Delta E_0/T_6^{5/6} = 0.75(Z_1^2 Z_2^2 M)^{1/6}$ (Mev)
$C^{12} + H^1 \rightarrow N^{13} + \gamma$	0.93004 ± 0.00004	5.7863 ± 0.0003	3.93	1.4
$N^{13} + C^{13} + e^+ + \nu$				
$C^{13} + H^1 \rightarrow N^{14} + \gamma$	0.93563 ± 0.00006	5.8037 ± 0.0002	3.94	1.4
$N^{14} + H^1 \rightarrow O^{15} + \gamma$	0.94046 ± 0.00003	6.7884 ± 0.0001	4.38	1.4
$O^{15} \rightarrow N^{15} + e^+ + \nu$				
$N^{15} + H^1 \rightarrow C^{12} + He^4$	0.94467 ± 0.00006	6.8036 ± 0.0002	4.38	1.4
$N^{15} + H^1 \rightarrow O^{16} + \gamma$	0.94467 ± 0.00006	6.8036 ± 0.0002	4.38	1.4
$O^{16} + H^1 \rightarrow F^{17} + \gamma$	0.94839 ± 0.00002	7.79082 ± 0.00006	4.80	1.5
$F^{17} \rightarrow O^{17} + e^+ + \nu$				
$O^{17} + H^1 \rightarrow N^{14} + He^4$	0.95172 ± 0.00005	7.8045 ± 0.0002	4.80	1.5

REACTION	$B_6 = 42.4834 (Z_1^2 Z_2^2 M)^{1/3}$	$2\pi\eta E^{1/2}$(kev) = $31.2853 (Z_1^2 Z_2^2 M)^{1/2}$	Q value (kev)	Neutrino E_{max}(kev) = $(\Delta m - 2m_e c^2)$
$C^{12} + H^1 \rightarrow N^{13} + \gamma$	136.926 ± 0.002	181.03 ± 0.02	1943.3 ± 1.3	
$N^{13} \rightarrow C^{13} + e^+ + \nu$			2221.1 ± 2.0	1199.0 ± 2.
$C^{13} + H^1 \rightarrow N^{14} + \gamma$	137.200 ± 0.003	181.57 ± 0.02	7549.4 ± 0.7	
$N^{14} + H^1 \rightarrow O^{15} + \gamma$	152.311 ± 0.002	212.38 ± 0.03	7291.1 ± 1.7	
$O^{15} \rightarrow N^{15} + e^+ + \nu$			2760.6 ± 2.6	1739. ± 3.
$N^{15} + H^1 \rightarrow C^{12} + He^4$	152.538 ± 0.003	212.85 ± 0.03	4964.3 ± 0.9	
$N^{15} + H^1 \rightarrow O^{16} + \gamma$	152.538 ± 0.003	212.85 ± 0.03	12125.8 ± 0.8	
$O^{16} + H^1 \rightarrow F^{17} + \gamma$	166.958 ± 0.001	243.74 ± 0.03	597.8 ± 2.3	
$F^{17} \rightarrow O^{17} + e^+ + \nu$			2761.7 ± 3.1	1740. ± 2.
$O^{17} + H^1 \rightarrow N^{14} + He^4$	167.154 ± 0.003	244.17 ± 0.03	1192.9 ± 0.9	

Table 7

REACTION	AVERAGE NEUTRINO ENERGY LOSS (Mev)	S(0) (kev - barns)	⟨dS/dE⟩ barns	$\left(\frac{P}{F_{L_1}} = \frac{A}{Afg \exp(-B/T_6^{1/3}) T^{-4/3}} \right)$
$C^{12} + H^1 \rightarrow N^{13} + \gamma$		(1.20 ± 0.15)	5.81×10^{-3}	$(1.7 \pm 0.3) \times 10^9$
$N^{13} \rightarrow C^{13} + e^+ + \nu$	0.710			
$C^{13} + H^1 \rightarrow N^{14} + \gamma$		(5.52 ± 0.7)	1.94×10^{-2}	$(8.0 \pm 1.0) \times 10^9$
$N^{14} + H^1 \rightarrow O^{15} + \gamma$		(3.12 ± 0.25)	-2.67×10^{-3}	$(4.7 \pm 0.4) \times 10^9$
$O^{15} \rightarrow N^{15} + e^+ + \nu$	1.00			
$N^{15} + H^1 \rightarrow C^{12} + He^4$		$(5.34 \pm \quad) \times 10^4$	8.22×10^2	$(8.0 \pm \quad) \times 10^{13}$
$N^{15} + H^1 \rightarrow O^{16} + \gamma$		$(2.74 \pm \quad) \times 10^1$	1.86×10^{-1}	$(4.2 \pm \quad) \times 10^{10}$
$O^{16} + H^1 \rightarrow F^{17} + \gamma$		$(1.06 \pm 0.18) \times 10^1$	-2.81×10^{-2}	$(1.7 \pm 0.3) \times 10^{10}$
$F^{17} \rightarrow O^{17} + e^+ + \nu$	0.94			
$O^{17} + H^1 \rightarrow N^{14} + He^4$				

Table 7

$$g = (1 + UT_6^{1/3} + VT_6^{2/3} + WT_6)$$

REACTION	U	V	W	f
	$U = 5/12B_6$	$V = \frac{B_o}{T_6^{2/3}} \frac{\langle dS/dE \rangle}{S(0)}$	$W = \frac{35}{36} \frac{\langle dS/dE \rangle_k}{S(0)}$	Electron Screening Factor (Weak)
$C^{12} + H^1 \rightarrow N^{13} + \gamma$	3.04×10^{-3}	1.90×10^{-2}	4.05×10^{-4}	$(1 + 1.5\rho^{1/2}/T_6^{3/2})$
$N^{13} \rightarrow C^{13} + e^+ + \nu$				
$C^{13} + H^1 \rightarrow N^{14} + \gamma$	3.04×10^{-3}	1.38×10^{-2}	2.94×10^{-4}	$(1 + 1.5\rho^{1/2}/T_6^{3/2})$
$N^{14} + H^1 \rightarrow O^{15} + \gamma$	2.74×10^{-3}	-3.74×10^{-3}	-7.17×10^{-5}	$(1 + 1.75\rho^{1/2}/T_6^{3/2})$
$O^{15} \rightarrow N^{15} + e^+ + \nu$				
$N^{15} + H^1 \rightarrow C^{12} + He^4$	2.73×10^{-3}	6.74×10^{-2}	1.29×10^{-3}	$(1 + 1.75\rho^{1/2}/T_6^{3/2})$
$N^{15} + H^1 \rightarrow O^{16} + \gamma$	2.73×10^{-3}	2.97×10^{-2}	5.69×10^{-4}	$(1 + 1.75\rho^{1/2}/T_6^{3/2})$
$O^{16} + H^1 \rightarrow F^{17} + \gamma$	2.50×10^{-3}	-1.27×10^{-2}	-2.22×10^{-4}	$(1 + 2.0\rho^{1/2}/T_6^{3/2})$
$F^{17} \rightarrow O^{17} + e^+ + \nu$				
$O^{17} + H^1 \rightarrow N^{14} + He^4$	2.50×10^{-3}			

Table 7

Table 8

Rate of the $O^{17} + H^1 \rightarrow N^{14} + He^4$ and Total Lifetime of the Bi-Cycle

T_6	$\frac{P_{17+1\rightarrow 14+4}}{\rho X_1 f_{17,1}}$	$\tau \rho X_1 f_{14,1} g_{14,1}$ bi-cycle sec
5	-31.6	29.7
6	-29.7	27.4
7	-28.0	25.6
8	-26.2	24.1
9	-24.8	22.9
10	-23.7	21.8
11	-22.8	20.8
12	-22.1	20.0
13	-21.4	19.3
14	-20.7	18.6
15	-20.0	18.0
16	-19.2	17.4
17	-18.4	16.9
18	-17.6	16.4
19	-16.7	16.0
20	-15.9	15.6
21		
22	-14.5	14.9
23		
24	-13.3	14.2
25	-12.8	13.9
26	-12.3	13.6
27		
28	-11.4	13.1
29		
30	-10.7	12.6
35	- 9.3	11.6
40	- 8.2	10.8
45	- 7.4	10.1
50	- 6.7	9.5
55	- 6.2	8.9
60	- 5.7	8.5
65	- 5.4	8.1
70	- 5.1	7.7
75	- 4.8	7.3
80	- 4.6	7.0
85	- 4.4	6.7
90	- 4.2	6.5
95	- 4.0	6.2
100	- 3.9	6.0

3.4 Nucleosynthesis from the CNO Cycle

Caughlan and Fowler (Caughlan 1962) have considered the equilibrium production of CNO during the carbon cycle. The relative abundance of a given isotope is obtained by comparing its life-time against destruction with the life-time of the cycle as a whole (remembering that for $T_6 \gtrsim 17$ the full bi-cycle gets into operation). In Table 8, the life-time of the cycle is given as a function of the temperature while in Figures 14 and 15, the relative isotopic abundances are plotted, normalized to the total abundance of carbon and nitrogen isotopes (CN) or to the total abundance of carbon, nitrogen and oxygen isotopes (CNO). In these graphs, the x are number densities, not mass densities.

Figure 14

Isotopic Abundances from the CNO Bi-cycle, Normalized to $X_{CN} = 1$ or to $X_{CNO} = 1$.

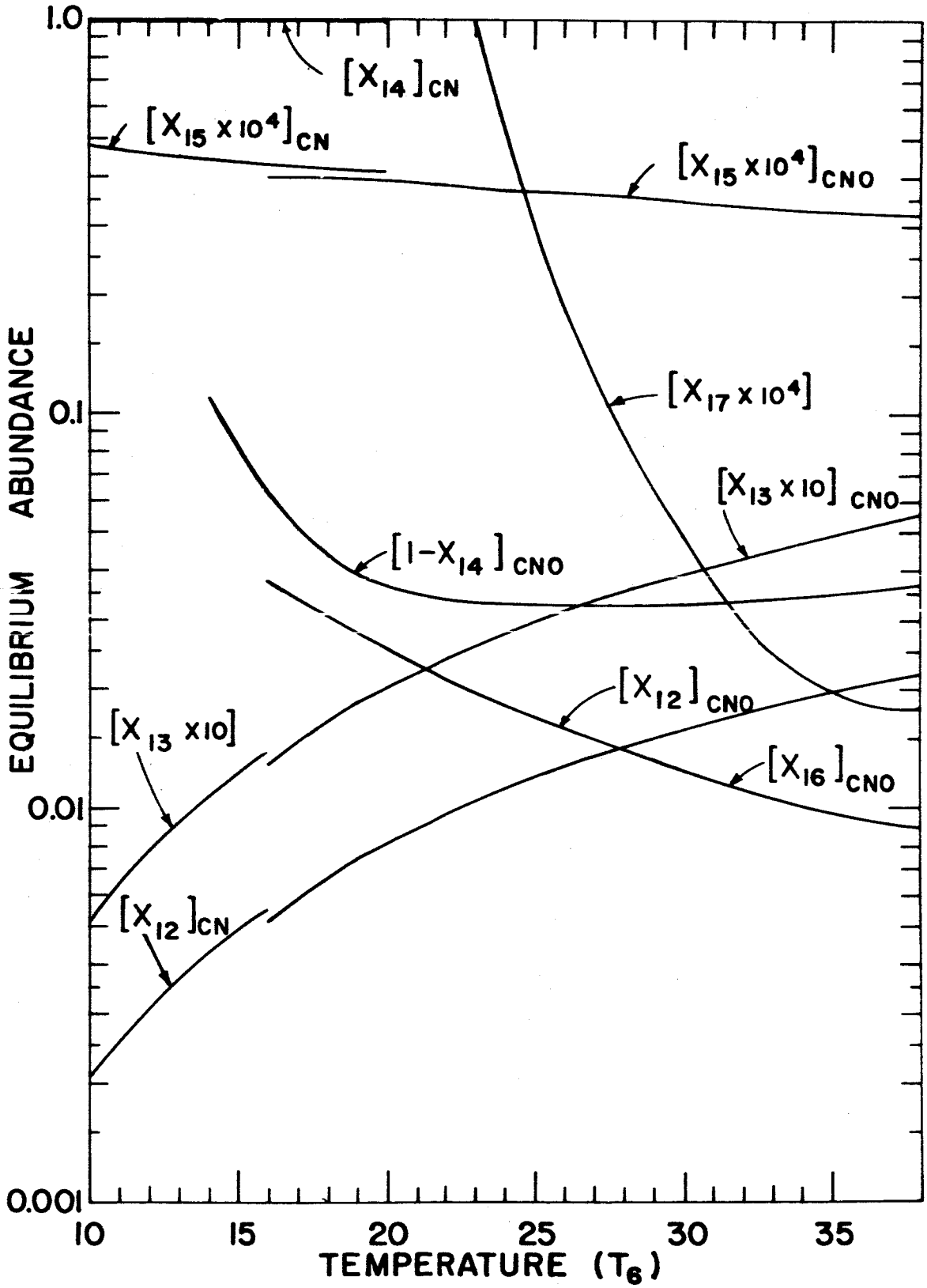

In these graphs, the x are number densities, not mass densities.

Figure 15

Isotopic Abundances from the CNO Bi-cycle, Normalized to $X_{CNO} = 1$.

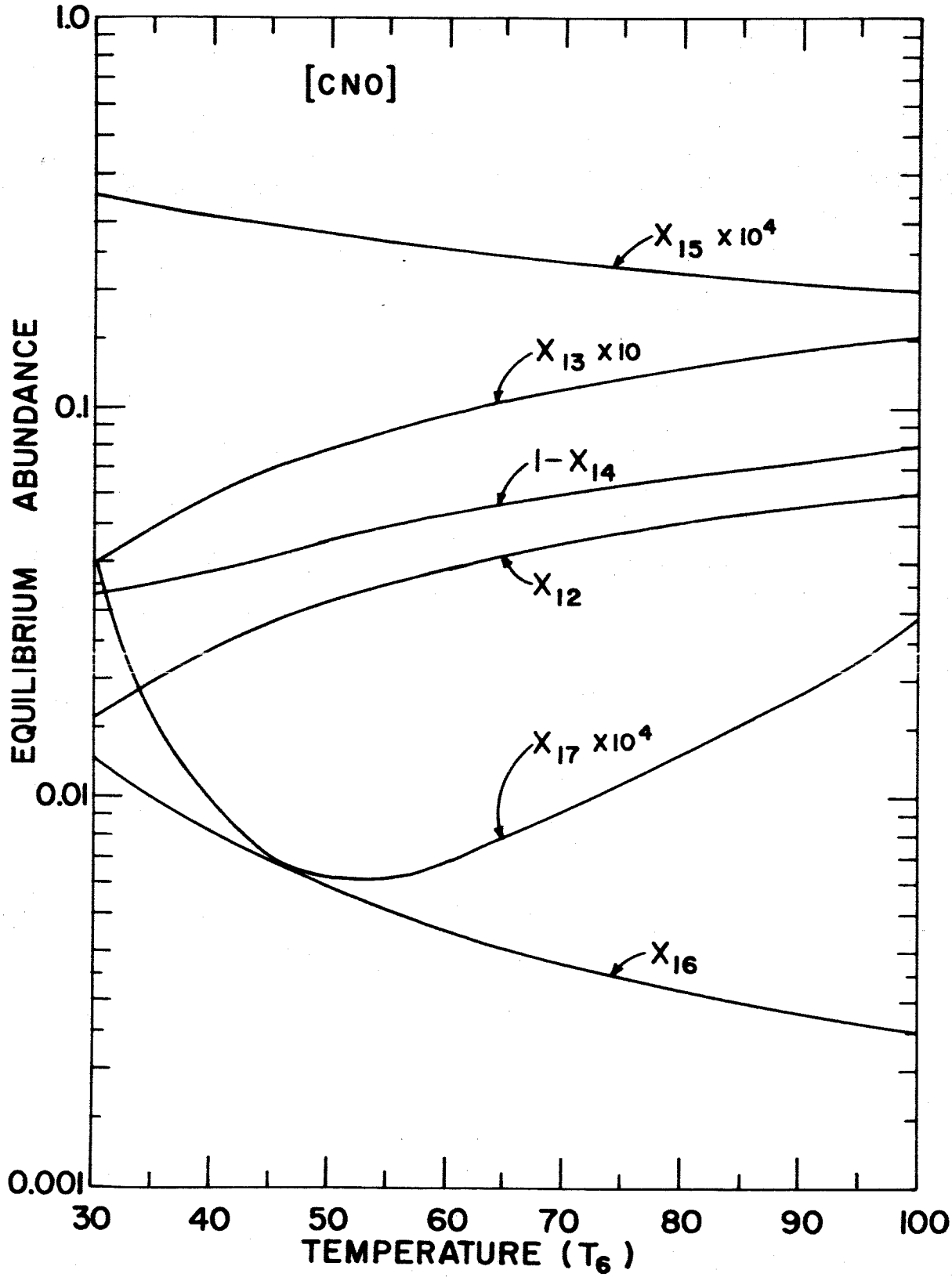

In these graphs, the x are number densities, not mass densities.

3.5 Neutrinos from the Hydrogen Burning Stage

From Tables 6 and 7 we see that there are six nuclear reactions which involve beta decay; namely:

$$H^1 + H^1 \rightarrow H^2 + e^+ + \nu$$

$$Be^7 + e^- \rightarrow Li^7 + \nu$$

$$B^8 \rightarrow Be^{8*} + e^+ + \nu$$

$$N^{13} \rightarrow C^{13} + e^+ + \nu$$

$$O^{15} \rightarrow N^{15} + e^+ + \nu$$

$$F^{17} \rightarrow O^{17} + e^+ + \nu$$

In principle each beta decaying nucleus ($A \rightarrow B + e^+ + \nu$) can also undergo an electron capture process ($A + e^- \rightarrow B + \nu$). In certain cases (e.g. Be^7 here) where the first mode is energetically forbidden, only the second mode is actually possible.

The importance of the second mode will be briefly investigated for the case of free electron capture (completely ionized gas) since, if it turned out to be important it would reduce the mean life of the beta decaying nucleus. This second mode is also interesting in the sense that it will generate sharp lines in the neutrino spectrum of the sun.

Indeed, whereas the first mode produces a hump spread from zero energy to $(\Delta M - 2m_e c^2)$, where ΔM is the energy difference between the mother and daughter atoms; the second mode (because it ends in a two-body breakup) will emit monoenergetic neutrinos (within kT; the thermal energy spread of the electrons) with $E_\nu = \Delta M$.

The relative rate of the two modes can be obtained by simply comparing the volume of phase space available to these modes (the f factor of beta decay). The volume of phase space available to the free electron capture can be obtained to a reasonable accuracy ($\simeq$ 25%) by the following formula:

$$f_{f.e.} = 4.7 \times 10^{-7} (Z) (\Delta M)^2 \frac{\rho(1 + \chi_1)}{T_6^{1/2}} \qquad (31)$$

where Z is the charge of the <u>mother</u> nucleus, ΔM is the mass difference defined above, in $m_e c^2$ ($m_e c^2 = 0.511$ Mev).

Using the experimentally known value of $\tau_{1/2}$ (the half life) and of the factor f for the reaction $A \rightarrow B + e + \nu$ we have:

$$P_{A+e \rightarrow B+\nu} = P_{A \rightarrow B+e+\nu} \left(\frac{f_{A+e \rightarrow B+\nu}}{f_{A \rightarrow B+e+\nu}} \right) = \frac{\ln 2}{(f \tau_{1/2})} (f_{A+e \rightarrow B+\nu})$$

where $P_{A+e\to B+\nu}$ is the inverse of the life-time of A against electron capture.

Salpeter has calculated the f factor for the first reaction ($H^1 + H^1$): he gets $f_{H^1+H^1\to H^2+e^-+\nu} = 0.145\,(1+0.054\,(\frac{T_6}{15})^{2/3})$

From our formula, the free capture rate is:

$$f_{H^1+H^2+e^-\to H^2+\nu} = 7.5\times 10^{-6}\,\rho\,(1+X_1)/T_6^{1/2} \qquad (32)$$

The ratio of the two processes is $\dfrac{5\times 10^{-5}(X_1+1)\rho}{T_6^{1/2}}$

In the center of the sun this ratio is about 0.003, hence, the contribution is negligible. In smaller stars it could well be much more important. It should be noticed, however, that Equation 31 is valid only for a non-degenerate gas. The case of a degenerate gas has been treated by Schatzman (1958).

The neutrino spectrum from this reaction contains a hump from E_ν = 0 to 0.42 Mev and then a peak at 1.440 Mev. In the sun the peak is slightly higher than the hump.

As mentioned before, because of its low Q value the Be^7 decays only by electron capture. The decaying nucleus goes eighty-eight per cent of the time to the ground state of Li^7 (0.861 Mev neutrino) and twelve per cent of the time

to the first excited state (0.383 Mev neutrino). In the previous section a detailed calculation of the electron capture probability by Bahcall (1962) was mentioned. Our approximate formula would give here a numerical constant eighteen per cent smaller. The spectrum in this case consists of two narrow lines. The relative heights are 7.3:1.

The B^8 isotope decays* eighty per cent of the time to the 2.9 Mev level in Be^8 (log ft = 5.72) and less than five per cent of the time to the ground state (log ft > 7.3). The rest goes through higher states (possibly a state at 11.7 Mev with log ft = 4.6). The outcoming neutrinos have on the average 7.2 Mev. They are by far the most energetic neutrinos coming from ordinary stars.

The peak from the B^8, N^{13}, O^{15}, F^{17} electron captures are all negligibly small in areas and in heights, as compared to the respective humps.

Looking at these neutrinos from the point of view of the cycles, we have the following situation: each PPI cycle is accompanied by two ($H^1 + H^1$) neutrinos (total E_ν = 0.53 Mev). PPII has one ($H^1 + H^1$) and one Be^7 neutrino (total E_ν = 1.06). PPIII has one ($H^1 + H^1$) and one B^8 neutrino)total E_ν = 7.5).

Note: Recent analyses of the branching ratio are in agreement with an $\simeq$100% decay to the 2.9 Mev level (Class, private communication). The formulae and graphs of the present work have been modified accordingly.

PPIV has one N^{13} and one O^{15} neutrino (total $E_\nu = 1.71$). F^{17} contributes negligibly to the spectrum.

In the next chapter we shall evaluate the relative contribution of each of these cycles in a star. If we call $\mathcal{E}_I$ the rate of energy generation from the PPI etc., the intensity of the $(H^1 + H^1)$ neutrinos will be proportional to $2\mathcal{E}_I + \mathcal{E}_{II} + \mathcal{E}_{III}$; the intensity of the Be^7 neutrinos to $\mathcal{E}_{II}$, the intensity of the B^8 neutrinos to $\mathcal{E}_{III}$ and the intensity of the N^{13} and O^{15} proportional to $\mathcal{E}_{IV}$. Using the results of the next chapter and a model of the sun by Sears (1959), we have built a neutrino spectrum from the sun. We recognize over the general background, made by the various humps, the three main lines of the spectrum (Figure 16).

Is there any hope of observing these solar neutrinos? To answer this question we shall briefly review the state of affairs in neutrino astronomy. The anti-neutrino was detected some two or three years ago in a famous experiment by Reines and Cowan (Reines, 1953). Let it be repeated for the sake of completeness that the decay of neutron or neutron-rich isotopes is accompanied by the emission of anti-neutrinos ($\bar{\nu}$) while the decay of proton (or proton-rich isotopes) is accompanied by neutrinos (ν).

Figure 16

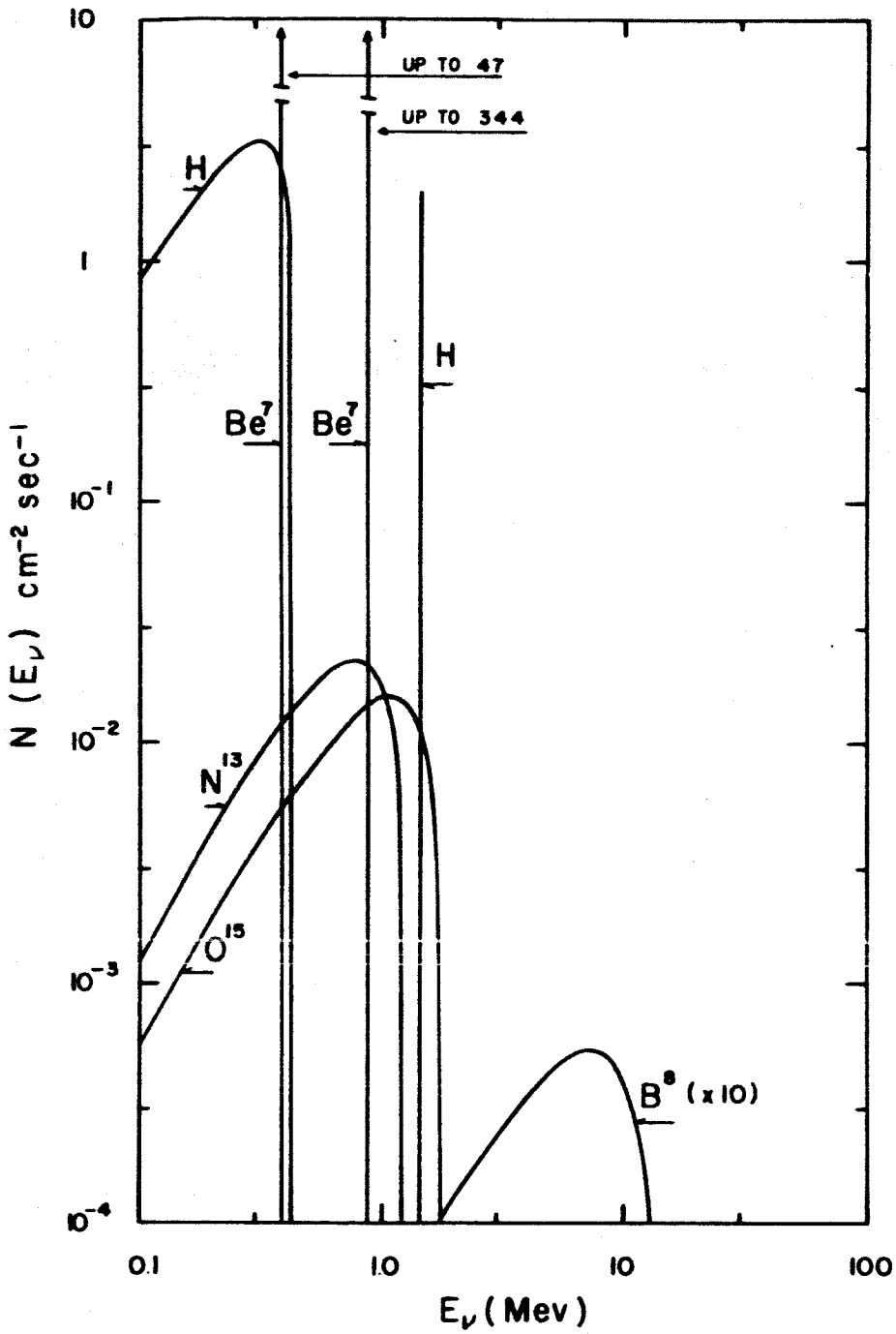

Figure 16.

Here, using a fashionable model of the present sun we have drawn the energy spectrum of the neutrinos coming from it.

Most remarkable is the presence of lines with very great height over the background (one of them to 100 in the units of the graph). These lines are associated with the processes of free electron capture by Be^7. The neutrinos emitted are monoenergetic except for a width of about one kev due to the thermal energies of the free electron gas.

All attempts to detect solar neutrinos have failed so far. However, the experimental upper limit on the integrated flux is gradually coming down. Improved technology should soon permit us to detect these neutrinos and give us the first direct experimental evidence for nuclear solar energy generation.

In a reactor, the nuclear reactions are sources of abundant fluxes of $\bar{\nu}$. Setting a detecting apparatus in a flux of $\simeq 10^{13} \bar{\nu}\ cm^{-2} sec^{-1}$, the experimenters succeeded in detecting a few $\bar{\nu}$ every hour. The neutrino (ν) has not yet been detected experimentally. The detection of ν is far more difficult than the detection of $\bar{\nu}$. Indeed, the fundamental process is now $n + \nu \rightarrow p + e^-$ instead of $p + \bar{\nu} \rightarrow n + e^+$. While the pair (n,e^+) is easily identified by the gamma rays it produces, the pair, (p,e^-) makes no effect of comparable ease in identification. One technique already used by Dr. Davis (Davis and Harmer, 1959) at Brookhaven is the following: a huge tank is filled with a material containing chlorine isotopes (1000 gallons of $C^2H^2Cl^4$). A flux of neutrinos may induce the following reaction in the Cl^{37} isotope of the material:

$$\nu + Cl^{37} \rightarrow A^{37} + e^-$$

The A^{37} is beta unstable with a period of 40 days:

$$A^{37} \rightarrow Cl^{37} + \nu + e^+$$

So, depending upon the flux there is an equilibrium concentration of A^{37} in the tank (a few hundred atoms). To isolate these atoms one bubbles some helium gas through the tank. The argon atoms stick to the helium and the whole is brought to a detection counter. Isotopes of A^{37} are detected by their beta activity. The number of A^{37} atoms detected allows us to evaluate:

number of A^{37} decaying per second =

number of A^{37} formed per second =

$$\int \sigma N(E_\nu)\, c\, dE_\nu .$$

where σ is the cross section for absorption of a neutrino by a Cl^{37} atom.

The strongest source of neutrinos, which reach the earth, is the sun. The sun emits almost exclusively neutrinos. Indeed, the nuclear reactions leading to beta unstable nuclei are of the (p, γ) form. They produce proton-rich isotopes which in turn decay to stable isotopes by emitting a neutrino (ν). According to the previous model of the sun, the flux of neutrinos at the earth would be:

$$\int N(E_\nu)\, c\, dE_\nu \simeq 6 \times 10^{10}\, \nu\ cm^{-2} sec^{-1} .$$

So far, the neutrino detection experiment of Dr. Davis

has failed to yield positive results. However, he has obtained an upper experimental limit:

$$\int \sigma \, NdE: \; < 5 \times 10^{-33} \text{ captures per second per atom.}$$

Such a rate is a lot more than the solar model predicts. It is about equal to the rate that would be obtained if the PPIII process was the only one active. Indeed, the decay of B^8 produces a high energy neutrino ($\bar{E}$ = 7 Mev). As the capture cross section varies with E_ν^2 such a decay has a far better chance to produce a click in Dr. Davis' tank than any other.

Dr. Davis plans to do another experiment with a tank of 10^5 gallons of $C^2H^2Cl^4$. He hopes to detect a flux if as little as 4% of the solar energy comes from PPIII. Due to the uncertainties in our knowledge of the solar structure such a contribution is indeed still quite possible.

Note: This problem was first considered by Marx and Menyhard (1960). Bahcall et <u>al</u> (1963) and Pochoda and Reeves (to be published) have made detailed analyses of this question from revised solar models. The detection power of the new apparatus is still too low (by a factor of about ten). However, an increase of $\Delta T_6 \simeq 3$ in the solar central temperature would bring the flux above threshold. The possibility of such a variation cannot be ruled out at the present time.

It is worth mentioning that if Dr. Davis obtains a positive result, that is, if he actually detects some neutrinos from the sun he will have given us for the first time a direct proof of the occurrence of nuclear reactions in the stars. He will then have settled definitely an age-old problem; how do the sun and stars generate energy at such a rate during so long a time. Today everybody believes in the nuclear mode of energy generation. At first this particular answer to the problem was accepted as no other one was available. Later, as stellar structures were studied in more detail, it became more and more evident in the light of the physical laws that nuclear reactions must go on inside the stars. The coherence of the whole framework necessitates their occurring. However, all these proofs remain indirect in nature. The clicks in Dr. Davis' tank would put a magnificant end point to our speculations.

By the same token the clicks could tell us more about the nature of stellar interiors. One could hope, for instance, that with improved techniques one would eventually be able to analyze, at least grossly, the spectrum. As we have discussed before, the respective shape of its various humps and lines would be a function of the physical conditions in

the core.

It is amusing to realize that a star of anti-matter would produce the same spectrum but with anti-neutrinos ($\bar{\nu}$). The lines identify the hydrogen-burning core, the $\bar{\nu}$ identify the anti-matter nature of the whole star. Before we finish the subject of the hydrogen burning stage, it might be worth while to consider one interesting corollary. All through the discussion we have neglected the reaction $He^3 + H^1 \rightarrow Li^4$ + gamma, $Li^4 \rightarrow He^4$ + electron + neutrino. Indeed, there are good reasons for neglecting that reaction; Li^4 is most likely a very unstable nucleus. It would much sooner break apart than beta decay. All the experimental evidence (analysed in the light of good theoretical models) points toward the particle-instability of Li^4, (Bashkin, Kavanagh, Parker 1959; Imhof, et al 1962).

In the chain of events leading to the formation of He^4 particles, the stability of Li^4 would produce some drastic changes. Because of the difference in Coulomb repulsion, the reaction $He^3 + H^1$ would be thousands of times faster than the $He^3 + He^4$. The solar energy would then be entirely obtained through that reaction. The crucial point now is

that the decay of Li^4, leading to He^4 would be accompanied by a high energy neutrino of maximum energy ~ 19 Mev, mean energy ~ 10 Mev. Since the capture cross section varies as E_ν^2, on the average these neutrinos have twice as large a capture probability as the B^8 neutrinos. Further, since the average neutrino emission per fusion of four protons into one helium would be larger than in the hypothetical case of pure PPIII burning, we should have to assume a higher rate of hydrogen burning to understand the present solar light output. This in turn implies a larger number (flux) of neutrinos.

Such a flux would produce an easily detectable effect in the Cl^{37} tank (way above the experimental limit quoted earlier). The absence of such an effect is an astronomical proof of the nuclear instability of Li^4.

3.6 Energy Generation from the Hydrogen Burning Stage

The first three PP cycles are governed by the rate for the proton-proton reaction. The number of reactions per sec per gram of matter is:

$$r = (1.0 \pm 0.1) \times 10^{11} f_{1,1}\, g_{1,1}\, \rho\, X_1^2\, e^{-33.810 T_6^{-1/3}} / T_6^{2/3} \qquad (33)$$

At temperatures below $T_6 \simeq 8$, only the two first reactions can come into equilibrium ($H^1 + H^1$ and $H^2 + H^1$). Excluding the energy carried by the neutrinos, these two reactions yield together Q = 6.675 Mev (1.069×10^{-5} ergs).
We obtain then for $T_6 \simeq 8$:

$$\varepsilon = (1.1 \pm 0.1) \times 10^{6} f_{1,1}\, g_{1,1}\, \rho\, X_1^2\, e^{-33.810/T_6^{-1/3}} / T_6^{2/3} \qquad (33a)$$

At higher temperatures the He^3 nuclei can react with themselves (leading to PPI) or with He^4 (leading to PPII or PPIII). PPII will be favored in the region of lower temperatures or of smaller He^4/H^1 ratio. Both factors will be found during the early periods of hydrogen burning.

In the case of PPII one needs two $H^1 + H^1$ reactions to form a He^4 nucleus, hence, the energy production <u>per proton-proton reaction</u> is only half of the nuclear energy released

by the formation of He^4. In other words, although Q_I = 26.20 Mev, we have to use here: ($\mathcal{E}'_I$, we define to be the energy generation rate when $X_4 = 0$).

$$\mathcal{E}'_I = \frac{Q_I}{2} r_{1,1} = 2.06 \pm 0.2 \times 10^6 f_{1,1} g_{1,1} \rho X_1^2 e^{-33.810 T_6^{-1/3}} / T_6^{2/3} \qquad (33b)$$

As the temperature increases (and/or the He^4/H^1 ratio increases) the PPII and PPIII branches may take over. The competition between these two cycles is tantamount to the competition between $Be^7(e^-, \nu)Li^7$ and $Be^7(H^1, \gamma)B^8$. Comparing the reaction rates (see Equation 39 or Figure 17) it appears that PPIII could predominate only at temperatures above T_6 = 20. For both processes each $H^1 + H^1$ reaction brings in the whole $4H^1 \rightarrow He^4$ process. Excluding neutrino losses again, we have Q_{II} = 25.67 Mev and Q_{III} = 19.2 Mev.

Thanks to the fact that for equilibrium conditions the relative abundances of the various elements involved can be expressed in terms of H^1 and He^4, the contribution from the three first branches can be grouped together in a formula which contains only the fractional densities of H^1 and He^4. Indeed, the rate of energy generation from these proton-proton branches can be written as:

$$\mathcal{E}_{pp} = Q_I N_3^2 \underline{\langle\sigma v\rangle_{3,3}} + Q_{II} N_7 p_{7+e} + Q_{III} N_7 N_1 \langle\sigma v\rangle_{7,1} \tag{34}$$

while the equilibrium abundance equations relate:

$$\frac{\langle\sigma v\rangle_{1,1}}{2} N_1^2 = \underline{\langle\sigma v\rangle_{3,3} N_3^2} + \langle\sigma v\rangle_{3,4} N_3 N_4 \tag{35}$$

for the equilibrium abundance of He^3, and

$$\langle\sigma v\rangle_{3,4} N_3 N_4 = \langle\sigma v\rangle_{7,1} N_1 N_7 + N_7 p_{7+e^-} \qquad \text{for } Be^7$$

We write our result in the form:

$$\mathcal{E}_{pp} = \mathcal{E}_I' \, \Psi_{pp}(\alpha, w) \tag{36}$$

where $\mathcal{E}_I' = \frac{Q_I}{2} \frac{N_1^2 \langle\sigma v\rangle_{1,1}}{2}$ as in Equations 33b and 34.

Then $\Psi_{pp} = \left[1 + \gamma\left(0.959 - \frac{0.492 w}{1+w}\right)\right]$

(37)

with the following definitions:

$$\gamma = \left(\left(1+\frac{2}{\alpha}\right)^{1/2} - 1\right)\alpha; \quad \alpha = \frac{\langle\sigma v\rangle_{3,4}^2}{\langle\sigma v\rangle_{1,1}\langle\sigma v\rangle_{3,3}} \left(\frac{N_4}{N_1}\right)^2 = \frac{S_{3,4}^2}{S_{1,1} S_{3,3}} e^{-100/T_6^{1/3}} \left(\frac{X_4}{4X_1}\right)^2 \tag{38}$$

The factor $\left(\alpha / \left(\frac{X_4}{4X_1}\right)^2\right)$ $S_{3,4}^2 / S_{1,1} S_{3,3} = 5.48 \times 10^{17}$ has been plotted in Figure 18 as a function of temperature. The factor γ varies from zero to one as the temperature increases.

In the last bracket:

Figure 17

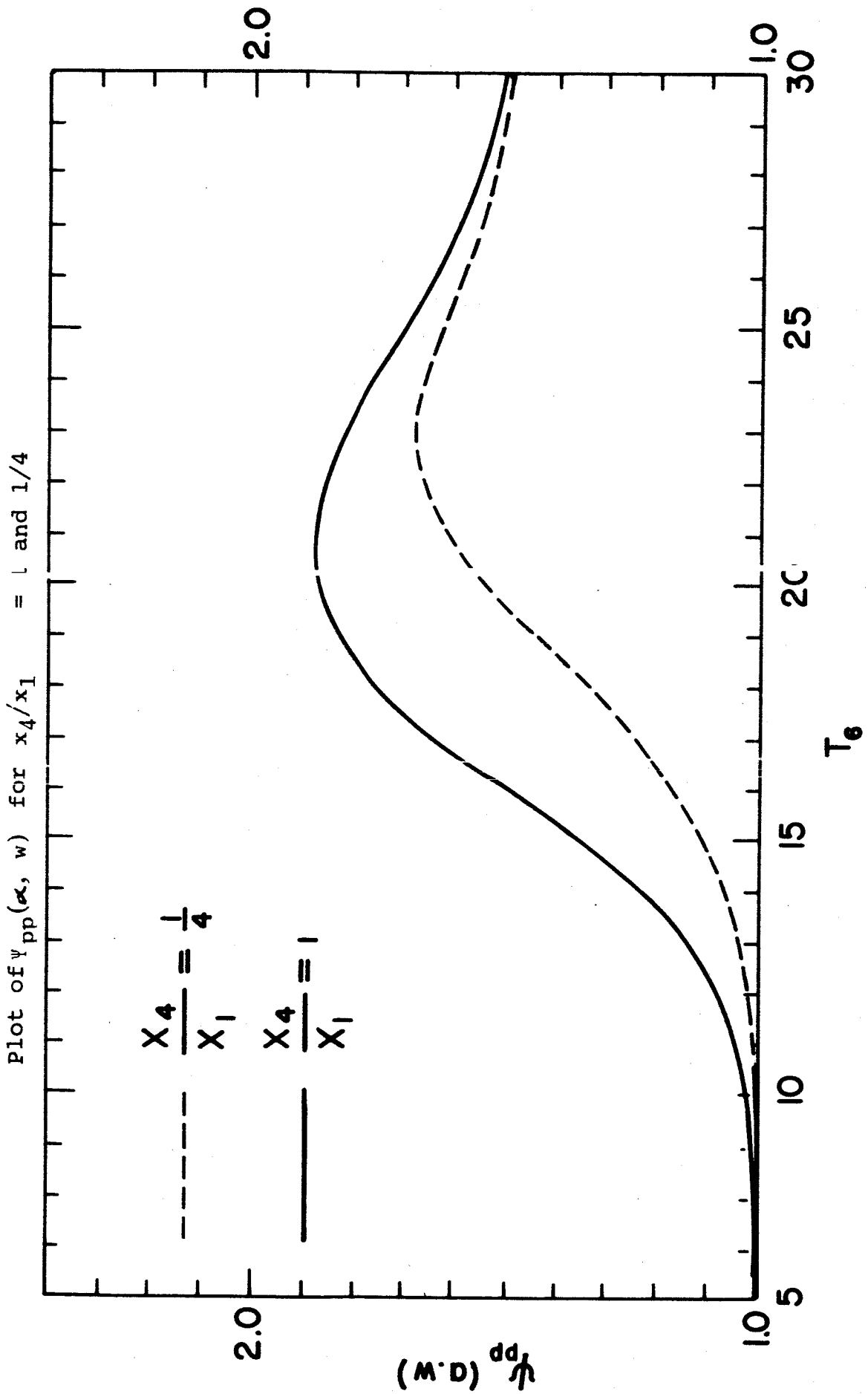
Plot of $\psi_{pp}(\alpha, w)$ for x_4/x_1 = 1 and 1/4
$\frac{x_4}{x_1} = \frac{1}{4}$
$\frac{x_4}{x_1} = 1$
2.0
1.0
5
10
15
20
25
30
T_6
ψ_{pp} (Q.W)

Table 9

Energy Generation from the Three Proton-Proton Branches

T_6	$g_{1,1}$	ε_o	n	$\left(\frac{\alpha/X_4}{4X_1}\right)^2$
1	1.02	4.27(-9)	10.61	2.03(-26)
2	1.03	2.88(-6)	8.29	1.85(-17)
3	1.04	6.53(-5)	7.17	4.22(-13)
4	1.04	4.60(-4)	6.46	2.39(-10)
5	1.05	1.82(-3)	5.95	2.19(-8)
6	1.05	5.18(-3)	5.56	6.88(-7)
7	1.06	1.19(-2)	5.26	1.08(-5)
8	1.06	2.34(-2)	5.00	1.06(-4)
9	1.07	4.16(-2)	4.79	7.23(-4)
10	1.07	6.79(-2)	4.60	3.80(-3)
11	1.07	1.04(-1)	4.44	1.62(-2)
12	1.08	1.52(-1)	4.30	5.87(-2)
13	1.08	2.12(-1)	4.17	1.85(-1)
14	1.08	2.87(-1)	4.06	5.23(-1)
15	1.09	3.77(-1)	3.95	1.34
16	1.09	4.83(-1)	3.86	3.18
17	1.09	6.07(-1)	3.77	7.04
18	1.10	7.49(-1)	3.69	1.47(1)
19	1.10	9.09(-1)	3.61	2.90(1)
20	1.10	1.09	3.54	5.48(1)

Table 9

T_6	$g_{1,1}$	ε_o	n	$\alpha/\left(\frac{X_4}{4X_1}\right)^2$
21	1.11	1.29	3.48	9.92(1)
22	1.11	1.51	3.42	1.73(2)
23	1.11	1.75	3.36	2.93(2)
24	1.12	2.01	3.30	4.81(2)
25	1.12	2.29	3.25	7.68(2)
26	1.12	2.59	3.21	1.20(3)
27	1.13	2.92	3.16	1.83(3)
28	1.13	3.26	3.12	2.73(3)
29	1.13	3.63	3.07	4.00(3)
30	1.13	4.01	3.03	5.77(3)
31	1.14	4.42	3.00	8.19(3)
32	1.14	4.85	2.96	1.14(4)
33	1.14	5.29	2.93	1.58(4)
34	1.14	5.76	2.89	2.15(4)
35	1.15	6.25	2.86	2.89(4)
36	1.15	6.75	2.83	3.85(4)
37	1.15	7.28	2.80	5.07(4)
38	1.16	7.82	2.77	6.61(4)
39	1.16	8.38	2.74	8.54(4)
40	1.16	8.96	2.72	1.09(5)
41	1.16	9.56	2.69	1.39(5)
42	1.17	1.02(1)	2.67	1.75(5)

Table 9

T_6	$g_{1,1}$	ε_o	n	$\alpha/\left(\frac{X_4}{4X_1}\right)^2$
43	1.17	1.08(1)	2.64	2.20(5)
44	1.17	1.15(1)	2.62	2.73(5)
45	1.17	1.21(1)	2.60	3.37(5)
46	1.18	1.28(1)	2.57	4.14(5)
47	1.18	1.35(1)	2.55	5.06(5)
48	1.18	1.42(1)	2.53	6.14(5)
49	1.18	1.49(1)	2.51	7.41(5)
50	1.19	1.57(1)	2.50	8.90(5)
55	1.20	1.96(1)	2.40	2.08(6)
60	1.21	2.38(1)	2.33	4.41(6)
65	1.22	2.84(1)	2.26	8.64(6)
70	1.23	3.32(1)	2.19	1.59(7)
75	1.24	3.82(1)	2.14	2.75(7)
80	1.25	4.34(1)	2.08	4.56(7)
85	1.26	4.88(1)	2.04	7.25(7)
90	1.27	5.43(1)	1.99	1.11(8)
95	1.28	5.99(1)	1.95	1.66(8)
100	1.29	6.56(1)	1.92	2.41(8)

$$w = \frac{\langle \sigma v \rangle_{7,1} N_1}{P_{7+e^-}} = 1.22 \times 10^{16} f_{7,1}\, g_{7,1}\, e^{-102.6/T_6^{1/3}} (T_6^{-1/6})(1 + 1/\chi_1)^{-1} \quad (39)$$

represents the influence of PPIII (through its high neutrino flux loss). Again, the contribution from this cycle is always negligible for $T_6 < 20$ and is usually negligible even for $T_6 > 20$, as the CN cycle becomes dominant. It could become important if the CNO abundance is abnormally low. In Figure 17 we have plotted $\Psi_{PP}(\alpha, w)$ for two values of the ratio. χ_4/χ_1.

The contribution from the three branches can be individually calculated from the following expression:

$$\mathcal{E}_{PP} = \mathcal{E}_{I} + \mathcal{E}_{II} + \mathcal{E}_{III} = \mathcal{E}'_{I} \left[(1-\gamma) + \frac{1.96\gamma}{1+w} + \frac{1.47\gamma w}{1+w} \right] \quad (40)$$

Using now a scheme described in the second section we write:

$$\mathcal{E}_{PP} = \rho \chi_1^2 f_{1,1}\, g_{1,1}\, \Psi_{PP}(\alpha, w) \mathcal{E}_0 \left(\frac{T}{T_0}\right)^n \quad (41)$$

where $[f_{1,1} = 1 + 0.25\, \rho^{1/2}/T_6^{3/2}]$ (the electron screening factor) and $[g_{1,1} = 1 + 0.012\, T_6^{1/3} + 0.0078\, T_6^{2/3} + 0.0006\, T_6]$ (a correction term). (See Table 6 and Table 9.) $\Psi(\alpha)$ is defined in the previous page with α plotted in Figure 18. $\Psi(\alpha)$ is plotted in Figure 17 for two values of (χ_4/χ_1) . In words, $\mathcal{E}_0$

Figure 18

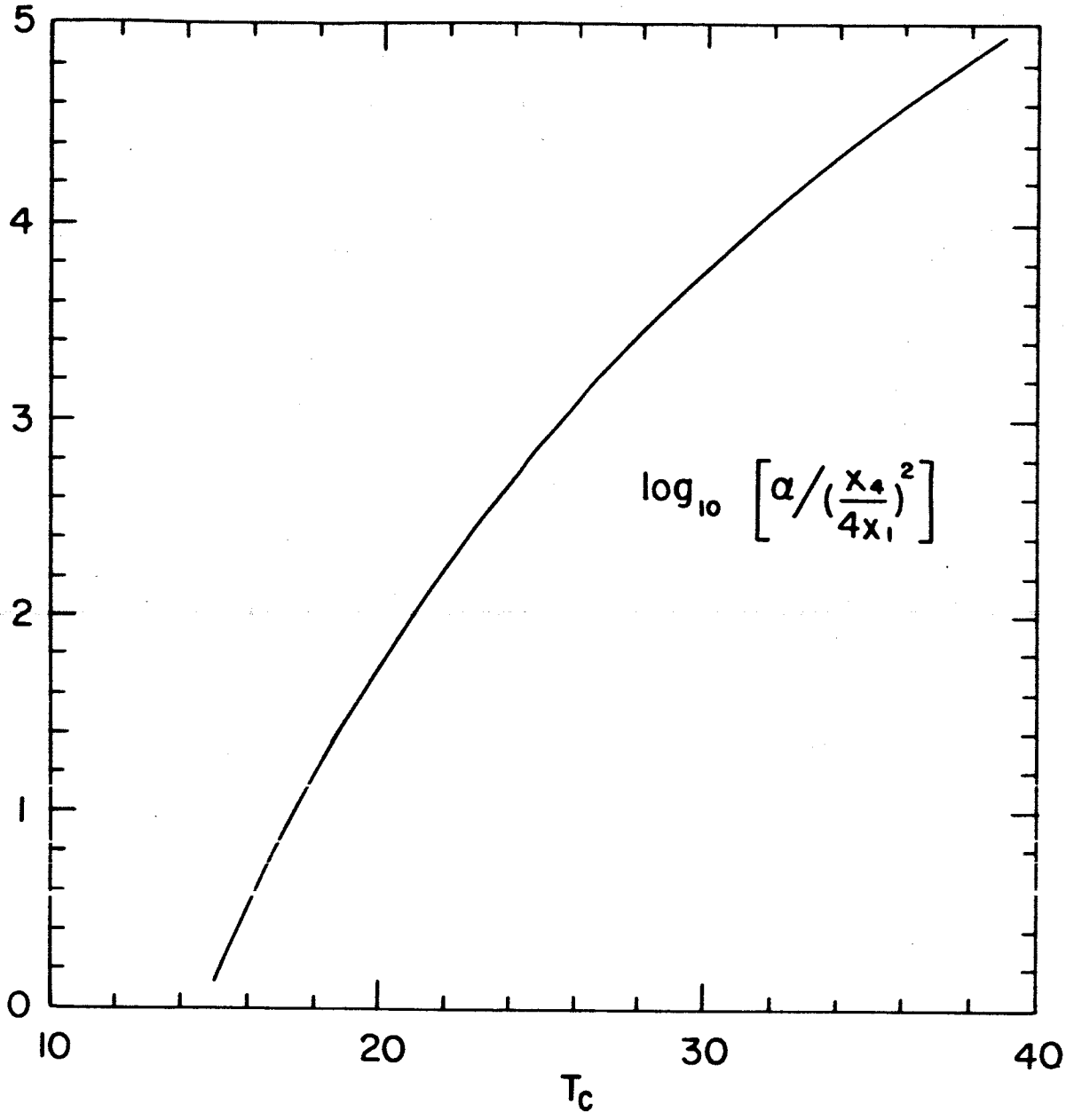

Plot of the parameter $\alpha/\left(X_4/_{4X_1}\right)^2$ as a function of T_6.

becomes the unscreened rate of energy generation at temperature T_0 per unit gram of hydrogen when helium-4 is absent from the core. Then n is the temperature exponent of the energy generation rate for the three PP branches of hydrogen burning. Although $f_{1,1}$ and $g_{1,1}$ and $\Psi_{pp}(\alpha)$ are functions of the temperature, their effect on the value of n is negligible.

The fourth PP cycle is governed by the rate of the $N^{14} + H^1$ reaction (the slowest one in the CNO cycle). The number of such reactions per unit gram is:

$$r = 1.98 \times 10^{32} f_{14,1}\, g_{14,1}\, \rho\, X_{14}\, X_1\, e^{-152.313/T_6^{1/3}} / T_6^{2/3} \tag{42}$$

The non-neutrino energy release is 25.02 Mev per cycle, hence:

$$\varepsilon_{CN} = 7.94 \times 10^{27} f_{14,1}\, g_{14,1}\, \rho\, X_{14}\, X_1\, e^{-152.313/T_6^{1/3}} / T_6^{2/3} \quad \text{erg/gm./sec.} \tag{43}$$

At temperatures below $T_6 \simeq 16$ within 10 per cent, the period of the CNO bi-cycle is too long to let the O^{16} atoms reach an equilibrium abundance concentration with the rest of the elements of the CN cycle. In this case, one only needs to consider the abundance of the carbon

and nitrogen isotopes in the original stellar gas. With the rate given here, for temperatures below $T_6 = 17$, the equilibrium abundance of N^{14} will always exceed 99 per cent of (X_{CN}) the original abundance of C and N. Hence, we replace X_{14} by X_{CN} in the formula. We write again:

$$\mathcal{E}_{CN} = \rho X_1 X_{CN} f_{1,14} g_{1,14} \mathcal{E}_0 \left(\frac{T}{T_0}\right)^n \tag{44}$$

where X_{CN} is the original abundance of carbon and nitrogen, $(X_{CN} = X_{14})$, $f_{14,1} = [1. + 1.75\rho^{1/2}/T_6^{3/2}]$ and $g_{14,1} = [1. + 0.0027T_6^{1/3} - 0.0037T_6^{2/3} - 0.0007T_6]$. In Tables 7 and 10 one finds $f_{14,1}$ $g_{14,1}$, $\mathcal{E}_0$ and n at various temperatures.

At higher temperature the bi-cycle is fully active and the O^{16} isotopes of the original stellar gas participate in the energy generation process. We can express the energy generation rate in terms of the $(N^{14} + H^1)$ rate and the fractional abundance of carbon, nitrogen and oxygen together. In this case $\mathcal{E} = \mathcal{E}_0 X_{CNO} \rho X_1 \left(\frac{X_{14}}{X_{CNO}}\right) f_{14,1} g_{14,1} \left(\frac{T}{T_0}\right)^n$

In Table 10 the values of X_{14}/X_{CNO} are tabulated. The effect of this quantity on n, the temperature exponent, is negligible.

Table 10

Energy Generation from the CN Cycle (PPIV)

T_6	$g_{14,1}$	ε_o	n	X_{14}/X_{CNO}
6	0.99	9.45(-10)	27.3	
7	0.99	5.67(-8)	25.9	
8	0.99	1.66(-6)	24.7	
9	0.99	2.87(-5)	23.7	
10	0.99	3.35(-4)	22.9	
11	0.99	2.86(-3)	22.2	
12	0.99	1.91(-2)	21.5	
13	0.98	1.04(-1)	20.9	
14	0.98	4.82(-1)	20.4	0.89
15	0.98	1.94	19.9	0.91
16	0.98	6.90	19.5	0.93
17	0.98	2.22(+1)	19.1	0.95
18	0.98	6.52(+1)	18.7	0.95
19	0.98	1.77(+2)	18.3	0.96
20	0.98	4.51(+2)	18.0	0.96
21	0.98	1.08(+3)	17.7	
22	0.98	2.44(+3)	17.4	0.97
23	0.98	5.27(+3)	17.2	
24	0.98	1.09(+4)	16.9	0.97
25	0.97	2.16(+4)	16.7	

Table 10

T_6	$g_{14,1}$	ε_o	n	X_{14}/X_{CNO}
26	0.97	4.14(+4)	16.4	0.97
27	0.97	7.66(+4)	16.2	
28	0.97	1.38(+5)	16.0	0.97
29	0.97	2.41(+5)	15.8	
30	0.97	4.11(+5)	15.6	0.97
31	0.97	6.85(+5)	15.5	
32	0.97	1.12(+6)	15.3	
33	0.97	1.78(+6)	15.1	
34	0.97	2.79(+6)	15.0	
35	0.97	4.30(+6)	14.8	
36	0.97	6.52(+6)	14.7	
37	0.97	9.73(+6)	14.5	
38	0.96	1.43(+7)	14.4	
39	0.96	2.08(+7)	14.3	
40	0.96	2.98(+7)	14.1	0.96
41	0.96	4.22(+7)	14.0	
42	0.96	5.90(+7)	13.9	
43	0.96	8.18(+7)	13.8	
44	0.96	1.12(+8)	13.7	
45	0.96	1.52(+8)	13.6	
46	0.96	2.05(+8)	13.5	

Table 10

T_6	$g_{14,1}$	ε_o	n	X_{14}/X_{CNO}
47	0.96	2.74(+8)	13.4	
48	0.96	3.62(+8)	13.3	
49	0.96	4.76(+8)	13.2	
50	0.96	6.20(+8)	13.1	0.95
55	0.95	2.11(+9)	12.6	
60	0.95	6.24(+9)	12.3	0.95
65	0.95	1.64(+10)	11.9	
70	0.94	3.93(+10)	11.6	0.94
75	0.94	8.66(+10)	11.3	
80	0.94	1.78(+11)	11.1	0.93
85	0.93	3.46(+11)	11.0	
90	0.93	6.39(+11)	10.6	0.93
95	0.93	1.13(+12)	10.4	
100	0.93	1.91(+12)	10.2	0.92

The large uncertainty in the rate of $O^{17} + H^1 \rightarrow N^{14} + He^4$ introduces an uncertainty on the quantity χ_{14}/χ_{CNO} and also on the temperature at which the bi-cycle gets in motion. With the values given in the table the contribution of the bi-cycle is governed by the $O^{16} + H^1$ rate at all temperatures where the bi-cycle plays any role ($T_6 > 14$). Hence, any increase in the rate of $O^{17} + H^1$ would be unnoticed as far as energy generation is concerned. On the other hand, a reduction of the rate by a factor of 30 would raise the effective operation of the bi-cycle to $T_6 = 17$ or 18, and would reduce by a non-negligible amount the fraction χ_{14}/χ_{CNO}.

TABLE 3

HELIUM REACTIONS

$$He^4 + He^4 \rightleftarrows Be^8$$

$$Be^8 + He^4 \rightleftarrows C^{12*}$$

$$C^{12*} \rightarrow C^{12} + \gamma$$

$$C^{12} + He^4 \rightarrow O^{16} + \gamma$$

$$O^{16} + He^4 \rightarrow Ne^{20} + \gamma$$

$$Ne^{20} + He^4 \rightarrow Mg^{24} + \gamma$$

etc...

4. Helium Burning Reactions

The fusion of two helium-4 produces the highly unstable Be^8 nucleus (lifetime $\simeq 10^{-6}$ sec.). In thermal equilibrium a certain concentration of Be^8 is established. A small number of these Be^8 will capture an extra He^4 to form C^{12} in its second excited state. The C^{12} may decay to its ground state liberating a gamma ray.

After a certain concentration of C^{12} has been built one may have $C^{12} + He^4 \rightarrow O^{16} + \gamma$, $O^{16} + He^4 \rightarrow Ne^{20} + \gamma$ etc. These exothermic reactions (mostly the first one, as we shall see later on) are expected to become the source of energy generation when the stellar core reaches temperatures of $T_8 = 1$ to 3 ($kT \simeq 10$ to 30 Kev).

In this section we shall study in detail the three reactions mentioned above. The parameters for these reactions are given in Table 11. Every resonance level in the range of stellar energies (see diagram) has been represented by a Breit-Wigner one level cross section formula (with Γ_α 's and Γ_γ 's). The value of $< \sigma v >$ has then been integrated numerically. The rate is well approximated by the resonant and non-resonant rate formulae when the Gamow peak is close

or far from the resonance. In the intermediate region, the agreement is not so good. However, since the rates are poorly known anyway, and since analytic approximations are useful for interpolation formulae, we have given such formulae whenever convenient. We have given the rates for temperature up to $T_8 = 5$. More complete discussion together with more extensive calculations will appear in a forthcoming paper (Cartledge, Marchant and Reeves, 1962).

At high densities we expect the rate to be accelerated by the effect of electron screening. For the first reaction ($3_\alpha \rightarrow c12$) the electron screening acts twice; once for the $He^4 + He^4$ reaction and then for the $He^4 + Be^8$ reaction. We shall consider a gas consisting mostly of He^4 atoms. According to the degree of degeneracy the value of $\mathcal{J}$ would vary from 1.22 to 1.0. We choose $\mathcal{J} = 1.1$ everywhere. Then:

$$
\begin{aligned}
-\frac{U_0}{kT} &\simeq 0.2\, Z_1 Z_2\, \rho^{1/2}/T_6^{3/2} && \text{(for weak screening)} \\
&= 2.4\, \rho^{1/2}/T_6^{3/2} && (\text{for } 3\alpha \rightarrow C^{12}) \qquad (46) \\
&= 2.4\, \rho^{1/2}/T_6^{3/2} && (\text{for } C^{12} + He^4 \rightarrow O^{16} + \gamma) \\
&= 3.2\, \rho^{1/2}/T_6^{3/2} && (\text{for } O^{16} + He^4 \rightarrow Ne^{20} + \gamma)
\end{aligned}
$$

In massive stars ($M \geq 2M_{\odot}$) the weak electron screening should apply. In smaller stars, and especially during the helium flash, one may have to consider the strong screening or even the extremely strong screening (pycnonuclear reactions) (Cameron 1962).

Table 11

REACTION	$He^4 + Be^8 \rightarrow C^{12} + \gamma$,	$He^4 + C^{12} \rightarrow O^{16} + \gamma$,	$He^4 + O^{16} \rightarrow Ne^{20} + \gamma$
REDUCED MASS $M = \frac{A_1 A_2}{A_1 + A_2}$ a.m.u.	2.66926 ± 0.00015	3.00242 ± 0.00008	3.20248 ± 0.00005
$Z_1 Z_2 \sqrt{M}$	13.0703 ± 0.0004	20.7930 ± 0.0003	28.6328 ± 0.0002
$\frac{E_o}{T_8^{2/3}} =$	146	199	246
$26.3\ (Z_1^2 Z_2^2 M)^{1/3}$			
$\frac{\Delta E_o}{T_8^{5/6}} =$	82	96	107
$35\ (Z_1^2 Z_2^2 M)^{1/6}$			
$T_8 = 9.1527$ $(Z_1^2 Z_2^2 M)^{1/3}$	50.786 ± 0.001	69.209 ± 0.001	85.663 ± 0.001
$2\pi\hbar E^{1/2}$(kev) = $31.1285\ (Z_1^2 Z_2^2 M)^{1/2}$	408.908 ± 0.048	650.52 ± 0.08	895.78 ± 0.10
Q value (kev)	7369.5 ± 1.0	7161.54 ± 0.39	4729.98 ± 0.47

4.1 Helium Thermonuclear Reactions

$3He^4 \rightarrow C^{12} + \gamma$

As seen from the diagram (Figure 19) the reaction is expected to be resonant, through the 7.656 $\pm$ 0.0007 Mev in C^{12}. The energy difference between this level and the masses of three He^4 has been determined by Cook, Fowler, Lauritsen and Lauritsen (Cook 1957). They find 372 $\pm$ 4 kev. Using the tables of USAEC (based on an ensemble of experimental data) one gets 381 $\pm$ 0.008 kev. We choose here 375 kev.

As a result of a series of experiments (Alburger 1960; Alburger and Pixley 1960; Alburger 1961; and Ajzenberg-Selove and Stelson 1960), we have the following sets of ratios:

$$(\Gamma_{e^\pm}/\Gamma) = (6.6 \pm 2.2) \times 10^{-6}$$
$$(\Gamma_\gamma/\Gamma) = (3.3 \pm 0.9) \times 10^{-4}$$

which yields $\Gamma_\gamma/\Gamma_{e^\pm} = 50 \begin{smallmatrix} +50 \\ -25 \end{smallmatrix}$

where Γ_γ, $\Gamma_{e^\pm}$ and Γ are respectively the radiation width to the 4.43 Mev state, the width for pair emission to the ground state and the total width of the 7.656 Mev level. The matrix element (M.E.) for the decay of this level through electron-positron pair emission has been estimated

by Fregeau (1956) from an analysis of the inelastic electron scattering. He gets (M.E.) = $(5.0 \pm 1.2) \times 10^{-26}$ cm^2.

To obtain from this matrix element the pair emission width, one must use a specific model. Using an incompressible liquid drop model of C^{12} (Welecka 1962), we obtain (with Fregeau's M.E.):

$$\Gamma_{e^\pm} = 4.5 \times 10^{-5} \text{ ev}$$

(this model also predicts M.E., one gets M.E. = 4.2×10^{-26} cm^2.) Since this value is model-dependent it cannot be considered very accurate. Dr. L. I. Schiff (private communication) has estimated for it an uncertainty of a factor two.

Using the experimental ratios quoted above, one gets $\Gamma_\gamma = 2.5 \times 10^{-3}$ ev (within a factor four) and $\Gamma = 7$ ev (within a factor three). Clearly $\Gamma \simeq \Gamma_\alpha$, (the alpha particle width). The Wigner-Teichmann limit of Γ_α is 7 ev (using a radius of 5.2 f. for the $Be^8 + He^4$ system). Hence, the level is almost a pure alpha level. Consequently, the upper limit of 21 ev for Γ_α is rather unlikely and hence also the upper limit on Γ_γ.

The theoretical model of Walecka predicts $\Gamma_\gamma = 1.0 \times 10^{-2}$ ev. In the view of the present discussion this appears

somewhat high. It does seem that his model gives a better estimate of Γ_{e^+} than of Γ_γ .

Note: Seeger, P.A., and Kavanagh, R.W. (to be published) have recently obtained $(\Gamma_\alpha / \Gamma) = (2.8 \pm 0.3) \times 10^{-4}$. Their analysis yield $\Gamma_\alpha = (2.4 \pm 1.5) \times 10^{-3}$ ev.

There is now strong evidence for an assigment of $J\pi = 3^-$ for the 9.63 Mev level (Bradford and Robson 1961 and Carlson 1961). We know also that the alpha width has the value $\Gamma_\alpha = 30 \pm 8$ kev (Douglas, Broer, Chiba, Herring, and Silverstein 1956); however, the radiation width is unknown. The most likely mode of radiative decay would be by a cascade through the 2^+ first excited state. If the width had an average value for uninhibited E 1 transitions, then $\Gamma_\gamma = 2.5$ ev (Carlson 1961); however, this transition would be of the form $0 \rightarrow 0$ in isotopic spin, so that selection rules will probably reduce the width by an order of magnitude. A calculation of Γ_γ has been quoted (Hoyle and Fowler 1960) which shows that an admixture of 4% of the T = 1 level at 17.63 Mev will reduce Γ_γ to 0.01 ev. We choose $\Gamma_\gamma = 0.03$ ev. with an uncertainty of about a factor ten either way.

Salpeter (1957) has shown that the resonant contribution

from these two levels can be written as:

$$P_\alpha = \omega(3)^{5/2} N_\alpha^2 \left(\frac{2\pi\hbar^2}{M_\alpha kT}\right)^3 \left(\frac{\Gamma_\gamma + \Gamma_{e^\pm}}{\hbar}\right) e^{-E_r/kT} \tag{47}$$

where M_α is the mass of the helium-4 nucleus, and ω a statistical factor defined earlier, involving this time the He^4 and the Be^8 nuclei. P_α is then the rate of destruction of He^4 per alpha particle per second.

With the data given earlier we find:

$$P_\alpha / (\rho X_4)^2 f_{3\alpha \to C^{12}} = \frac{5.92 \times 10^{-7}}{T_8^3} \times 10^{-18.9/T_8} \quad \text{(7.65 level)} \tag{48}$$

within a factor four each way.

The resonant rate from the second level (9.65) is given by:

$$P_\alpha / (\rho X_4)^2 f_{3\alpha \to C^{12}} = \frac{5.0 \times 10^{-5}}{T_8^3} \times 10^{-119.0/T_8} \tag{49}$$

In our range of temperatures ($T_8 < 6$), the first level dominates everywhere. The resonant rate given in Equation 48 is valid for $T_8 > 0.85$. At lower temperatures the rate has been integrated numerically, the result is given in Table 12.

We recall here that P_α is the rate of destruction of He^4 per alpha particle per second. The mean rate of formation of C^{12} per alpha particle $P_{3\alpha \to C^{12}}$ is three times smaller.

Figure 19

Energy Diagram of C^{12}

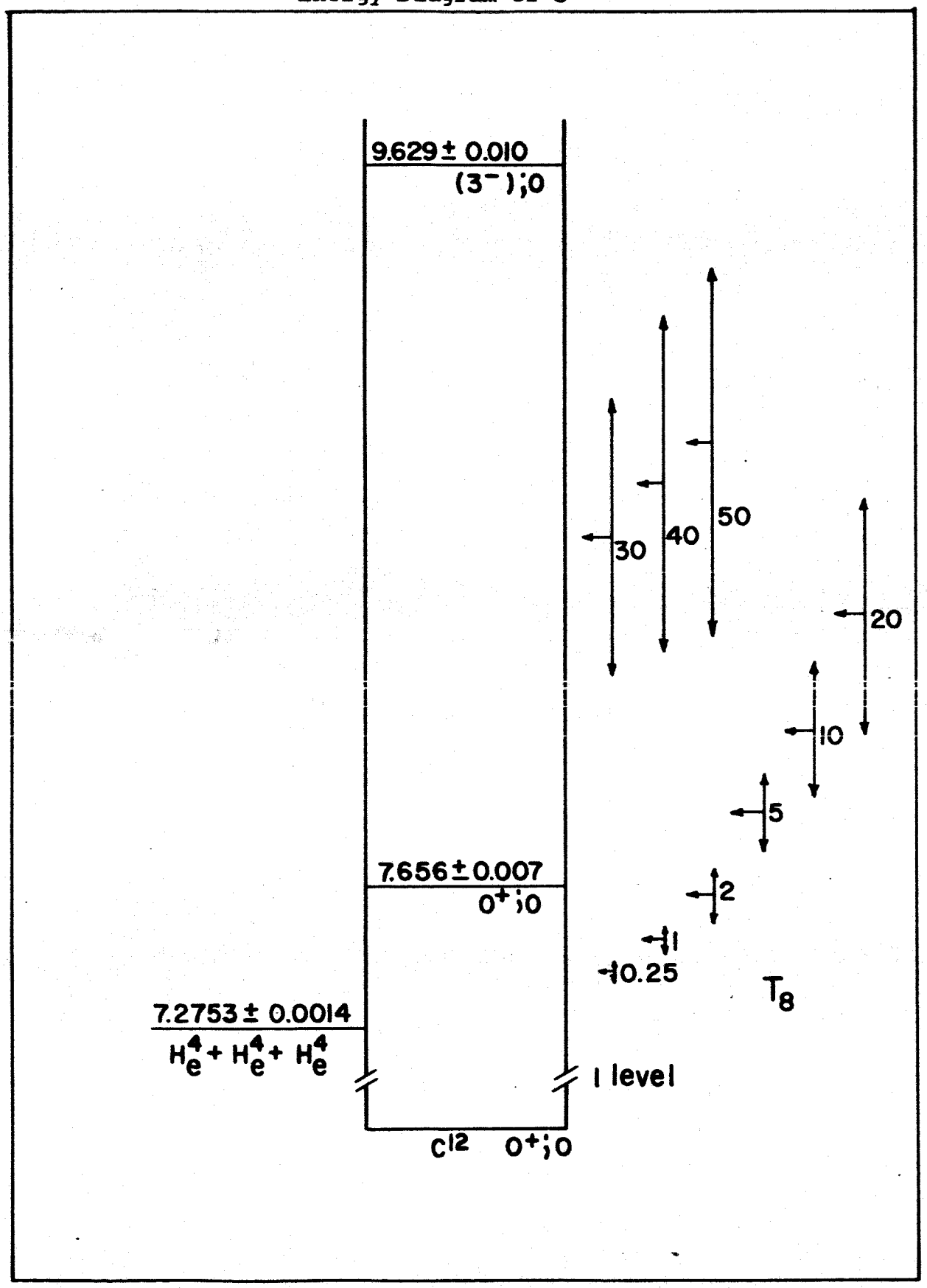

$C^{12} + \alpha \rightarrow O^{16} + \gamma$

The level at 7.12 Mev lies 40 kev below the sum of the masses of $C^{12} + He^4$. Its radiation width is 6.6×10^{-2} ev within 30% (Swann and Metzger 1957; Reibel and Mann 1960).

The value of the alpha width is still unknown. More specifically, we know nothing of the value of θ_α^2 which measures the overlap of this state with the system of $C^{12} + He^4$. Statistically, the spectrum of values of θ_α^2 is distributed between 0.001 and 1 (Roth and Wildermuth 1960). There is some theoretical reason (quoted in Cameron 1958) to believe that this state should have a rather large alpha particle width. We shall choose $\theta_\alpha^2 = 0.1$ with a possible error of a factor ten each way. The rate has been integrated numerically. The non-resonant approximation comes to within 30% of the computed value everywhere except at the highest temperature:

$$\frac{P_{12,4}(7,12)_{n.r.}}{(\rho X_4 f_{12,4})} = \frac{4.6 \times 10^9 \times 10^{-(30.05/T_8^{1/3} - \delta)}}{T_8^2 \left[1 - 4 \times 10^{-3} T_8 + 0.2\, T_8^{-2/3}\right]^2} \qquad (50)$$

where $\delta = 0.06\ T_8^{2/3}\ (1 + 0.07\ T_8^{1/3})$

This rate is uncertain by a factor of about twenty.

The level at 8.88 is a 2^-, hence it cannot contribute

to the capture process. The next level at 9.58 Mev has Γ_α = (0.65 ± 0.03) Mev (Segal, Olness and Sprenkel 1961). Its radiation width is Γ_γ = 6 x 10^{-3} ev within a factor of about two (Bloom, Toppel and Wilkinson 1957). The computed rate should be correct within a factor of five:

$$\frac{P_{12,4}\,(9.58)_r}{(\rho X_4) f_{12,4}} = \frac{4.3 \times 10^3 \times 10^{-122/T_8}}{T_8^{3/2}} \tag{51}$$

The next level (2^+ at 9.84 Mev) has Γ_γ = (2 ± 1) x 10^{-2} ev (Meads and McIldowie 1960) and Γ_α = (7.5 ± 4) x 10^2 ev (Hill 1953). This makes the rate uncertain by less than a factor of two:

$$\frac{P_{12,4}\,(9.84)_r}{(\rho X_4) f_{12,4}} = \frac{2.35 \times 10^4 \times 10^{-135/T_8}}{T_8^{3/2}} \tag{52}$$

The 7.12 level contribution dominates the rate for $T_8 < 5$. The 9.58 level enters the picture at $T_8 > 5$, while the 9.85 comes in only above T_8 = 20 to 30. The total reaction rate (the sum of these contributions) is given in Table 12.

Figure 20

Energy Diagram of O^{16}

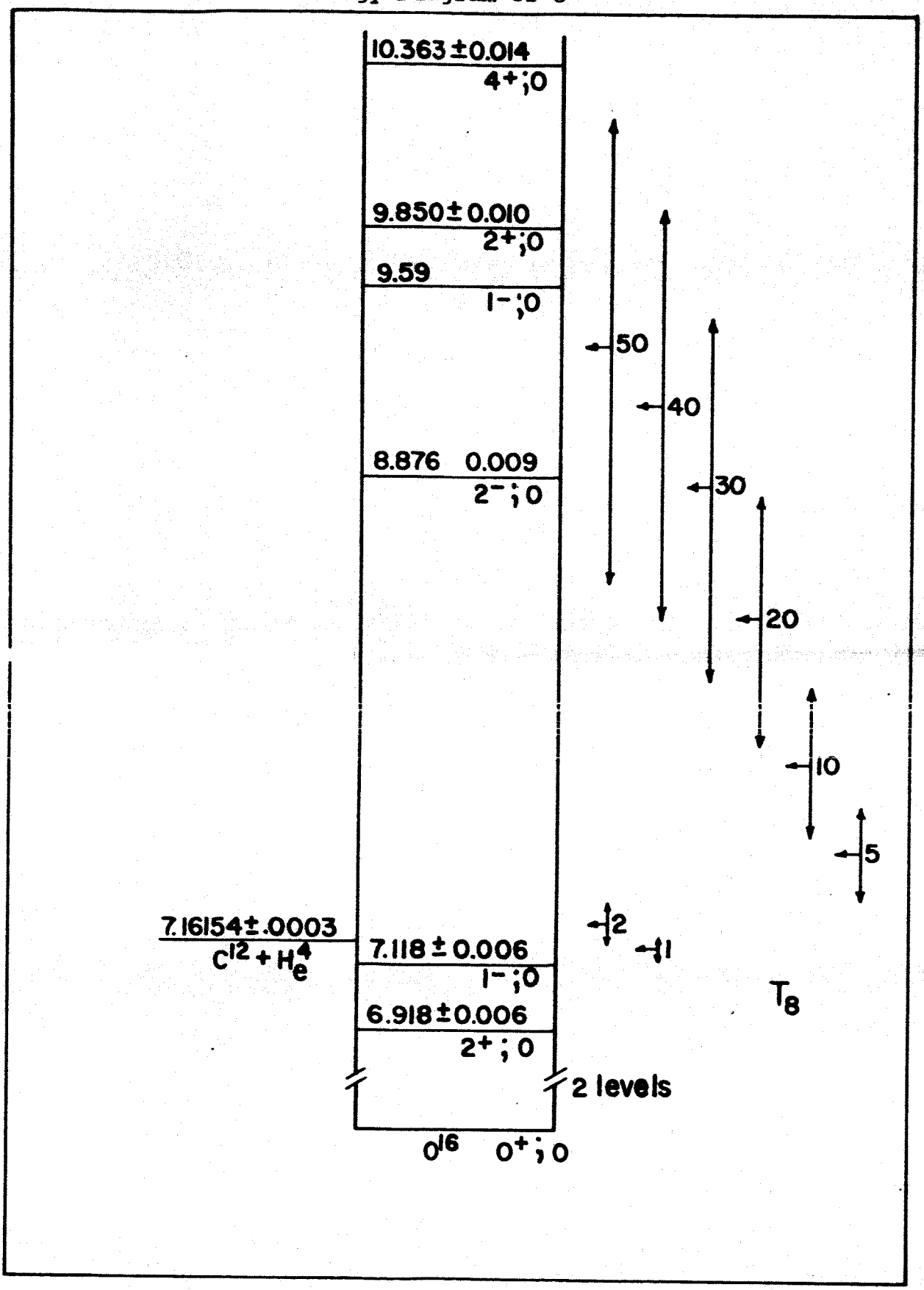

$O^{16} + \alpha \rightarrow Ne^{20} + \gamma$

The situation is described in Figure 21. We have incorporated in these the new data from the Chalk River group (Kuehner, Gove, Litherland, Clark and Almqvist 1961). The Q value and the various resonance energies are known within about 10 kev. The 4.97 level is a (2^-); hence not active for $O^{16}(\alpha,\gamma)Ne^{20}$. For the 5.64 Mev (3^-) level, we have two independent measurements:

$$(2\ell+1)\frac{\Gamma_\alpha \Gamma_\gamma}{\Gamma} = 0.003 \pm 0.002 \text{ ev and}$$

$$\Gamma_\gamma/\Gamma = 0.07 \pm 0.01$$

From these we get:

$$\Gamma_\alpha = 6 \pm 4 \times 10^{-3} \text{ ev}$$

$$\Gamma_\gamma = 4 \pm 3 \times 10^{-4} \text{ ev}$$

For the 5.80 Mev (1^-) level we have only one piece of information:

$$\Gamma_\gamma/\Gamma < 0.006.$$

The single particle limit for Γ_α is 16 ev; the actual Γ_α has been estimated to be about 10% of this value, or $\Gamma_\alpha \approx 2$ ev. We adopt this value and from the experimental information $\Gamma_\gamma/\Gamma_\alpha < 0.006$, we chose $\Gamma_\gamma = 0.01$ ev. Both

choices should be valid within factors of 10 either way. The product $(2\ell+1)\frac{\Gamma_\alpha \Gamma_\gamma}{\Gamma}$ should be about 0.03 ev, again within a factor of ten.

For the 6.75 Mev level the radiation width is not known. On the basis of single particle estimates, we take Γ_γ = 0.1 ev. The alpha width is 19 kev (Cameron, J. R. 1953).

In the range $1 < T_8 < 2.1$ the total rate comes mostly from the non-resonant contribution of the 5.80 Mev and 6.72 Mev levels

$$\frac{P_{16,4}\ (5.8+6.7)_{n.r.}}{(\rho X_4)} = \frac{4.5 \times 10^9 \times 10^{-37.2/T_8^{1/3}}}{T_8^{2/3}}$$

(within a factor of 10) (53)

For $2.5 < T_8 < 8$, the resonant contribution from the 5.64 Mev dominates:

$$\frac{P_{16,4}\ (5.64)_{r.}}{(\rho X_4)} = \frac{6.3 \times 10^3 \times 10^{-45.9/T_8}}{T_8^{3/2}}$$

(within a factor of 2) (54)

Above $T_8 = 8$, the resonant rate from the 5.80 Mev takes over:

$$\frac{P_{16,4}\ (5.80)}{(\rho X_4)} = \frac{6.3 \times 10^3 \times 10^{-54.4/T_8}}{T_8^{3/2}}$$

(within a factor of 10) (55)

Figure 21

Energy Diagram of Ne^{20}

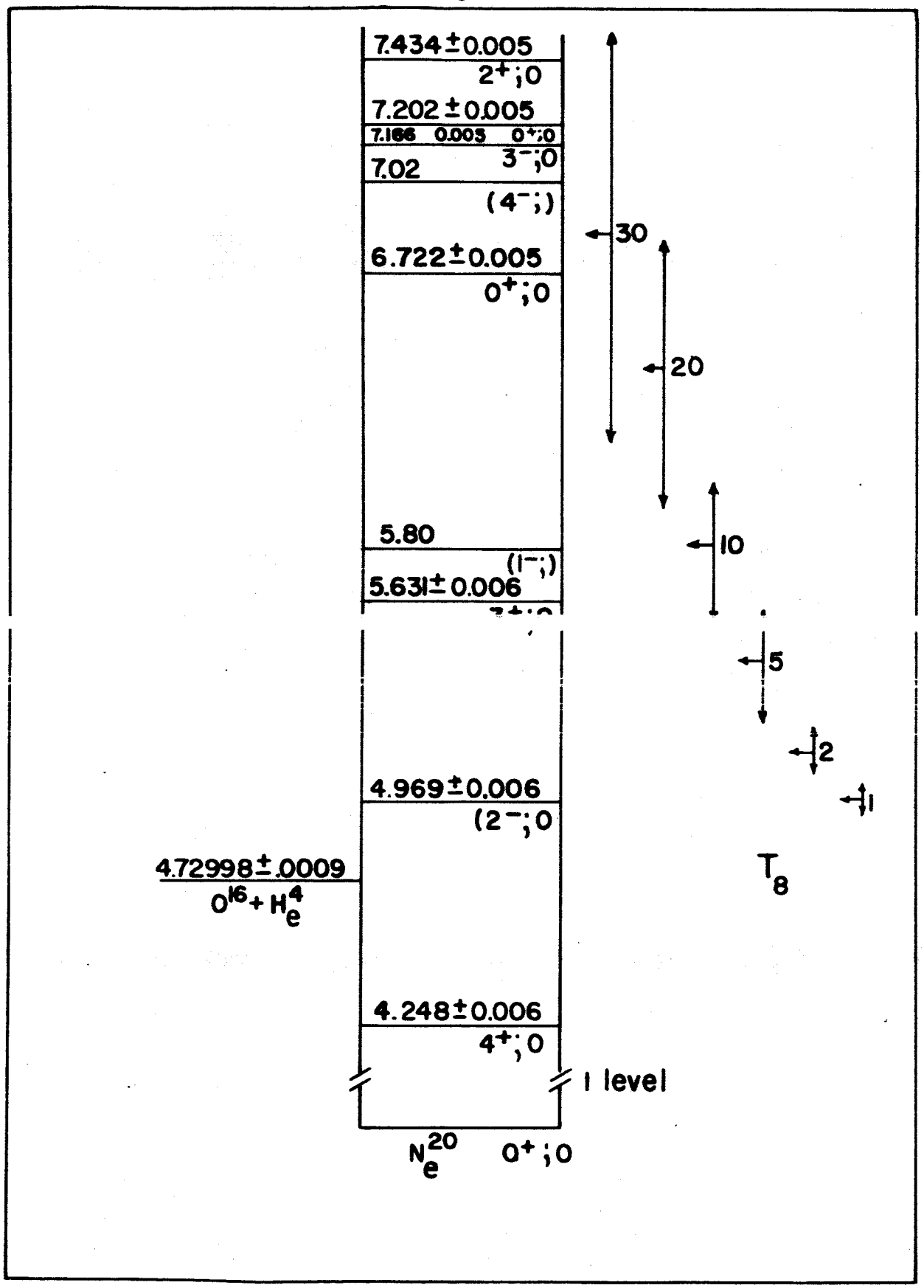

4.2 Nucleosynthesis from Helium Burning Stage

The rate of isotope formation in the helium thermonuclear reactions can be obtained by solving the following equations:

$$\frac{dN_{12}}{dt} = N_4 N_8 \langle\sigma v\rangle_{4,8} - N_4 N_{12} \langle\sigma v\rangle_{4,12}$$

$$\frac{dN_{16}}{dt} = N_4 N_{12} \langle\sigma v\rangle_{4,12} - N_4 N_{16} \langle\sigma v\rangle_{4,16}, \text{ etc.} \tag{56}$$

$$\frac{dN_4}{dt} = -3N_4 N_8 \langle\sigma v\rangle_{4,8} - N_4 N_{12} \langle\sigma v\rangle_{4,12} - N_4 N_{16} \langle\sigma v\rangle_{4,16}, \text{ etc.}$$

From our previous definitions we have:

$$N_4 N_8 \langle\sigma v\rangle_{4,8} = P_{3\alpha\to C^{12}} N_4 = \frac{P_{\alpha} N_4}{3}$$

$$N_4 N_{12} \langle\sigma v\rangle_{4,12} = P_{12,4} N_{12} \tag{57}$$

together with $N_{12} = \frac{\mathcal{N}\rho X_{12}}{12}$ etc., where $\mathcal{N}$ is the Avogadro's number.

We re-write these equations in a more convenient form:

$$\frac{dX_4}{d\tau} = -3X_4^3 - \frac{q_{16} X_4 X_{12}}{3} - \frac{q_{20} X_4 X_{16}}{4} \quad \text{etc.}$$

$$\frac{dX_{12}}{d\tau} = 3X_4^3 - q_{16} X_4 X_{12} \tag{58}$$

$$\frac{dX_{16}}{d\tau} = \frac{4}{3} q_{16} X_4 X_{12} - q_{20} X_4 X_{16}, \text{ etc.}$$

where:

Figure 22

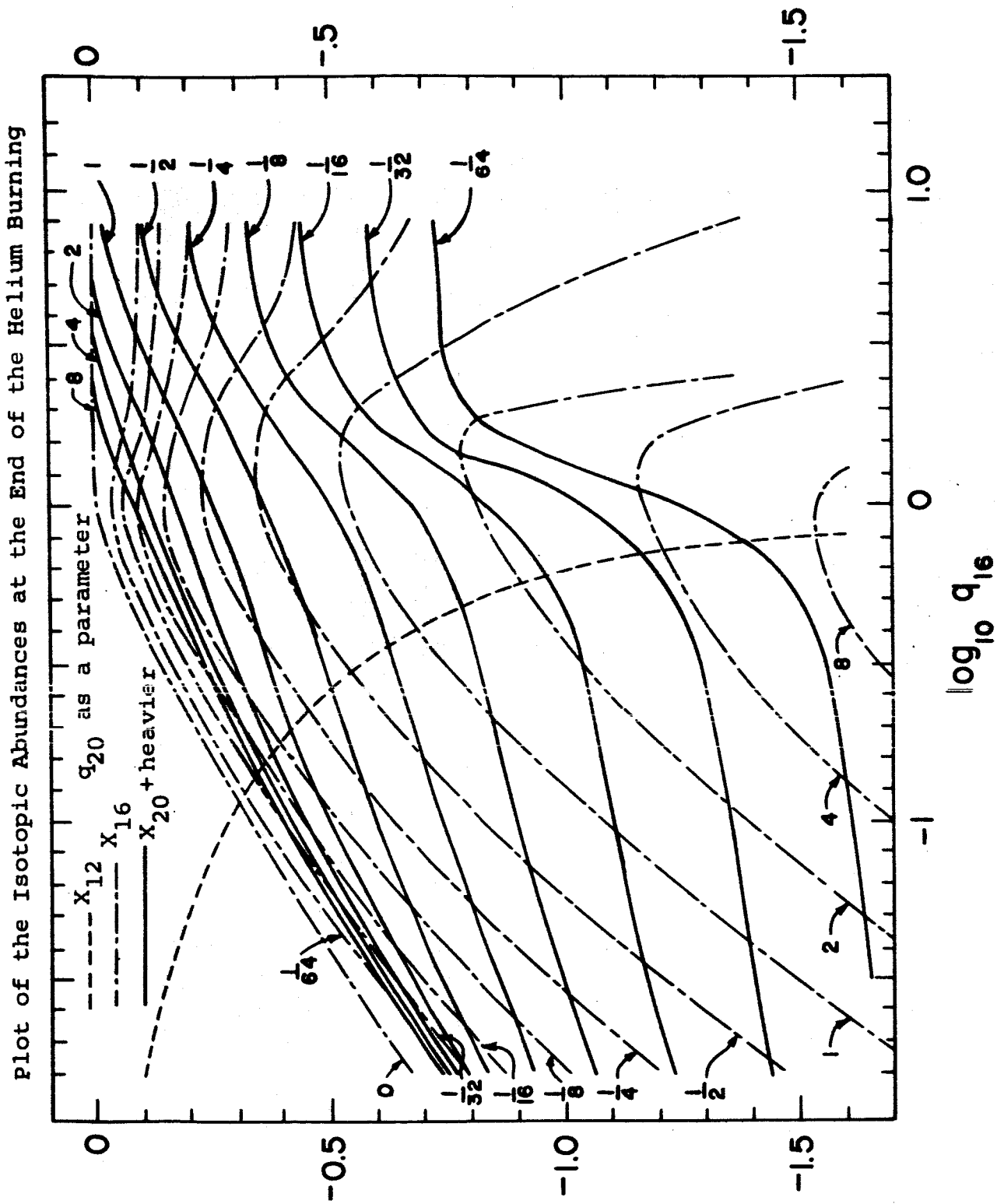
Plot of the Isotopic Abundances at the End of the Helium Burning
X_{12}
X_{16}
X_{20} + heavier
q_{20} as a parameter
$\log_{10} q_{16}$
0
-0.5
-1.0
-1.5
1.0
-1

$$\log(q_{16}\rho) = [\log(P_{12,4}/\rho\chi_4) - \log(P_{3\alpha\to C^{12}}/(\rho\chi_4)^2)] \tag{59}$$

Note that q_{16} is unaffected by electron screening (Eq. 46).

$$\log(q_{20}\rho) = [\log(P_{16,4}/\rho\chi_4) - \log P_{3\alpha\to C^{12}}/(\rho\chi_4)^2] \tag{60}$$

The variable $\tau \equiv \left(\frac{P_{3\alpha\to C^{12}}}{(\chi_4)^2}\right)t$ is a convenient time scale. The equations are solved with the assumption that: $\chi_4(0)=1$, $\chi_i(0)=0$, all other i (in other words, a pure Helium core).

The behavior of the variables χ_i as a function of the q is depicted in Figure 22. The fractional weight of C^{12} at the end of the process depends only upon the value of q_{16}. In the graph we give the final value of χ_{12} as a function of q_{16}. It appears that if $q_{16} > 0.1$, $\chi_{12} < 0.5$ and if $q_{16} > 1.0$, χ_{12} is completely negligible.

On the same graph we have used q_{20} as a parameter and studied the effect of a variation in q_{16}. The combination of q_{16} and q_{20} fixes the weight of all the material heavier than O^{16} (Ne^{20}, Mg^{24}, etc.).

In Figure 23 we have plotted the ratio $\frac{\chi_{16}}{\chi_{12}}$ in the case $q_{20} = 0$ (no Ne^{20} production) as a function of χ_4 with

Figure 23

Plot of $\frac{X_{16}}{X_{12}}$ as a Function of X_4 for Various Values of q_{16}

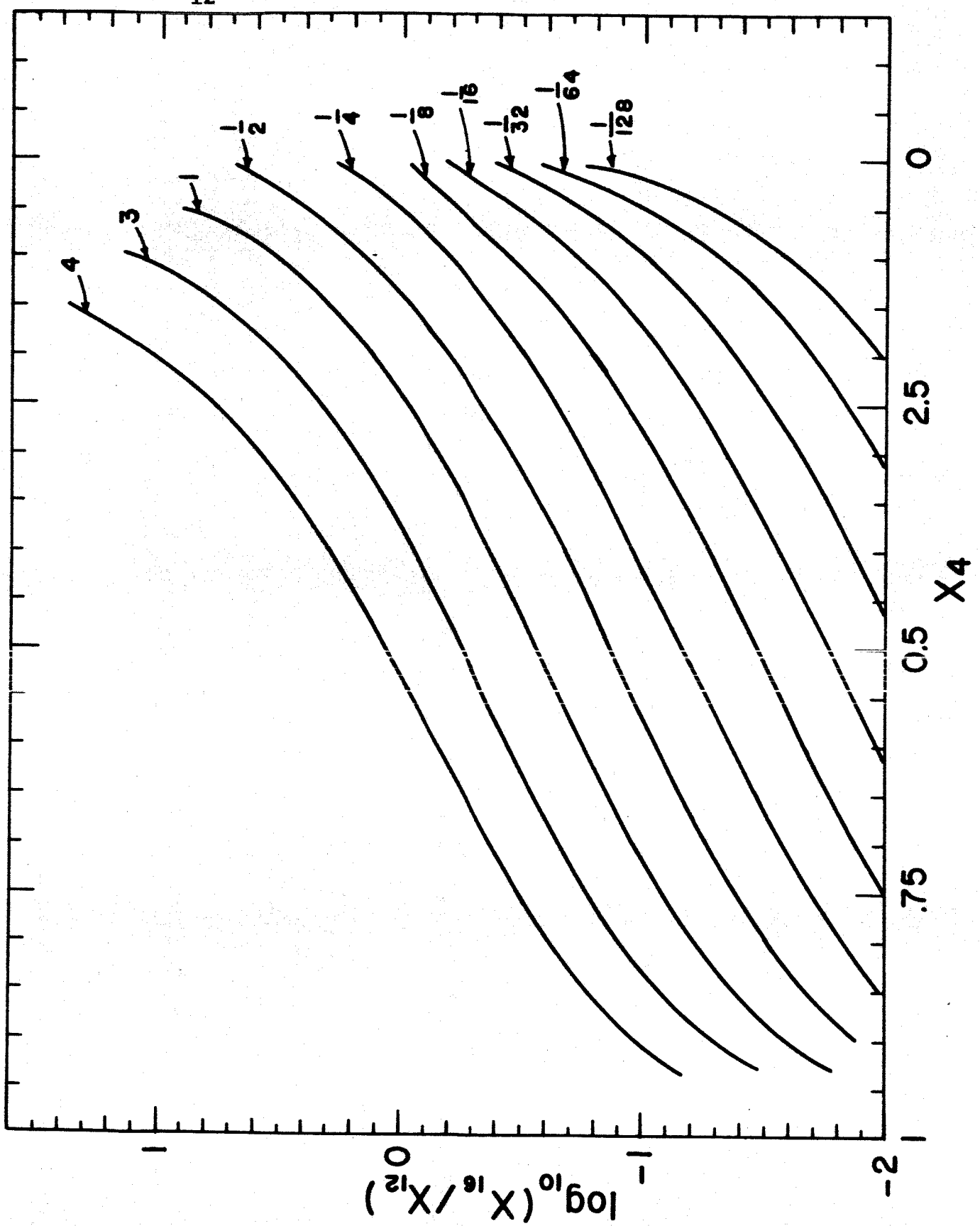

q_{16} as a parameter. Using the fact that $X_4 + X_{12} + X_{16} = 1$ one may obtain at any time the abundance of X_{12} and X_{16} This will be useful later when we shall consider over-all energy generation rates.

Using the rate computed previously we have plotted $\log_{10}(q_{16}\rho)$ and $\log_{10}(q_{20}\rho)$ as a function of T_8 (Figure 24). Then from a given set of ρ_c and T_c (central density and temperature), one can obtain first q_{16} and q_{20} from this figure and then from Figure 22 X_{12}, X_{16}, X_{20} at the end of the helium burning process. Although we have made the underlying assumption that ρ_c and T_c were remaining constants all through the helium burning stage, the isotopic abundances obtained should not be badly approximated.

Figure 24

Plot of $q_{16}\ \rho$ and $q_{20}\ \rho$ as a Function of T_8

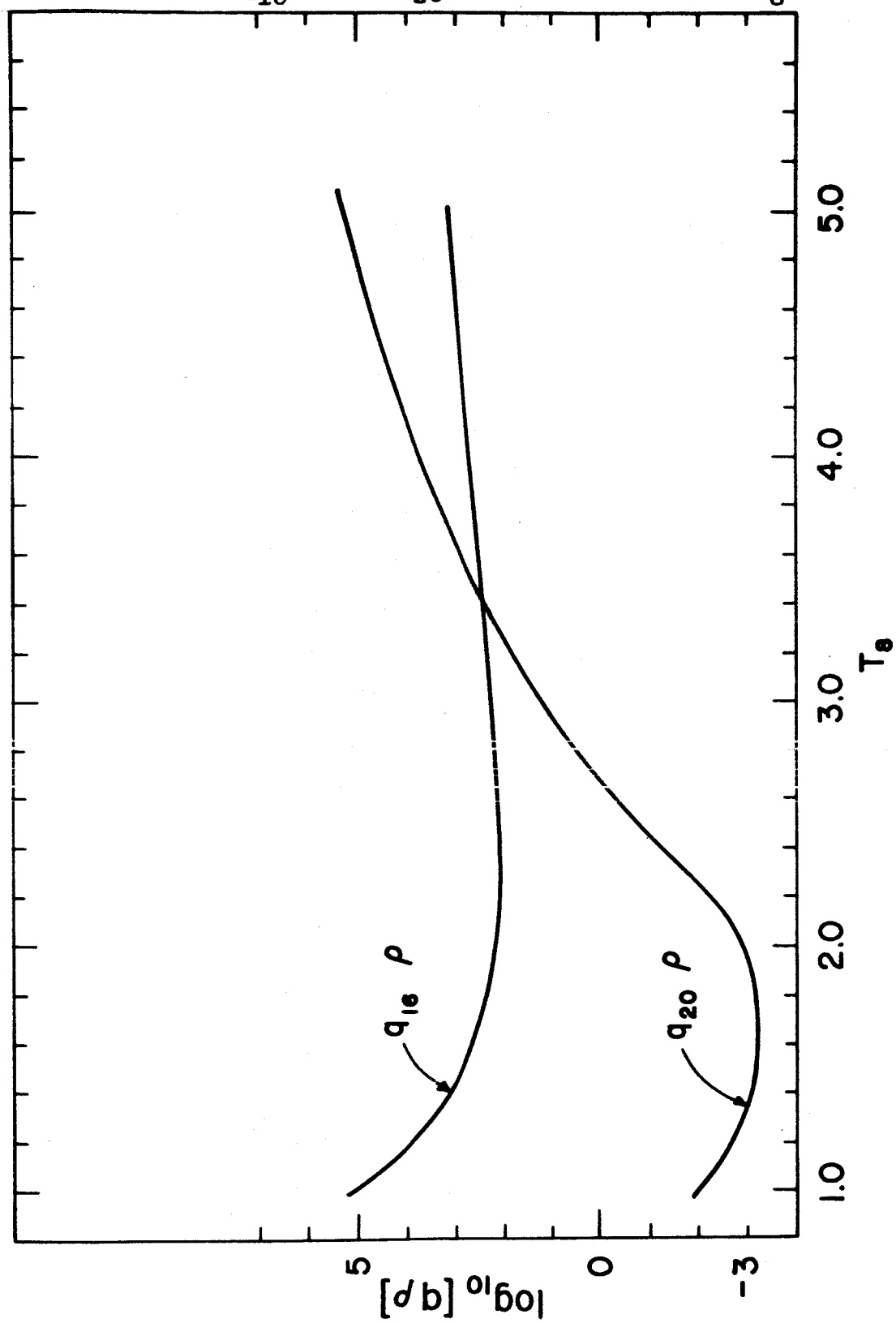

4.3 Energy Generation from the Helium Burning Stage

The rate of energy generation from the helium burning reactions depends primarily on the rate of the $3He^4$ to C^{12}. (Q = 7.275 Mev per reaction.) The rate of energy production in ergs/gm/sec of the $3He^4 \rightarrow C^{12}$ reaction we write as:

$$\mathcal{E}_{3\alpha \rightarrow C^{12}} = 1.75 \times 10^{18} P_{3\alpha \rightarrow C^{12}} X_4 f_{3\alpha \rightarrow C^{12}} \tag{61}$$

In the resonant range ($0.85 < T_8 < 50$) we have:

$$\mathcal{E}_{3\alpha \rightarrow C^{12}} = 3.46 \times 10^{11} \rho^2 X_4^3 T_8^{-3} (10^{-13.9/T_8}) f_{3\alpha \rightarrow C^{12}} = \rho^2 X_4^3 f_{3\alpha \rightarrow C^{12}} \mathcal{E}_0 \left(\frac{T}{T_0}\right)^n \tag{62}$$

The value of $\mathcal{E}_0$ and n are tabulated in Table 12. For $T_8 > 0.85$; $n = \frac{43.5}{T_8} - 3$. Below that value of T , the n were computed by numerical interpolation.

Using the previous definitions, the contribution to the energy generation from the following reactions can be written down as:

$$\mathcal{E} = \frac{\mathcal{E}_{3\alpha \rightarrow C^{12}}}{(X_4^3)} \Psi_\alpha \tag{63}$$

with $$\Psi_\alpha = [X_4^3 + 0.33 q_{16} X_4 X_{12} + 0.15 q_{20} X_4 X_{16}] \tag{64}$$

In Figure 25 we have plotted the value of (Ψ_α) in Equation

Figure 25

Plot of Ψ_α as a function of X_4 and q_{16}

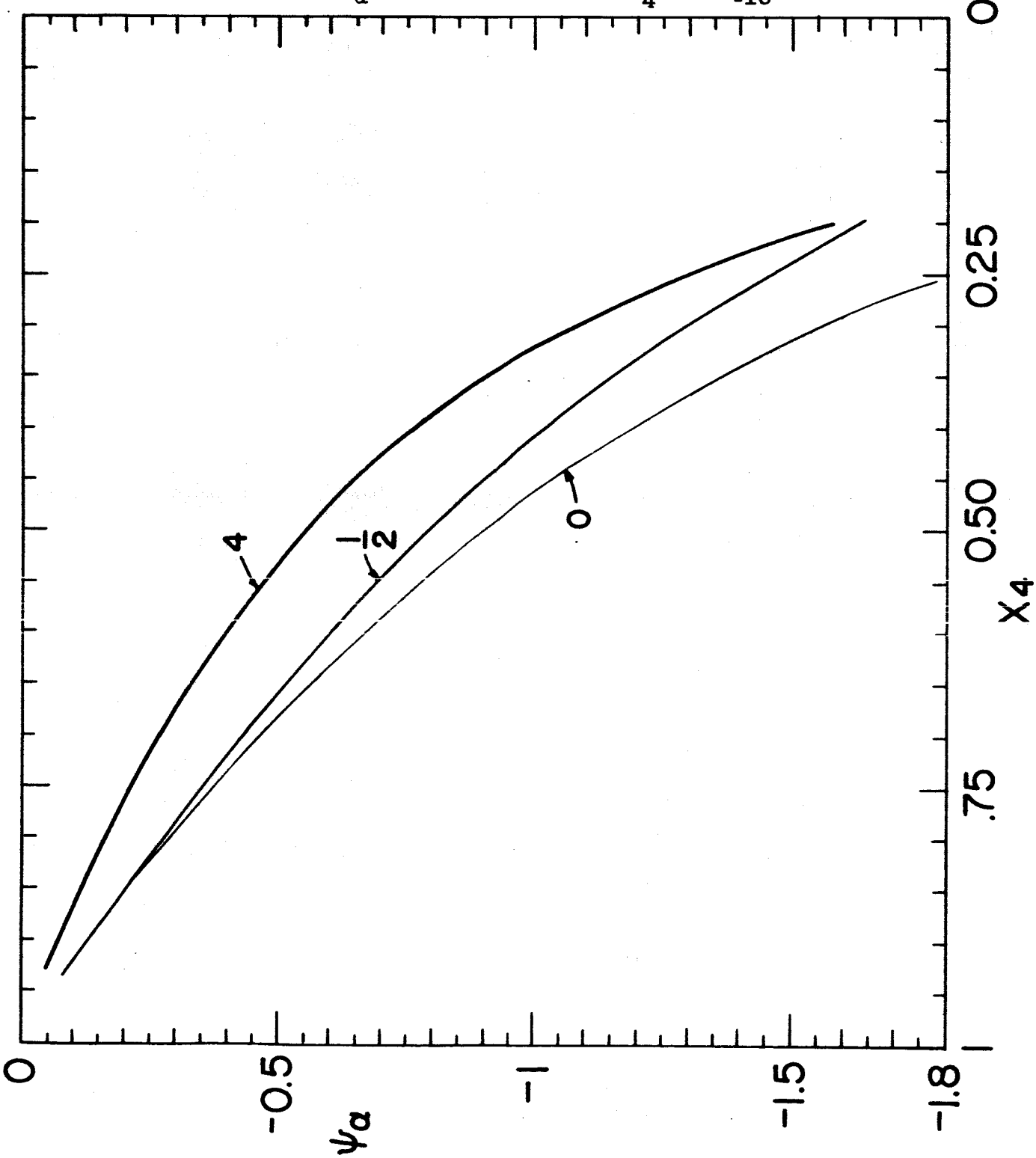

64 as a function of χ_4 for various q_{16} (assuming again that $q_{20} = 0$).

TABLE 12

T_8	$P_\alpha/(\rho X_4)^2 f_{3\alpha\to C^{12}}$	$\frac{P_{12,\alpha}}{(\rho X_4) f_{12,4}}$	$\frac{P_{16,\alpha}}{(\rho X_4) f_{16,4}}$	$\mathcal{E}_0$	n
0.7	7.2(-33)			4.2(-15)	42
0.8	3.1(-30)			1.8(-12)	49
0.9	8.1(-28)	3.4(-22)		4.7(-10)	45
1.0	7.5(-26)	3.3(-21)	3.0(-28)	4.4(-8)	41
1.1	2.9(-24)	2.4(-20)	4.1(-27)	1.7(-6)	37
1.2	6.1(-23)	1.4(-19)	4.1(-26)	3.6(-5)	33
1.3	7.8(-22)	6.5(-19)	3.3(-25)	4.6(-4)	31
1.4	6.8(-21)	2.6(-18)	2.1(-24)	4.0(-3)	29
1.5	4.4(-20)	9.5(-18)	1.2(-23)	2.6(-2)	26
1.6	2.2(-19)	3.0(-17)	5.4(-23)	1.3(-1)	24
1.7	9.2(-19)	8.7(-17)	2.2(-22)	5.4(-1)	23
1.8	3.2(-18)	2.3(-16)	8.4(-22)	1.9	21
1.9	9.7(-18)	5.8(-16)	2.8(-21)	5.7	20
2.0	2.6(-17)	1.3(-15)	8.8(-21)	1.5(1)	19
2.1	6.4(-17)	3.0(-15)	3.0(-20)	3.7(1)	18
2.2	1.4(-16)	6.2(-15)	2.7(-19)	8.3(1)	17
2.3	2.9(-16)	1.2(-14)	2.1(-18)	1.7(2)	16
2.4	5.7(-16)	2.4(-14)	1.3(-17)	3.3(2)	15
2.5	1.0(-15)	4.4(-14)	7.2(-17)	6.1(2)	14
2.6	1.8(-15)	7.9(-14)	3.4(-16)	1.1(3)	14

(7.65 - R - 4)

(7.12 - N - R - 10)

(5.80 and 6.72 - N - R - 10)

(5.64 - R - 2)

Table 12 (continued)

T_8	$P_{14}/(\rho\chi_4)^2 f_{3\alpha\to C^{12}}$	$\frac{P_{12,4}}{(\rho\chi_4)f_{12,4}}$	$\frac{P_{16,4}}{(\rho\chi_4)f_{16,4}}$	$\mathcal{E}_0$	n
2.7	3.0(-15)	1.4(-13)	1.5(-15)	1.8(3)	13
2.8	4.8(-15)	2.3(-13)	5.6(-15)	2.8(3)	13
2.9	7.4(-15)	3.8(-13)	2.0(-14)	4.3(3)	12
3.0	1.1(-14)	6.1(-13)	6.3(-14)	6.4(3)	12
3.1	1.6(-14)	9.6(-13)	1.9(-13)	9.3(3)	11
3.2	2.2(-14)	1.5(-12)	5.1(-13)	1.3(4)	11
3.3	3.1(-14)	2.2(-12)	1.3(-12)	1.8(4)	10
3.4	4.2(-14)	3.3(-12)	3.3(-12)	2.4(4)	9.8
3.5	5.5(-14)	4.9(-12)	7.6(-12)	3.2(4)	9.4
3.6	7.1(-14)	7.0(-12)	1.7(-11)	4.2(4)	9.1
3.7	9.1(-14)	1.0(-11)	3.6(-11)	5.3(4)	8.8
3.8	1.1(-13)	1.4(-11)	7.3(-11)	6.7(4)	8.5
3.9	1.4(-13)	2.0(-11)	1.4(-10)	8.3(4)	8.2
4.0	1.7(-13)	2.7(-11)	2.7(-10)	1.0(5)	7.9
4.1	2.1(-13)	3.6(-11)	4.9(-10)	1.2(5)	7.6
4.2	2.5(-13)	4.9(-11)	8.8(-10)	1.5(5)	7.4
4.3	3.0(-13)	6.5(-11)	1.5(-9)	1.8(5)	7.1
4.4	3.5(-13)	8.5(-11)	2.6(-9)	2.1(5)	6.9
4.5	4.1(-13)	1.1(-10)	4.2(-9)	2.4(5)	6.7
4.6	4.7(-13)	1.4(-10)	6.8(-9)	2.7(5)	6.5
4.7	5.4(-13)	1.9(-10)	1.1(-8)	3.2(5)	6.3
4.8	6.2(-13)	2.4(-10)	1.7(-8)	3.6(5)	6.1

(7.65-R-4) (7.12-NR-10) (5.64-R-2)

Table 12 (continued)

T_8	$P_\alpha / (\rho X_4)^2 f_{3\alpha \to C^{12}}$		$\frac{P_{12,4}}{(\rho X_4) f_{12,4}}$		$\frac{P_{16,4}}{(\rho X_4) f_{16,4}}$		$\mathcal{E}_0$	n
4.9	7.0(-13)	(7.65-R-4)	3.0(-10)	(7.12-NR-10)	2.5(-8)	(5.64-R-2)	4.1(5)	5.9
5.0	7.9(-13)		3.8(-10)		3.8(-8)		4.6(5)	5.7

5. Subsequent Burning Stages

After the exhaustion of He^4, the least charged nucleus to be found in a stellar core is C^{12}. If the temperature keeps on rising, the rate of nuclear reaction between C^{12} will become large enough to meet the energy requirements of the star. Approximate models have shown that the consequent carbon burning stage would take place around $T_9 = 0.6$ to 1.0. The set of reactions following the initial fusion are described in Table 13.

The next source of energy generation will be either the $O^{16} + O^{16}$ reaction or the photodisintegration of Ne^{20} ($Ne^{20} + \gamma \rightarrow O^{16} + He^4$) (followed by the capture of the He^4), depending upon the physical conditions in the stars. The Ne^{20} mode will precede the O^{16} mode when the densities are low and/or the temperature is high. The same models mentioned before show that stars with less than one solar mass will go through the O^{16} stage before the Ne^{20} stage. In the range $1 \lesssim M_\odot \lesssim 4$ the two stages should be about simultaneous (at $T_9 \simeq 1.2$) while bigger stars should see the order reversed. Again it should be repeated that these estimates are approximate.

TABLE 13

REACTION	$C^{12} + C^{12}$	$O^{16} + O^{16}$
REDUCED MASS		
$M = \frac{A_1 A_2}{A_1 + A_2}$ a.m.u.	6.00191 ± 0.00007	8.00000 ± 0.00000
$Z_1 Z_2 \sqrt{M}$	88.1956 ± 0.0005	181.019 ± 0.000
$\frac{E_0}{T_9^{2/3}} = 122 (Z_1^2 Z_2^2 M)^{1/3}$ (kev)	2418	3905
$\frac{\Delta E_0}{T_9^{5/6}} = 237 (Z_1^2 Z_2^2 M)^{1/6}$ (kev)	1056	1342
$B_G = 4.248 (Z_1^2 Z_2^2 M)^{1/2}$	84.175 ± 0.001	135.947 ± 0.000
$2\pi\eta E^{1/2}$ (kev) $= 31.285 (Z_1^2 Z_2^2 M)^{1/2}$	2759.22 ± 0.01	5663.24 ± 0.00

TABLE 13

REACTION	Q value (kev)
$C^{12} + C^{12} \rightarrow Mg^{24} + \gamma$	13930.1 ± 2.2
$C^{12} + C^{12} \rightarrow Na^{23} + H^{1}$	2237.5 ± 2.0
$C^{12} + C^{12} \rightarrow Mg^{23} + n$	-2605 ± 11
$C^{12} + C^{12} \rightarrow Ne^{20} + He^{4}$	4616.2 ± 1.1
$C^{12} + C^{12} \rightarrow O^{16} + He^{4} + He^{4}$	-113.8 ± 1.1
$O^{16} + O^{16} \rightarrow S^{32} + \gamma$	16538.8 ± 0.9
$O^{16} + O^{16} \rightarrow P^{31} + H^{1}$	7676.2 ± 1.5
$O^{16} + O^{16} \rightarrow S^{31} + n$	1459 ± 17
$O^{16} + O^{16} \rightarrow Si^{28} + He^{4}$	9593.1 ± 3.3
$O^{16} + O^{16} \rightarrow Mg^{24} + He^{4} + He^{4}$	-393.0 ± 2.5

$C^{12} + C^{12} \rightarrow Mg^{24*}$

The low energy yield of the $C^{12} + C^{12}$ reaction has been studied experimentally by the Chalk River group (Almqvist, Bromley, and Kuehner 1960; Bromley, Kuehner, and Almqvist 1960). The results have been studied by Reeves (1962a) and by Fowler (private communication), with the help of rather different extrapolation methods. The rates obtained are numerically in very good agreement, although the analytic formulation is slightly different. Agreement was reached that Reeves' formula is accurate over a wider range of temperature.

$$\log_{10} \frac{P_{12,12}}{\rho X_{12}} \frac{1}{f_{12,12}} = 27.0 - \frac{36.55}{T_9^{1/3}} \left[1 + 0.1\, T_9\right]^{1/3} - \frac{2}{3} \log_{10} T_9 \qquad (65)$$

It is difficult to estimate the accuracy of these rates; although the experimental points were valid within 50%, they were still quite remote from the energies of astrophysical interests. The extrapolations were not easy since the $C^{12} + C^{12}$ reaction is a rather complicated process (e.g. exhibiting resonances in the excitation curve). At the lowest temperature ($T_9 \simeq 0.5$) the uncertainty in the rate may reach a value of ten each way. At higher temperatures ($T_9 \simeq 1$) it is probably less than five. For large densities

we must again consider the effect of electron screening ($f_{12,12} = e^{-U_0/kT}$. For weak screening cases we use $\mathcal{J} \simeq 1.7$ then $-U_0/kT \simeq 12\rho^{1/2}/T_6^{3/2}$. When this last quantity is larger than one, we use $(-U_0/kT) = 3.5\rho^{1/3}/T_6$. (strong screening).

The Q value of the $C^{12} + C^{12}$ reactions brings these particles into a region of the energy diagram of the compound nucleus (Mg^{24}) where the levels overlap each other. The experimental branching ratio between the $Na^{23} + H^1$ mode and the $Ne^{20} + He^4$ mode is about 1 to 1 at all measured energies. Comparing the Q values to the respective Coulomb barrier energies, it seems safe to assume that this ratio is the same in the stellar energy region. In view of its negative Q value, the branching ratio to $Mg^{23} + n$ is negligible.

The protons and the alphas released by this reaction will in turn get captured by some of the nuclei in the gas, thereby building some of the isotopes, mainly in the range $20 < A < 28$. On the average, the net amount of energy released per each $C^{12} + C^{12}$ collision is about 13 Mev. Hence, we write as before:

$$\mathcal{E}_c = 10^{17.7} X_{12} P_{12,12} = \rho (X_{12})^2 f_{12,12} \mathcal{E}_0 \left(\frac{T}{T_0}\right)^n \text{erg/gm/sec.} \quad (66)$$

Figure 26

Energy Diagram of Mg^{24}

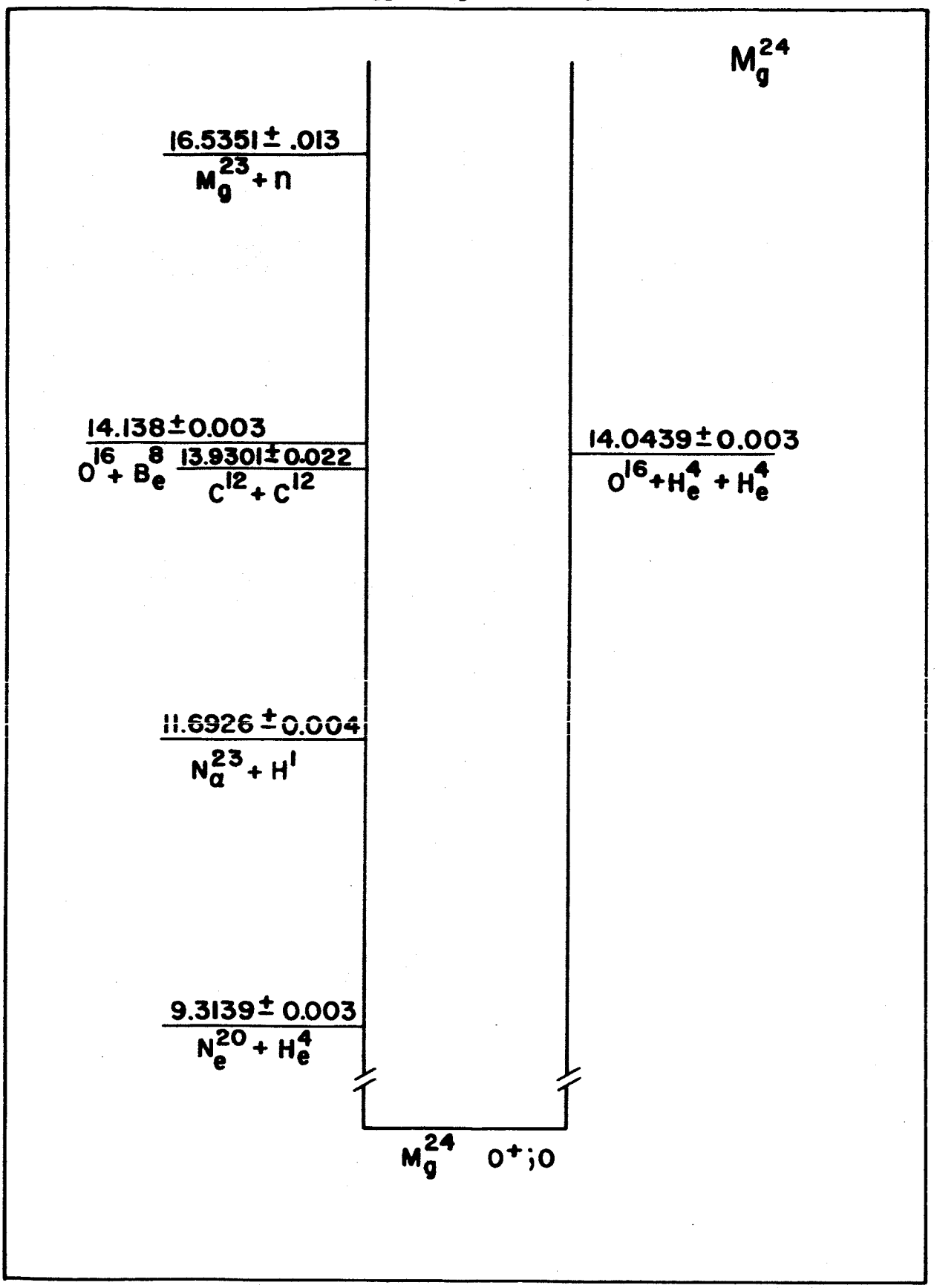

In Table 14 values of $\mathcal{E}_o$ are given, together with n, the logarithmic derivative.

$$C^{12} + O^{16}$$

Experimental results show that as expected from Coulomb barrier comparison, this reaction is much slower than $C^{12} + C^{12}$. Hence, C^{12} will be almost completely exhausted before it has a chance to start. It most likely never plays an important astrophysical role as far as energy generation is concerned.

$$O^{16} + O^{16} \rightarrow S^{32*}$$

Again we have experimental information from the experimental Chalk River group but of much poorer value this time. The yield has been obtained at only one angle, and only the alpha break-up has been studied (Figure 27). The data has been studied by Reeves (1962a) and Fowler (private communication). The rate obtained by Fowler is about ten to twenty times smaller than the rate obtained by Reeves. Such a difference is within the expected uncertainties since

the extrapolation has to be brought quite a long way down. In a private discussion it was agreed that Reeves' analysis gave a better fit to the data.

$$\log_{10} \frac{P_{16,16}}{\rho \chi_{16} f_{16,16}} = 40.5 - \frac{59.02\,(1 + 0.14 T_9)^{1/3}}{T_9^{1/3}} - \frac{2}{3} \log_{10} T_9 \quad (67)$$

The weak electron screening factor is $\exp 25(\rho^{1/2}/T_6^{3/2})$ and the strong screening factor, $\exp[6.2\,\rho^{1/3}/T_6]$

Again the compound nucleus (S^{32}) will be formed in a region of excitation energy where the levels are heavily crowded. The proton decay mode has not been studied but it is probably safe to assume a 1 to 1 ratio between alpha and proton branching ratio. Although the neutrons have a positive Q value their branching ratio should still be negligible.

The mean energy release per each $O^{16} + O^{16}$ reaction is 19 Mev. Hence:

$$\mathcal{E}_0 = 10^{17.8} \chi_{16} P_{16,16} = \rho \chi_{16}^2 f_{16,16} \mathcal{E}_0 \left(\frac{T}{T_0}\right)^n \text{ erg/gm.sec.} \quad (68)$$

Values of $\mathcal{E}_0$ together with the logarithmic derivative are to be found in Table 14.

Figure 27

Energy Diagram of S^{32}

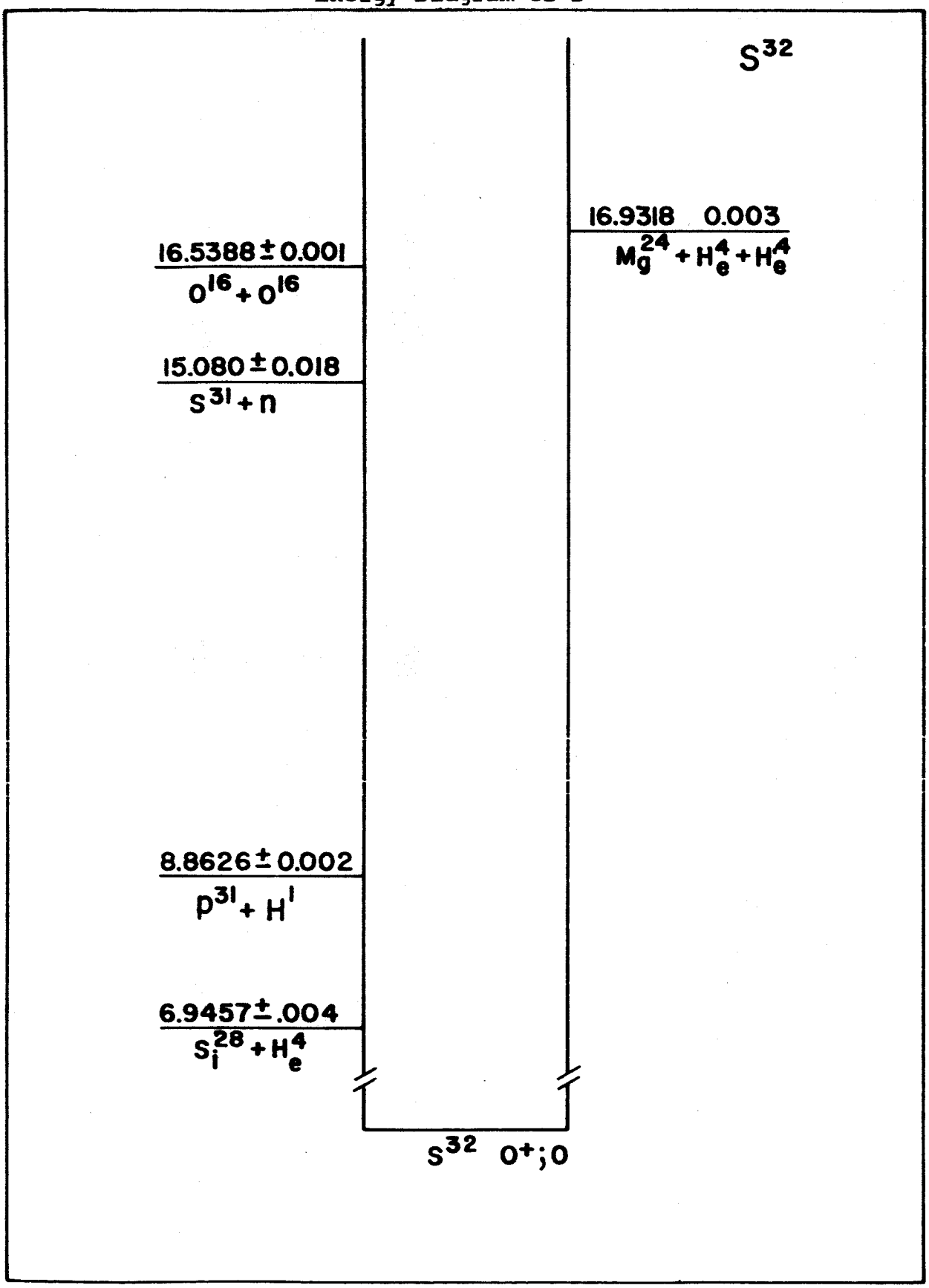

$$Ne^{20} + \gamma \rightarrow O^{16} + He^{4}$$

The experimental situation has been analyzed in the chapter on helium thermonuclear reactions. The rate of photodisintegration from the level at 5.64 Mev is:

$$\log_{10} P_{20\rightarrow 16+4}\,(5.64) = 12.7\begin{pmatrix}+0.2\\-0.5\end{pmatrix} - \frac{28.4}{T_9} \qquad (69)$$

while the level at 5.80 gives:

$$\log_{10} P_{20\rightarrow 16+4}\,(5.81) \simeq 13.40 - \frac{29.3}{T_9} \quad \text{within a factor of 10.} \qquad (70)$$

Below $T_9 = 1.3$, the 5.64 Mev level dominates the rate while in the region from 1.3 to 2.0, they become very similar. The total rate is given in Table 14. The uncertainty is about a factor three in the low temperature range and (due to the uncertainty in the second level) grows to about a factor of five in the higher temperature range. The effect of electron screening is negligible.

The alpha coming out could be captured by some of the constituents of the gas (O^{16}, Ne^{20}, Mg^{25} are probably the best represented isotopes at this point in the game). Of these Ne^{20} has by far the largest cross section (by a factor of about ten). Hence, the most frequent set of reactions will be represented by:

$$2Ne^{20} \rightarrow O^{16} + Mg^{24} \qquad Q = 4.583 \text{ Mev.}$$

The two reactions involved will almost always be in equilibrium, hence, the energy generation rate will be given by the photo-disintegration rate:

$$\mathcal{E}_{Ne} = 10^{17.13} (P_{20 \rightarrow 16+4}) \chi_{20} = \chi_{20} \mathcal{E}_0 \left(\frac{T}{T_0}\right)^n \tag{71}$$

The values of $\mathcal{E}_0$ and n are given in Table 14.

The carbon burning stage generates elements in the range A = 20 to 27. Detailed calculations indicate that Ne^{20} would retain its preponderance over its neighbors, but it is doubtful whether Mg^{24} would be much more abundant than Mg^{25} or Mg^{26}. The neon-burning, on the other hand, would be an important source of Mg^{24}, most likely the dominant one. The oxygen-burning is responsible for the isotopes in the range A = 25-32, with a strong peak at Si^{28}, most likely strong enough to make it preponderant over the background of the isotope-curve.

It does seem, then, that the alpha process of Burbidge, Burbidge, Fowler and Hoyle (Burbidge 1957) could be responsible for isotopes 36-46 but may not be the main source of the isotopes 24, 28, and 32.

The carbon-burning gives rise to a neutron flux which is strong enough to produce large amounts of metals in over-abundance. Such a process could be an important mechanism for

heavy-nuclei building.

Table 14

Energy Generation from C + C, O + O and Ne

T_9	$C_{12}+C_{12}$ ε_0	$C_{12}+C_{12}$ n	$O_{16}+O_{16}$ ε_0	$O_{16}+O_{16}$ n	$Ne+\gamma$ ε_0	$Ne+\gamma$ n
0.4	5(-6)	38				
0.45	3(-4)	36				
0.50	1(-2)	35				
0.55	3(-1)	34				
0.60	5	32				
0.65	5(1)	32				
0.70	5(2)	31				
0.75	4(3)	30				
0.80	2(4)	29	3(-8)	47	3(-6)	81
0.85	1(5)	29				
0.90	6(5)	28	5(-6)	45		73
0.95	3(6)	27				
1.0	9(6)	27	4(-4)	43	5(1)	65
1.05	3(7)	26				
1.1	1(8)	26	2(-2)	42	2(4)	59
1.15	3(8)	25				
1.2			6(-1)	40	4(6)	54
1.3	6(9)	24	1(1)	39	2(8)	50
1.4	3(10)	24	2(2)	38	9(9)	47
1.5	1(11)	23	2(3)	37	3(11)	44
1.6	5(11)	22	2(4)	36	4(12)	41
1.7	2(12)	22	1(5)	35	4(13)	38
1.8	6(12)	21	7(5)	34	3(14)	36

Table 14

T_9	$C_{12}+C_{12}$ ε_0	$C_{12}+C_{12}$ n	$O_{16}+O_{16}$ ε_0	$O_{16}+O_{16}$ n	$Ne+\gamma$ ε_0	$Ne+\gamma$ n
1.9	2(13)	21	4(6)	34	2(15)	34
2.0	5(13)	20	2(7)	33	2(16)	33
2.1	1(14)	20	7(7)	32		
2.2	3(14)	20	3(8)	31		
2.3	6(14)	19	1(9)	31		
2.4	1(15)	19	3(9)	30		
2.5	3(15)	19	9(9)	30		
2.6	5(15)	18	3(10)	29		
2.7	1(16)	18	7(10)	29		
2.8	2(16)	18	2(11)	28		
2.9	3(16)	17	4(11)	28		
3.0	5(16)	17	1(12)	27	2(21)	22

6. Neutrinos in the Late Stages of Stellar Evolution

6.1 Neutrinos from the Urca Process

One factor which will play an ever more important role in the energy balance of stars is the emission of neutrinos. As we saw before, in the hydrogen burning phase, at most ten per cent of the energy was carried away by neutrinos. In the helium burning reactions no neutrinos were emitted accompanying the formation of carbon, oxygen or neon. However, another mechanism was becoming increasingly operant, the so-called Urca process of Gamow and Schonberg (1941). One isotope of the gas can capture an electron and decay into a new isotope with the emission of an anti-neutrino. The new isotope is unstable and would soon beta-decay to the original nucleus with the emission of a neutrino, and the process could start again. At every round of the game the star loses a pair of neutrino - anti-neutrinos. Such a process represents a leak through which the star could in principle lose energy at a very high rate. In reality the energy loss depends on the electron capture rate, hence, on the temperature and also on the actual

Figure 28

isotopic abundances of the gas. More exactly it depends to a very high degree on the presence of some special nuclei which differ very little in mass from another (unstable) nucleus into which they can be transformed by a weak interaction. In that case an electron of very small energy could generate the transformation. Since low energy electrons are well represented in a Maxwell-Boltzman or Fermi distribution, the rate would be correspondingly higher. In Figure 28 we have described the best Urca nucleus (He^3).

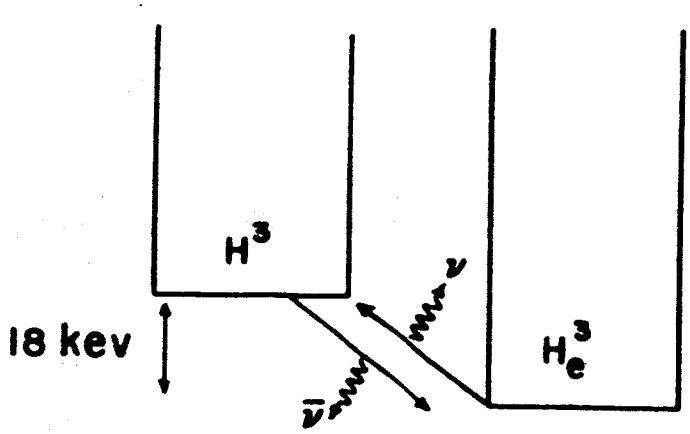

Ordinary Urca Process

The mass difference between a tritium nucleus plus an electron and a helium nucleus is only 18 Kev. At a temperature of $T_8 = 1$ the value of kT is $\sim$ 9 Kev, hence, the mean kinetic energy is about 14 Kev. Other privileged nuclei are N^{14} (150 Kev), S^{33} (249 Kev) and Cl^{35} (167 Kev). Unfortunately, at the temperatures where the process could become important He^3 has completely disappeared and the C^{14} formed by the electron capture on N^{14} decays too slowly back to the original state (life-time of 5600 years). The stellar abundance of Cl^{35} and S^{33} is not known, but these isotopes could well catalyse a large production of neutrinos shortly after the end of the helium burning stage.

These neutrino producing processes can be further enhanced by the stellar heat. Consider a beta-unstable nucleus, newly formed, e.g., by the Urca process, waiting for its lifetime to run out. By a thermal collision it can be excited in a higher state, out of which it can beta-decay back directly to the original nucleus with a possibly highly reduced lifetime, thereby decreasing the period of the cycle and increasing its energy output (see Figure 29). Consider next a nucleus which has a beta-stable ground state but a low energy beta-unstable excited state. From Figure 29

Figure 21

it is easy to see how such a nucleus could itself participate in the process under investigation.

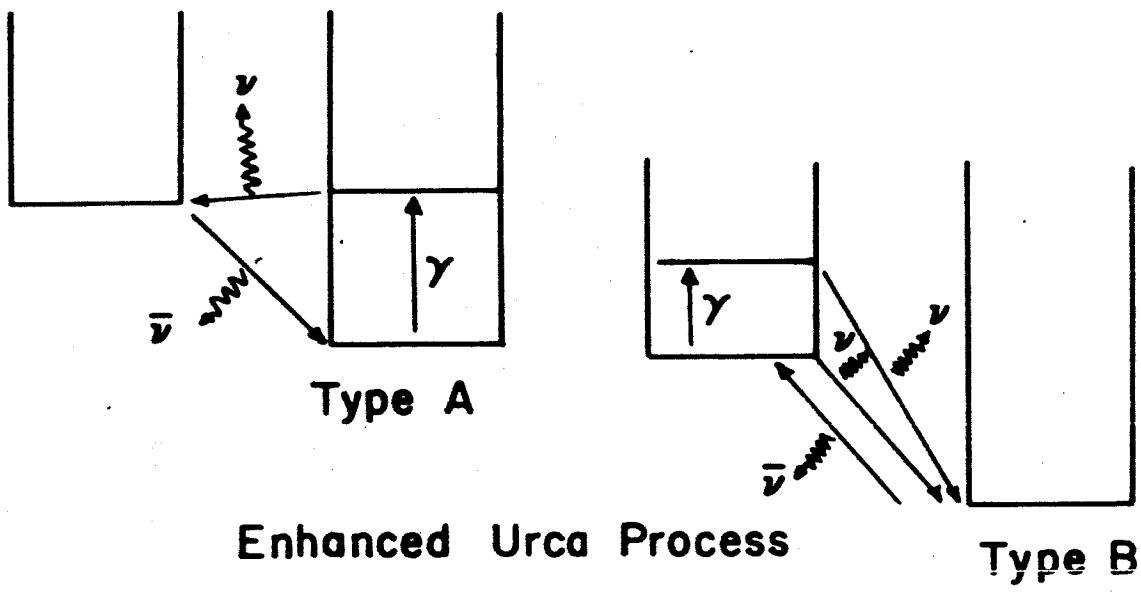

In Chiu (1961a) one finds a table illustrating the Urca energy loss for various elements. The rate of energy loss in ergs per gm-sec, in a gas entirely made of a given element i (i.e. $x_i = 1$), is given at various temperatures. In this work, Chiu had not considered the possible enhancement of the Urca process. Hence, the rate of energy loss becomes "saturated" when the time for electron capture becomes much smaller than the time for beta-decay.

The enhancement of the Urca process (the photo-beta

reaction) is treated in Cameron (1959a). He shows that the life-time of certain beta-decaying nuclei can be shortened by several orders of magnitude, thereby postponing the onset of saturation.

In the next section we shall describe other modes of neutrino emission. The modes turn out to be much more important than the Urca process for just about any realistic conditions of temperature, density and chemical composition. However, as it turns out, there is still a slight aura of doubt surrounding the existence of the newly discovered neutrino processes, the Urca process should be kept in the background

6.2 Neutrinos from Weak Interaction Processes

Experiments of recent years have called for an overhaul of the classical beta decay theory. A new formalism has been put forward by a number of theorists, in particular, by Feynman and Gell-Mann (1958).

The form of the theory suggests the possibility of a direct interaction between electrons and neutrinos even in the absence of nucleons (Pontecorvo 1959).

Indeed, in this theory (called the universal Fermi interaction), the transition amplitude is written down as:

$$J = (e, \bar{\nu}_e) + (p, \bar{n}) + (\mu, \bar{\nu}_\mu) \tag{72}$$

In the jargon of quantum mechanics, this means that the transition probability formula, $P = J^* J$, should describe all the processes made possible by the weak interaction. In other words, we should observe in nature the processes

$(\nu_e, \bar{e})(e, \bar{\nu}_e)$, $(\nu_\mu, \bar{\mu})(e, \bar{\nu}_e)$, $(\nu_\mu, \bar{\mu})(p, \bar{n})$ etc.

And with due regard to kinetic variables, the probability of each such process should be the same.

So far in laboratories, only the cross term $(n, \bar{p})(e, \bar{\nu}_e)$ (for instance, $n \rightarrow p + e^- + \bar{\nu}$, the decay of the neutron),

$(\bar{\nu}_\mu, \mu)(e, \bar{\nu}_e)$ (i.e. $\mu \to e + \nu_e + \nu_\mu$, the decay of the muon), and $(n, \bar{p})(\mu, \bar{\nu}_\mu)$ (i.e. $p + \bar{\mu} \to n + \nu_\mu$, the muon capture) have been observed. Their transition probabilities are as predicted by the theory. None of the square terms have been observed so far, which, indeed, is not a drawback for the theory; their cross sections are too small for present technologies.

We shall assume that these square terms actually represent real physical processes. Such an assumption is most probably correct, although it is not easy to evaluate its degree of validity. Later we shall discuss how a confirmation of its validity may actually come from astrophysical observations.

In particular, we concentrate our attention on the first square terms, i.e. we assume the existence of a direct weak interaction between electrons and neutrinos. We look at two different groups of processes; group A involves the fundamental process:

$$e^- \to e^- + \nu + \bar{\nu} \qquad \text{(A)}$$

For energy momentum considerations this process will always

require another particle. We shall have:

$\gamma + e^- \rightarrow e^- + \nu + \bar{\nu}$	photoneutrinos	A 1
$e^- + e^- \rightarrow e^- + e^- + \nu + \bar{\nu}$		A 2
$e^- + (Z,A) \rightarrow e^- + (Z,A) + \nu + \bar{\nu}$	bremstrahlung	A 3

The second group (B) involves the reaction:

$e^- + e^+ \rightarrow \nu + \bar{\nu}$	(actually or virtually).	
$e^- + e^+ \rightarrow \nu + \bar{\nu}$	pair annihilation neutrinos	B 1
$\gamma + \gamma \rightarrow (e^+ + e^-) \rightarrow \nu + \bar{\nu}$		B 2
$\gamma + \gamma \rightarrow (e^+ + e^-) \rightarrow \gamma + \nu + \bar{\nu}$		B 3
$\gamma + (Z,A) \rightarrow (Z,A) + \nu + \bar{\nu}$		B 4
plasmon $\rightarrow \nu + \bar{\nu}$		B 5

The process B 2 is absent if the weak interaction is a local interaction and if there is no intermediate boson (Gell-Mann 1961). Even if the intermediate boson exists the cross section is expected to be vanishingly small. We shall not consider it.

The rate for the processes A 1, A 3, B 1, B 4 and B 5 have been computed (Chiu and Stabler 1961), (Ritus 1962), Gandel'man and Penaev 1960) (Chiu 1961b) (Matinyan and

Tsilosani 1962) (Adams, Ruderman, Woo 1962). A 2 is presently being computed; preliminary results show that it is of less importance than the other processes. B 3 has been evaluated approximately (Chiu and Morrison 1960). It also seems to be of less importance.

Of course, these rates are functions of the density and the temperature. For astrophysical discussion we shal consider the region of the ρ-T plane defined by the following inequalities:

$$10^2 < \rho < 10^8 \text{ gr/cm}^3$$
$$10^8 < T < 5 \times 10^9 \text{ gr/cm}^3$$

At such temperatures all the stellar constituents have atomic numbers equal or larger than 4. Hence, we have $A/Z \simeq 2$. So, the mean number of nucleons per electron $(\mu_e) \simeq 2$.

In this range, three main processes are dominant: A 1, B 1 and B 5. In Figure 30 their respective domains are roughly delineated.

B 5 (plasma neutrinos) takes over the low T-high ρ part of the range; it is far less affected by the onset of degeneracy than any of the other processes. This

Figure 30

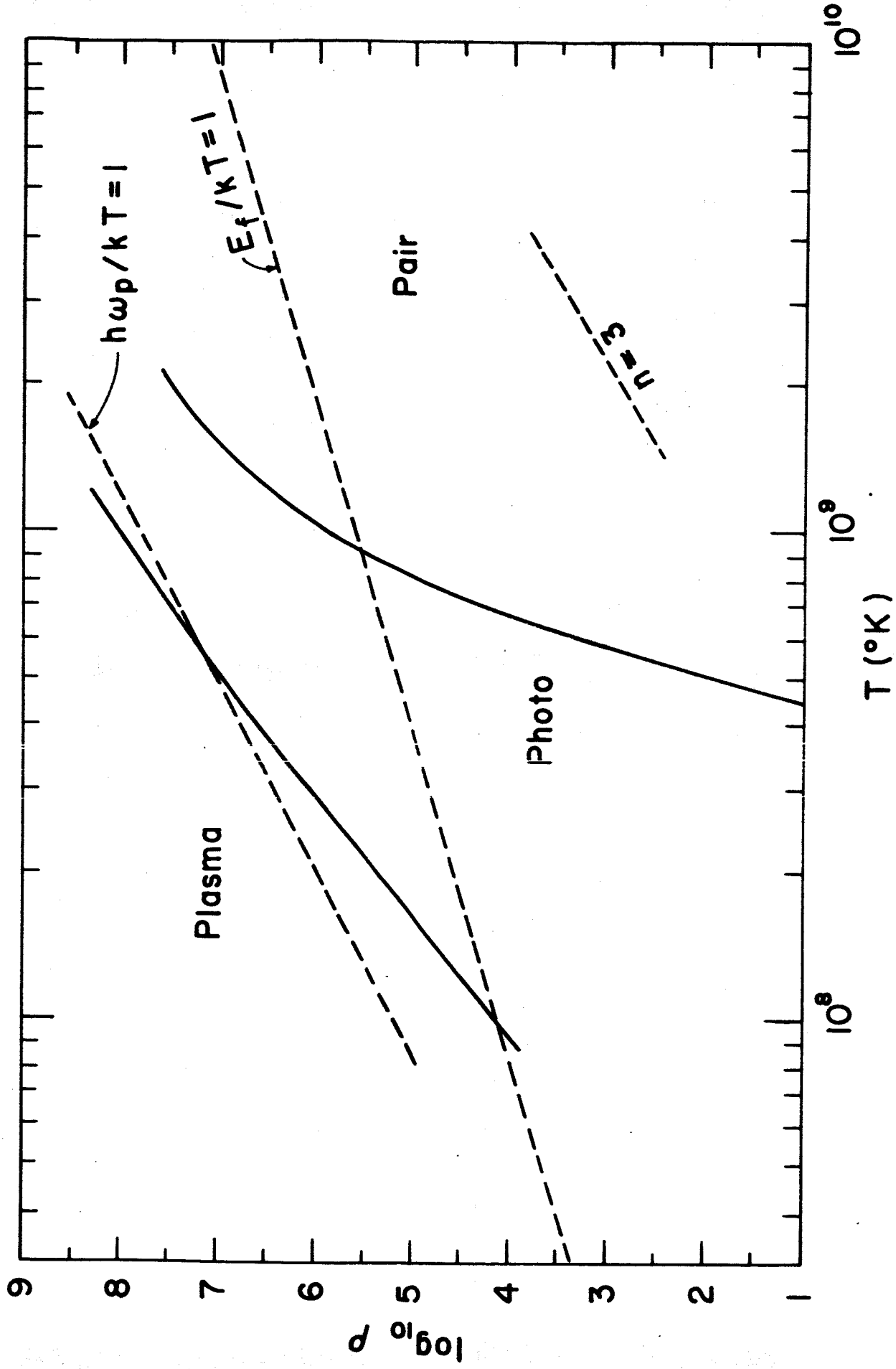
$h\omega_p/kT=1$
$E_f/kT=1$
Pair
$n=n$
Photo
Plasma
10^8
10^9
10^{10}
T (°K)
1
2
3
4
5
6
7
8
9
$\log_{10} \rho$

process can be described as resulting from the interaction of electromagnetic waves with an ionized gas. The coupled system then has a normal mode (plasmon) whose frequency a_p is greater than $\frac{2\pi}{\lambda}c$ where λ is the wavelength, i.e. it acts like a particle with non-zero mass. In particular, it can decay into a $\nu - \bar{\nu}$ pair with energy-momentum conservation.

Although neutrinos are generated by the action of both transverse and longitudinal electromagnetic waves, the first type is more effective in our range of physical conditions.

The computation of the rate is too involved to be repeated here. We shall merely quote the results together with some useful approximations.

One important parameter is ω_p, the natural frequency of the plasma. For a completely degenerate gas:

$$\left(\frac{\hbar\omega_p}{m_e c^2}\right) \simeq \frac{4\alpha x_f^3}{3\pi(1+x^2)^{1/2}} \tag{73}$$

where x_f is the Fermi momentum in units of $m_e c\,[x_f^3 \simeq 1.02\times 10^{-6}(\rho/\mu_e)]$, and α is the fine structure constant. Numerically:

$$\frac{\hbar\omega_p}{m_e c^2} = 5.62\times 10^{-5}(\rho/\mu_e)^{1/2}\left[1+1.01\times 10^{-4}(\rho/\mu_e)^{2/3}\right]^{-1/4} \tag{74}$$

We shall also use:

$$\frac{\hbar\omega_p}{kT} = \frac{3.34\times10^{-4}}{T_9}(\rho/\mu_e)^{1/2}\left[1+1.01\times10^{-4}(\rho/\mu_e)^{2/3}\right]^{-3/4} \quad (75)$$

and $(kT/m_e c^2) = 0.169\, T_9$

For $T_9 < 5$ the plasma frequency is quite insensitive to the temperature; accordingly these formulae remain approximately valid even in partially degenerate gases.

The rate is given by:

$$\varepsilon_{B5} = \frac{2.96\times10^{22}}{\rho}\left(\frac{\hbar\omega_p}{m_e c^2}\right)^6\left(\frac{kT}{m_e c^2}\right)^3 \text{ ergs/gm sec for } \frac{\hbar\omega_p}{kT} \ll 1 \quad (76)$$

and

$$\varepsilon_{B5} = \frac{1.54\times10^{22}}{\rho}\left(\frac{\hbar\omega_p}{m_e c^2}\right)^{7.5}\left(\frac{kT}{m_e c^2}\right)^{1.5}\exp\left[-\hbar\omega_p/kT\right] \text{ ergs/gm sec} \quad (77)$$

for $\frac{\hbar\omega_p}{m_e c^2} \gg 1$ (see Figure 30).

The intermediate region has not been investigated adequately. However, a first approximation can be obtained by a smooth joining of the curves.

Numerically we get

$$\varepsilon_{B5} = \frac{5.55\times10^{-7}\rho^2 T_9^3}{\left[1.+0.63\times10^{-4}\rho^{2/3}\right]^{3/2}} \text{ for } \frac{\hbar\omega_p}{kT} \ll 1 \quad (78)$$

$$\varepsilon_{B6} = \frac{10^{-12}\rho^{2.75}T_9^{1.5}e^{-\frac{\hbar\omega_p}{kT}}}{\left[1+0.63\times10^{-4}\rho^{2/3}\right]^{15/2}} \text{ for } \frac{\hbar\omega_p}{kT} \gg 1 \quad (79)$$

The temperature exponent n is always small. It has the value n = 3 in the region $\hbar\omega_p/kT < 1$, while in the region $\hbar\omega_p/kT > 1$ it gets slightly larger. Only for extreme conditions such as $T_9 < 0.2$, $\rho > 10^8$ does it ever reach values larger than five or six.

Next we have to investigate the photoneutrino mechanism. The probability of the photoneutrino process depends linearly on the density of the electron gas (provided the electrons are non-degenerate). It depends very strongly on the temperature, since both the density of the photon gas and the phase space available to the outgoing neutrinos are rapidly increasing with the temperature.

The detailed calculation is too complicated to be reproduced here. We shall only quote a result valid in the non-degenerate non-relativistic range. We define $\mathcal{E}^{\nu}_{A1}$ as the rate of neutrinic energy generation per gram per sec. from photoneutrino processes.

Then:

$$\mathcal{E}^{\nu}_{A1} = 10^{7.7}\, T_9^{3}\ \mathrm{erg\ gm^{-1}\ sec^{-1}} \tag{80}$$

Because of the definition of $\mathcal{E}^{\nu}_{A1}$ we do expect this

TABLE 15

NEUTRINO RATES (NON DEGENERATE)

T_9	photo	pair		range	T_9	photo	pair		range
	$\log_{10}(\mathcal{E}_{Ai})$	$\log_{10}(\mathcal{E}_{Bi})$	n	$[\log \rho_c]$		$\log_{10}(\mathcal{E}_{Ai})$	$\log_{10}\mathcal{E}_{Bi}$	n	$[\log \rho_c]$
0.2	2.1			4.6	1.4	8.9	16.1	13	6.0
0.3	3.5	0		4.8	1.6	9.3	16.8	12	6.4
0.4	4.5	4.70	32	5.0	1.8		17.4	11	
0.5	5.3	7.7	27	5.2	2.0		17.9		6.8
0.6	5.9	9.7	23	5.4	2.5		19.0		7.0
0.7	6.5	11.2	20	5.4	3.0		19.7		7.5
0.8	6.9	12.3	18	5.6	3.5		20.4		
0.9	7.3	13.2	16	5.6	4.0		21.0		
1.0	7.7	14.0	15	5.6	5.0		21.9		
1.2	8.3	15.2	14	5.8	6.0		22.6		

quantity to be independent of the density. In Table 15 values of $\mathcal{E}_{\nu}^{\nu}$ are given for several temperatures at which the photoneutrino rate may dominate over the pair annihilation process (if the density is high enough).

The effect of degeneracy would be to reduce the rate. Indeed, in the process A 1 the electron is expected to change its momentum and hence its cell of momentum space. Degeneracy, however, implies that very few cells are still available, except at higher energies. This cuts considerably the total probability of a reaction. Computations show, indeed, this effect. However, some ambiguities have recently appeared between different computations, so that the results cannot be used at the present time. A recalculation is being made and should soon be available.

The third process of importance is the pair annihilation neutrino process, (B 1). It owes its presence to the existence of electron-positron pairs in the gas. These pairs are themselves created by the gamma rays populating the high energy tail of the black body radiation. As the temperature is increased, the number of these photons increases enormously ($\sim T^3$) and so does the equilibrium concentration of the positron-electron gas. A small fraction

of the ensuing recombination results in the neutrino - anti-neutrino pairs:

$$\gamma + \gamma \rightarrow (e^+ + e^-) \rightarrow \nu + \bar{\nu}$$

In a vacuum, the neutrino energy output <u>per unit volume</u> would be a function of the temperature <u>only</u> (since the population of photons is a function of T only) and again, a very steep function for reasons similar to those given in the discussion of the A 1 process.

We shall derive approximately (Chiu and Morrison 1960) the expression for $\mathcal{E}^{\nu}_{B1}$ as this derivation illustrates the nature of the processes involved. For electrons of energies less than $m_e c^2$ (0.5 Mev) the probability of the reaction $e^+ + e^- \rightarrow \nu + \bar{\nu}$ per unit pair of electron and positron per cm^3 is almost independent of energy:

$$P_{B1} \simeq 1.35 \times 10^{-34} \, sec^{-1} cm^{-3} \tag{81}$$

Each reaction releases about 2 $m_e c^2$ in the form of neutrinos. Hence, the total rate of energy generation should be given by:

$$E \propto \int P_{B1} (2 m_e c^2) \times N_{e^-}(p_-) \times N_{e^+}(p_+) \, d^3p_+ d^3p_- \tag{82}$$

The population of electrons or positrons in a vacuum can be found from statistical thermodynamics. Since these are fermions we have:

$$N(p)d^3p = \frac{2d^3p}{h^3[e^{+(\alpha+E/kT)}+1]} \tag{83}$$

Now we need not impose the restriction that N (their total number) be constant (it is a function of T). Hence, we set $\alpha = 0$. Further, since these particles can be annihilated, we must use for E the total $E^2 = (p^2c^2 + m_e{}^2c^4)$. Defining $\chi = p/m_ec^2$ and $\beta = m_ec^2/kT$, we have

$$\int Ne^-(p_-)d^3p_- = \frac{1}{\pi^2}\left(\frac{\hbar}{m_ec}\right)^{-3} f(\beta) \tag{84}$$

with

$$f(\beta) = \int_0^\infty \exp[-\beta(1+\chi^2)^{1/2}]\chi^2 dx \tag{85}$$

If β is large (as will be the case for $T_9 \lesssim 3$), the integrand decreases very rapidly with increasing χ. Indeed, most of its value comes from $\chi < 1$. So we can expand:

$$(1+\chi^2)^{1/2} \simeq 1 + \frac{\chi^2}{2} - \frac{\chi^4}{8} + \ldots \tag{86}$$

and keep only the first terms:

$$f(\beta) = \frac{\sqrt{\pi}}{4}\left(\frac{2}{\beta}\right)^{3/2} e^{-\beta} \qquad \beta > 1 \tag{87}$$

$\mathcal{E}^{\nu}_{BI}$ becomes:

$$\mathcal{E}^{\nu}_{BI} = \frac{P_{BI}(2m_ec^2)\,f^2(\beta)}{\rho\pi^4(\hbar/m_ec)^6} = \frac{10^{18.7}e^{-2m_ec^2/kT}}{\rho}\,T_9^3 \quad \text{(vacuum)} \tag{88}$$

We note that $\mathcal{E}$ is actually a decreasing function of the density. This explains why it gets dominated by the photoneutrinos in the high density range.

The previous discussion was restricted to a vacuum. What happens if we introduce a gas of matter in the box? The answer depends upon the state of degeneracy of the gas. A non-degenerate gas will not modify the rate of neutrinic energy production; true enough the electron gas will reduce the equilibrium concentration of positrons but it will not affect the rate of creation of positrons and, also, the rate of annihilation since both are (by definition of equilibrium) equal. Hence, the neutrino energy output per unit volume is independent of the density of the gas, provided again that the density corresponds to a state of non-degeneracy.

The presence of degenerate electrons will hinder the

formation of electron-positron pairs, and consequently decrease the output of neutrinos. Extensive calculations have been made all through the relevant range of density and temperature. Table 16 reproduces some of the results (Chiu 1961).

TABLE 16

PAIR ANNIHILATION NEUTRINO ENERGY YIELD

(ϵ_ν^a) in erg/gm-sec.

	← $\log_{10}\rho$ (gr/cm^3) →							
T_9	2	3	4	5	6	7	8	9
0.3								
0.4								
0.5	5.7	4.7	3.7	2.6	1.2			
0.6	7.7	6.7	5.7	4.6	3.3	0.3		
0.7	9.2	8.2	7.2	6.1	4.9	2.3		
0.8	10.3	9.3	8.3	7.3	6.1	3.8		
0.9	11.2	10.2	9.2	8.2	7.0	5.0	0	
1.0	12.0	11.0	10.0	9.0	7.8	5.9	1.5	
1.2	13.2	12.2	11.2	10.2	9.1	7.4	3.7	
[illegible]	[illegible]	[illegible]	[illegible]	[illegible]	[illegible]	8.5	5.4	
1.6	14.8	13.8	12.8	11.8	10.8	9.4	6.6	0.4
1.8	15.4	14.4	13.4	12.4	11.4	10.1	7.6	2.1
2.0	15.9	14.9	13.9	12.9	11.9	10.7	8.4	3.5
2.5	17.0	16.0	15.0	14.0	13.0	11.8	10	6.1
3.0	17.7	16.7	15.7	14.7	13.7	12.7	11.1	7.9

6.3 Neutrinos and Stellar Evolution

The intensity of neutrino emission in the temperature range above a few hundreds of millions of degrees is quite remarkable (see Figure 3). If we realize that the sun pours out 2 erg/gm-sec and that the most brilliant steady stars yield only a few thousand times more optical photons, we see that neutrino emission may be of paramount importance during the late stages of the life of a star. Supernovae do reach luminosities of 10^{10} erg/gm/sec and novae 10^{6} erg/gm/sec, but only for very short periods of time (hours to days) denoting highly unstable situations.

The effect on stellar evolution of neutrino emitting [illegible] are far from being well understood.

Through the virial theorem (which applies to photons and neutrino emission as well) we learn that to every quantum of energy emitted there must correspond a quantum of energy to be used in increasing the interal (kinetic) energy of the star.

In a non-degenerate core (for a stellar mass exceeding the solar mass) this growth in the thermal energy raises the temperature. The specific effect of these neutrino processes

is then to accelerate the contraction rate and hence to shorten the life of the star (that is, compared to what would be the case if these mechanisms were inactive).

On the nuclear burning of the remaining isotopes the neutrino emission has the following effect: as discussed before, contraction of a star can be halted only if the nuclear energy generation is high enough to provide the energy requirement of the star, and will be halted at the temperature where such a condition is met. For a specific nuclear fuel this temperature range can be obtained by comparing the rate of nuclear energy generation from this fuel with the rate of neutrino and photon emission. The temperature range will be much higher than it would have been in a case of pure photonic emission. The equivalent burning stage would be postponed until this higher temperature is reached.

Experimental evidence for or against the existence of neutrino emission from a direct coupling between electrons and neutrinos (such as discussed in the beginning of this chapter) may actually come from astrophysics.

The plasma neutrinos appear to be intense enough to

influence even the helium burning stage. Hayashi and Cameron (1962) have recently discussed models of carbon burning red supergiants with and without neutrino emission. Reeves (1962b) has investigated crudely the effect of the neutrino emission on carbon, oxygen and neon stages. Finally, we expect the supernovae explosion and cooling to be highly influenced by neutrino losses.

Although the present neutrino emission hypothesis seems to rest on fairly safe ground, we would have to reject it should improved models persistently find better agreement with experimental results when the neutrinos from such processes are ignored. In the meantime experimental physicists are busy preparing a crucial experiment; the scattering of anti-neutrinos from a reactor of electrons. Detection of scattered electrons would confirm the validity of our assumption.

7. More Thermonuclear Reaction Rates

In this section we shall consider a number of nuclear reactions which are of interest especially for studies of nucleosynthesis. For instance, the reactions:

$$Li^6 + H^1 \rightarrow He^3 + He^4$$
$$Be^9 + H^1 \rightarrow Li^6 + He^4$$
$$B^{10} + H^1 \rightarrow Be^7 + He^4$$
$$B^{11} + H^1 \rightarrow Be^8 + He^4$$

are most important for the theories of the origin of the solar system, (Cameron 1962; Fowler, Greenstein and Hoyle 1962; Bashkin and Peaslee 1961). While the reactions:

$$C^{13} + He^4 \rightarrow O^{16} + n$$
$$H^1 + Ne^{20} \rightarrow Na^{21} + \gamma$$
$$Ne^{21} + He^4 \rightarrow Mg^{24} + n$$

are expected to provide neutron fluxes for the formation of heavy elements (Clayton, Fowler, Hull and Zimmerman 1961). The reaction $N^{14} + He^4 \rightarrow O^{17} + H^1$ may act as a trigger for the helium burning flash (Cameron 1959b). The parameters belonging to the proton reactions are given in Table 17.

They come mostly from the work of Salpeter (1955), Fowler (1959) and Fowler, Greenstein and Hoyle (1961). Most of them <u>have not been</u> revised during the course of the present work.

Three reactions involving He^4 ($C^{13} + He^4$, $N^{14} + He^4$, $N^{15} + He^4$) have been recomputed by Thibaudeau (1962)*. The most recent data on the energy levels of F^{18} do allow the $N^{14} + He^4$ reaction to be resonant through the 4.651 Mev level. Consequently the rate given here is much larger than the rate given in Burbidge, Burbidge, Fowler and Hoyle (Table 18 and Table 19). Other helium reactions have been listed in Tables 18 and 19; they come from Salpeter (1955) or Burbidge, Burbidge, Fowler and Hoyle (1957).

*Some of these rates are taken from a recent analysis of Dr. G. R. Caughlan.

Table 17

REACTION	REDUCED MASS $M = \frac{A_1 A_2}{A_1 + A_2}$ a.m.u.	$Z_1 Z_2 \sqrt{M}$	$\frac{E_o}{T_6^{2/3}} = 1.220 (Z_1^2 Z_2^2 M)^{1/3}$ (kev)	$\frac{\Delta E_o}{T_6^{5/6}} = 0.75 (Z_1^2 Z_2^2 M)^{1/6}$ (kev)
$H^1 + Li^6 \rightarrow He^3 + He^4$, $\rightarrow Be^7 + \gamma$	0.8635 ± 0.0001	2.7877 ± 0.0002	2.42	1.1
$H^1 + Be^9 \rightarrow Li^6 + He^4$, $\rightarrow B^{10} + \gamma$	0.90675 ± 0.00009	3.8089 ± 0.0002	2.98	1.2
$H^1 + B^{10} \rightarrow Be^7 + He^4$, $\rightarrow C^{11} + \gamma$	0.91595 ± 0.00008	4.7853 ± 0.0002	3.47	1.3
$H^1 + B^{11} \rightarrow Be^8 + He^4$, $\rightarrow C^{12} + \gamma$	0.92360 ± 0.00006	4.8052 ± 0.0002	3.48	1.3
$H^1 + O^{18} \rightarrow N^{15} + He^4$, $\rightarrow F^{19} + \gamma$	0.95469 ± 0.00002	7.8167 ± 0.0001	4.81	1.5
$H^1 + F^{19} \rightarrow O^{16} + He^4$, $\rightarrow Ne^{20} + \gamma$	0.95736 ± 0.00004	8.8060 ± 0.0002	5.20	1.6
$H^1 + Ne^{20} \rightarrow Na^{21} + \gamma$	0.95976 ± 0.00003	9.7968 ± 0.0002	5.59	1.6
$H^1 + Ne^{21} \rightarrow Na^{22} + \gamma$	0.96197 ± 0.00006	9.8080 ± 0.0003	5.59	1.6
$H^1 + Ne^{22} \rightarrow Na^{23} + \gamma$	0.96397 ± 0.00003	9.8182 ± 0.0002	5.60	1.6

Table 17

REACTION	REDUCED MASS	$Z_1 Z_2 \sqrt{M}$	$\frac{E_o}{T_6}^{2/3} =$	$\frac{\Delta E_o}{T_6}^{5/6} =$
	$M = \frac{A_1 A_2}{A_1 + A_2}$ a.m.u.		$1.220 (Z_1^2 Z_2^2 M)^{1/3}$ (kev)	$0.75 (Z_1^2 Z_2^2 M)^{1/6}$ (kev)
$H^1 + Na^{23} \rightarrow Ne^{20} + He^4$; $Ne^{20} \rightarrow Mg^{24} + \gamma$	0.96581 ± 0.00005	10.8103 ± 0.0003	5.97	1.7

Table 17

REACTION		$B_6 = 42.483(Z_1^2 Z_2^2 M)^{1/3}$	$2\pi\eta E^{1/2}$ (kev) = $31.285(Z_1^2 Z_2^2 M)^{1/2}$	Q VALUE (KEV)
$H^1 + Li^6$	$He^3 + He^4$	84.149 ± 0.005	87.21 ± 0.01	4021.9 ± 1.0
	$Be^7 + \gamma$			5609.3 ± 1.4
$H^1 + Be^9$	$Li^6 + He^4$	103.615 ± 0.004	119.16 ± 0.01	2124.7 ± 0.9
	$B^{10} + \gamma$			6587.2 ± 1.0
$H^1 + B^{10}$	$Be^7 + He^4$	120.640 ± 0.003	149.71 ± 0.02	1146.8 ± 1.0
	$C^{11} + \gamma$			8691.1 ± 3.1
$H^1 + B^{11}$	$Be^8 + He^4$	120.974 ± 0.003	150.33 ± 0.02	8586.4 ± 1.1
	$C^{12} + \gamma$			15955.87 ± 0.44
$H^1 + O^{18}$	$N^{15} + He^4$	167.327 ± 0.002	244.55 ± 0.03	3980.4 ± 0.9
	$F^{19} + \gamma$			7992.2 ± 0.7
$H^1 + F^{19}$	$O^{16} + He^4$	181.164 ± 0.003	275.50 ± 0.03	8114.0 ± 0.7
	$Ne^{20} + \gamma$			12843.93 ± 0.7
$H^1 + Ne^{20}$	$Na^{21} + \gamma$	194.510 ± 0.002	306.49 ± 0.04	2454 ± 3.0
$H^1 + Ne^{21}$	$Na^{22} + \gamma$	194.658 ± 0.004	306.85 ± 0.04	6743.0 ± 4.9
$H^1 + Ne^{22}$	$Na^{23} + \gamma$	194.793 ± 0.002	307.17 ± 0.04	8790.1 ± 1.5
$H^1 + Na^{23}$	$Ne^{20} + He^4$	207.704 ± 0.004	338.20 ± 0.04	2378.7 ± 1.5
	$Mg^{24} + \gamma$			11692.6 ± 2.2

Table 17

REACTION	S(0) (kev-barns)	A $p/\rho\lambda_1 = Afg\exp(-B/T_6^{1/3})T_6^{-2/3}$	$g = (1 + UT_6^{1/3})$ U (U = 5/12B)	f Electron Screening Factor
$H^1 + Li^6 \rightarrow He^3 + He^4$, $\rightarrow Be^7 + \gamma$	5.06×10^3	5.96×10^{12}	4.95×10^{-3}	$(1 + 0.75\rho^{1/2}/T^{3/2})$
$H^1 + Be^9 \rightarrow Li^6 + He^4$, $\rightarrow B^{10} + \gamma$	3.01×10^4	3.84×10^{13}	4.02×10^{-3}	$(1 + 1.00\rho^{1/2}/T^{3/2})$
$H^1 + B^{10} \rightarrow Be^7 + He^4$, $\rightarrow C^{11} + \gamma$	1.79×10^4	2.45×10^{13}	3.45×10^{-3}	$(1 + 1.25\rho^{1/2}/T^{3/2})$
$H^1 + B^{11} \rightarrow Be^8 + He^4$, $\rightarrow C^{12} + \gamma$	8.99×10^4	1.23×10^{14}	3.44×10^{-3}	$(1 + 1.25\rho^{1/2}/T^{3/2})$
$H^1 + O^{18} \rightarrow N^{15} + He^4$, $\rightarrow F^{19} + \gamma$	10^5	1.5×10^{14}	2.49×10^{-3}	$(1 + 2.00\rho^{1/2}/T^{3/2})$
$H^1 + F^{19} \rightarrow O^{16} + He^4$, $\rightarrow Ne^{20} + \gamma$	10^6	1.5×10^{15}	2.30×10^{-3}	$(1 + 2.25\rho^{1/2}/T^{3/2})$
$H^1 + Ne^{20} \rightarrow Na^{21} + \gamma$	55 ± 20	9.33×10^{10}	2.14×10^{-3}	$(1 + 2.50\rho^{1/2}/T^{3/2})$
$H^1 + Ne^{21} \rightarrow Na^{22} + \gamma$	> 5.6	$> 10^{10}$	2.14×10^{-3}	$(1 + 2.50\rho^{1/2}/T^{3/2})$
$H^1 + Ne^{22} \rightarrow Na^{23} + \gamma$	≥ 550	$\geq 10^{12}$	2.14×10^{-3}	$(1 + 2.50\rho^{1/2}/T^{3/2})$

Table 17

REACTION	S(0) (kev-barns)	A $p/\rho\,\chi_1 = Afg\,\exp(-B/T_6^{1/3})\,T_6^{-2/3}$	$g = (1 + UT_6^{1/3})$ U (U = 5/12B)	f Electron Screening Factor
$H^1 + Na^{23} \rightarrow Ne^{20} + He^4$	3×10^3	5.3×10^{12}	2.01×10^{-3}	$(1 + 2.75\,\rho^{1/2}/T^{3/2})$
$H^1 + Na^{23} \rightarrow Mg^{24} + \gamma$	$> 10^4$	7.2×10^{13}		

Table 18

REACTION	$He^4 + C^{13} \rightarrow O^{17} + \gamma$, $\rightarrow O^{16} + n$	$He^4 + N^{14} \rightarrow F^{18} + \gamma$	$He^4 + N^{15} \rightarrow F^{19} + \gamma$
REDUCED MASS $M = \frac{A_1 A_2}{A_1 + A_2}$ a.m.u.	3.06150 ± 0.00011	3.11383 ± 0.00007	3.16053 ± 0.00011
$Z_1 Z_2 \sqrt{M}$	20.9966 ± 0.0004	24.7045 ± 0.0003	24.8890 ± 0.0004
$\frac{E_o}{T_8}^{2/3} = 26.3 (Z_1^2 Z_2^2 M)^{1/3}$	200	223	224
$\frac{\Delta E_o}{T_8}^{5/6} = 35 (Z_1^2 Z_2^2 M)^{1/6}$	96	101	101
$B_8 = 9.1527 (Z_1^2 Z_2^2 M)^{1/3}$	69.660 ± 0.001	77.637 ± 0.001	78.023 ± 0.001
$2\pi\hbar E^{1/2}$ (kev) $31.1285 (Z_1^2 Z_2^2 M)^{1/2}$	652.97 ± 0.08	768.86 ± 0.09	774.77 ± 0.09
Q value (kev)	6356.6 ± 1.1 ($O^{17} + \gamma$) 2214.5 ± 0.9 ($O^{16} + n$)	4403.9 ± 4.0	4011.8 ± 1.1

Table 19

$$\log_{10}\left(\frac{P_{13,4}}{\rho x_4 f_{13,4}}\right) = 17.1 - \frac{2}{3}\log T_8 - 30.24T_8^{-1/3}$$

$$\log_{10}\left(\frac{P_{20,4}}{\rho x_4 f_{20,4}}\right) = 19.8 - \frac{2}{3}\log T_8 - 43.73T_8^{-1/3} - 0.09T_8^{2/3}$$

$$\log_{10}\left(\frac{P_{24,4}}{\rho x_4 f_{24,4}}\right) = 20.7 - \frac{2}{3}\log T_8 - 49.8\,T_8^{-1/3} - 0.1\,T_8^{2/3}$$

$$\log_{10}\left(\frac{P_{28,4}}{\rho x_4 f_{28,4}}\right) = 22.0 - \frac{2}{3}\log T_8 - 55.6\,T_8^{-1/3} - 0.12T_8^{2/3}$$

T_8	$\log_{10}\left(\frac{P_{14,4}}{\rho x_4 f_{14,4}}\right)$	$\log_{10}\left(\frac{P_{15,4}}{\rho x_4 f_{15,4}}\right)$
0.8	-20.05	-23.82
1.0	-17.10	-19.26
1.1	-16.00	-17.55
1.2	-15.07	-16.13
1.5	-12.84	-13.00
2.0	-10.28	- 9.82
2.5		
3.0	- 6.91	- 6.17
4.0	- 4.92	- 3.85
5.0	- 3.62	- 2.30
6.0	- 2.66	- 1.18
8.0	- 1.43	0.34
10.0	- 0.47	1.32

(4.65-R-as)→

(4.65-R-20) ↔ (4.65-R-as)

(4.38-R-50)

(MANY-R-10)

(MANY-R-10)

TABLES

Table 1 Reactions involved in the proton-proton chains.

Table 2 Reactions involved in the CNO bi-cycle.

Table 3 Reactions involved in helium burning.

Table 4 Masses of the stable elements from A = 1 to 58.

Table 5 Useful parameters for computation of thermonuclear reaction rates.

Table 6 Parameters for the proton-proton chains.

Table 7 Parameters for the CNO bi-cycle.

Table 8 Rate of the $O^{17} + H^{1} \rightarrow N^{14} + He^{4}$ and total lifetime of the bi-cycle.

Table 9 Energy generation from the proton-proton branches.

Table 10 Energy generation from the CNO bi-cycle.

Table 11 Parameters for the helium thermonuclear reactions.

Table 12 Helium burning rates and energy generation.

Table 13 Reaction involved in $C^{12} + C^{12}$, $O^{16} + O^{16}$, and relevant nuclear parameters.

Table 14 Energy generation from $C^{12} + C^{12}$, $O^{16} + O^{16}$ and Ne^{20}.

Table 15 Non-degenerate neutrino rates.

Table 16 Pair annihilation neutrino rates, including degeneracy. (With Chiu 1961b.)

Table 17 Parameters for some secondary proton reactions.

Table 18 Parameters for some secondary He^{4} reactions.

Table 19 Rates for some secondary He^{4} reactions.

FIGURES

Figure 1 Overall energy generation rate.

Figure 2 Nuclear history of a star.

Figure 3 Average neutrino luminosity of a typical star.

Figure 4 Energy diagram of N^{14}.

Figure 5 Plot of the electron screening parameter (f'/f) as a function of D, the degeneracy parameter.

Figure 6 Energy diagram of Be^{7}.

Figure 7 Energy diagram of Be^{8}.

Figure 8 Energy diagram of B^{8}.

Figure 9 Energy diagram of N^{13}.

Figure 10 Energy diagram of O^{15}.

Figure 11 Energy diagram of O^{16}.

Figure 12 Energy diagram of F^{17}.

Figure 13 Energy diagram of F^{18}.

Figure 14 Isotopic abundances from the CNO bi-cycle normalized to $X_{CN} = 1$, or to $X_{CNO} = 1$. $(10 < T_6 < 35)$.

Figure 15 Same as Figure 14 with $(30 < T_6 < 100)$.

Figure 16 The neutrino spectrum from the sun.

Figure 17 Plot of $\Psi_{pp}(\alpha, w)$ for $X_4/X_1 = 2$ and $1/2$.

Figure 18 Plot of the parameter $\alpha/\left(X_4/4X_1\right)^2$ as a function of T_6.

Figure 19 Energy diagram of C^{12}.

Figure 20 Energy diagram of O^{16}.

Figure 21 Energy diagram of Ne^{20}.

Figure 22 Plot of the isotopic abundances at the end of the helium burning as a function of q_{16} and q_{20}. (See Equation 64.) X_{20} + heavier means the sum of $X_{20} + X_{24} + X_{28}$ etc.

Figure 23 Plot of $\frac{X_{16}}{X_{12}}$ as a function of X_4 for various values of q_{16} (assuming $q_{20} = 0$).

Figure 24 Plot of $q_{16}\rho$ and $q_{20}\rho$ as a function of T_8.

Figure 25 Plot of Ψ_α in Equation 64 as a function of X_4 and q_{16}, illustrating the influence of the $C^{12} + \alpha$ on the rate of energy generation from helium thermonuclear reactions.

Figure 26 Energy diagram of Mg^{24}.

Figure 27 Energy diagram of S^{32}.

Figure 28 Ordinary Urca process.

Figure 29 Enhanced Urca process (photobeta reaction).

Figure 30 Respective domains of the various neutrino processes. On the same graph are shown the lines $hw_p/kT = 1$, $E_f/kT = 1$, (bordering the region of degeneracy) and the slope of the $\rho \propto T^3$ function applicable to the interior of an $n = 3$ polytropic model.

REFERENCES

ADAMS, J. B.; RUDERMAN, M.A.; and WOO, C.H.	1962	U.C.R.L. 10343.
AJZENBERG-SELOVE, F., and STELSON, P.H.	1960	Phys. Rev., 120, 500.
ALBURGER, D.E.	1960	Phys. Rev., 118, 235.
	1961	Phys. Rev., 124, 193.
ALBURGER, D.E., and PIXLEY, R.W.	1960	Phys. Rev., 119, 1970.
ALMQVIST, E.; BROMLEY, D.A.; and KUEHNER, J.A.	1960	Phys. Rev., Letters, 4, 515.
BAHCALL, J.H.	1962	To be published.
	1963	Ap. J.
BASHKIN, S.; KAVANAGH, R.W.; and PARKER, P.D.	1959	Phys. Rev. Letters, 3, 518.
BASHKIN, S., and PEASLEE, D.C.	1961	Astrophys. J., 134, 981.
BLOOM, S.D.; TOPPEL, B.J.; and WILKINSON, D.H.	1957	Phil. Mag. 2, 57.
BRADFORD, E., and ROBSON, B.A.	1961	Nuclear Phys., 29, 442.
BROMLEY, D.A.; KUEHNER, J.A.; and ALMQVIST, E.	1960	Phys. Rev. Letters, 4, 365.
BROWN, R.E.	1962	Phys. Rev., 125, 347.
BURBIDGE, E.M.; BURBIDGE, G.R.; FOWLER, W.A.; and HOYLE, F.	1957	Rev. Mod. Phys., 29, 547.
BURGE, E.J., and PROWSE, D.J.	1956	Phil. Mag., 1, 912.
CAMERON, A.G.W.	1958	Chalk River Report CRL-41.
	1959a	Astrophys. J., 130, 452.
	1959b	Astrophys. J., 130, 916.
	1962	Icarus, 1, 13.
CAMERON, J.R.	1953	Phys. Rev. 90, 839.

CARLSON, R.R.	1961	Nuclear Phys., 28, 443.
CARTLEDGE, W.; MARCHANT, G.; and REEVES, H.	1962	To be published.
CAUGHLAN, G.R., and FOWLER, W.A.	1962	To be published.
CHIU, H.Y.	1961a 1961b	Ann. Phys., 15, 1. Phys. Rev., 123, 1040.
CHIU, H.Y., and MORRISON, P.	1960	Phys. Rev. Letters, 5, 573.
CHIU, H.Y., and STABLER, R.C.	1961	Phys. Rev., 122, 1317.
CHRISTY, R.F., and DUCK, I.	1961	Nuclear Phys., 24, 89.
CLAYTON, D.D.	1962	To be published.
CLAYTON, D.D.; FOWLER, W.A.; HULL, T.E.; and ZIMMERMAN, B.A.	1961	Ann. Phys., 12, 331.
COOK, C.W.; FOWLER, W.A.; LAURITSEN, C.C.; and LAURITSEN, T.	1957	Phys. Rev., 107, 508.
DAVIS, R., and HARMER, D.S.	1959	Bull. Am. Phys. Soc. 4, 217.
DOUGLAS, R.A.; BROER, J.W.; CHIBA, REN; HERRING, D.F.; and SILVERSTEIN, E.A.	1956	Phys. Rev., 104, 1059.
EVERLING, F.; KOENIG, L.A.; MATTAUCH, J.H.E.; and WAPSTRA, A.H.	1960	Nuclear Data Tables, Part I, U.S.A.E.C. Report.
FESHBACH, H.; SHAPIRO, M.M.; and WEISSKOPF, V.F.	1953	Tables of Penetrabilities of Charged Particle Reactions (N.Y.O.-3077).
FEYNMAN, R.P., and GELLMANN, M.	1958	Phys. Rev., 109, 193.

FOWLER, W.A.	1951	Phys. Rev. 81, 655 (1951)
FOWLER, W.A.	1959	Ninth International Astroph. Symposium, Liege, 203.
FOWLER, W.A.; GREENSTEIN, J.L.; and HOYLE, F.	1962	Geophysical Journal of the Royal Astronomical Soc., 6, 148.
FREGEAU, J.H.	1956	Phys. Rev., 104, 225.
GANDEL'MAN, G.M., and PINAEV, V.S.	1960	JETP 10, 764.
GAMOW, G., and SCHOENBERG, M.	1941	Phys. Rev., 59, 539.
GELL-MANN, M.	1961	Phys. Rev. Letters, 6, 70.
GOOD, W.M.; KUNZ, W.E.; and MOAK, C.D.	1954	Phys. Rev. 94, 87.
GRIFFITHS, G.; LAL, M.; and SCARFE, C.	1961	Bull. Am. Phys. Soc., 6, 506.
HAYASHI, C., and CAMERON, R.C.	1962	To be published.
HEBBARD, D.F.	1960	Nuclear Phys., 15, 289.
HEBBARD, D.F., and VOGL, J.L.	1960	Nuclear Phys., 21, 652.
HESTER, R.E.; PIXLEY, R.E.; and LAMB, W.A.B.	1958	Phys. Rev.111, 1604.
HILL, R.W.	1953	Phys. Rev., 90, 845.
HOLMGREN, H.D., and JOHNSTON, R.L.	1959	Phys. Rev. Letters, 2, 275, 381.
HOYLE, R., and FOWLER, W.A.	1960	Astrophys. J., 132, 565.
IMHOF, W.L., et al	1962	Lockheed Report AF 29(601)-1765.
KAVANAGH, R.W.	1960	Nuclear Phys., 15, 411.
KELLER, G.	1953	Astrophys. J., 118, 142.
KUEHNER, J.A.; GOVE, H.E.; LITHERLAND, A.E.; CLARK, M.A.; and ALMQVIST, E.	1961	Chalk River Report, PD-317

KUMAR, S.S.	1962	To be published.
LAL, M.	1961	(Thesis) University of British Columbia.
LAMB, W.A.S., and HESTER, R.E.	1957a 1957b	Phys. Rev., 107, 550. Phys. Rev., 108, 1304.
LANDOLT-BORNSTEIN	1961	New Series Group I, Vol. 1, (Springer-Verlag, Berlin).
MARX, C., and MENYHARD, N.,	1960	Mitteilungen der Sternwarte der Ungarishen Akademie der Wissenschaften, Budapest.
MATINYAN, G., and TSILOSANI	1962	JETP, 14, 1195.
MEADS, R.E., and MC ILDOWIE, J.E.C.	1960	Proc. Phys. Soc., A75, 257.
PIXLEY, R.E.	1962	To be published.
POCHODA P., and REEVES, H.	1963	To be published in Space Science Reviews.
PONTECORVO, B.M.	1959	JETP, 9, 1148.
REEVES, H.	1962a 1962b	Astrophys. J., 135, 779. To be published.
REIBEL, K., and MANN, A.K.	1960	Phys. Rev., 118, 701
REINES, R., and COWAN, C.L., JR.	1953	Phys. Rev., 92, 830.
RITUS, V.I.	1962	JETP, 14, 915.
ROTH, B., and WILDERMUTH, K.	1960	Nuclear Phys., 20, 10.
SALPETER, E.E.	1952 1954 1955 1957	Phys. Rev., 88, 547. Austral. J. Phys., 7, 373. Phys. Rev., 97, 1237. Phys. Rev., 107, 516.
SAWYER, G.A., and PHILLIPS, J.A.	1953	Los Alamo Report 1578.
SCHARDT, A.; FOWLER, W.A.; and LAURITSEN, C.C.	1952	Phys. Rev., 86, 527.

ACKNOWLEDGMENTS

I wish to thank Dr. R. Jastrow and the Institute for Space Studies for their hospitality; Dr. A.G.W. Cameron, H.Y. Chiu, E.E. Salpeter and B. Stromgren for their comments; Mr. J. Hauben, W. Hatt, Miss B. Forman, A. Weisswasser and M. Golub for their help in the numerical calculations.

Finally I acknowledge gratefully the patience of Mrs. Judith Sprott, Mr. Ted Psaropulos and Mr. W. Cartledge in preparing and revising the manuscript.